# NANOSTRUCTURES FOR THERAPY AND DIAGNOSIS

by


## ROSARIA ARUTA


In partial Fulfillment of the Requirements for the Degree of Doctor of Philosophy in Engineering Materials and Structures at the Federico II University for Naples


Advisor
Prof. Paolo Antonio Netti

Tutor
Dr. Ing. Enza Torino

Chairman
Prof. Giuseppe Mensitieri

## EXTENDED ABSTRACT

The **preparation of Nanostructures of desired shape, composition and with tailored properties** is of wide scientific and technological interest. Indeed, a variety of nanoparticle architectures have been proposed as nanocarriers, these include liposomes, quantum dots (QD), gold-nanoshells, mesoporous materials, micelles, magnetic nanoparticles, dendrimers, and Carbon Nanotubes (CNTs) as so as several materials have been studied for use in active agents targeting. Among them, as asserted by different authors, **hollow biopolymeric nanocapsules** or (nanoencapsulated systems) as active substance carriers, compared to other particulated systems, show higher drug encapsulation efficiency due to optimized drug solubility in the core, low polymeric content compared such as to nanospheres, drug polymeric shell protection against degradation factor like pH and light and the reduction of tissue irritation due to the polymeric shell.

Several research teams have extensively studied the nanoparticles formation mechanism, and generally there are several classical methods for the preparation of nanocapsular systems: nanoprecipitation, emulsion diffusion, emulsion evaporation, double emulsification, emulsion coacervation, polymer coating and layer by layer.

Despite the fact the research proposed on these methods has shown important strategies, all these methods present critical challenges with a view of the industrial development. Indeed, it is important to take into account that the method chosen should also considerer other aspects such as active substance stability under operational conditions, particularly stirring, encapsulation efficiency, method feasibility, the generation of contaminants and the need for subsequent purification steps, solvent nature, the water volume required and time consumption. Likewise, the feasibility of scaling-up and cost should be considered.

In these perspectives, **to overcome some limitations of traditional processes in nanocapsular structure productions**, such as sufficient scale-up to produce the cost reduction required to target volume markets and more complicated procedure not suitable to be industrialized, we focused our attention on the **three main approaches**:

- the first one based on the **Thermally Induced Phase Separation** (TIPS) to produce nanocapsules for **therapy**
- the second one related to the study of the **micellization of block-copolymer** to apply in the field of **enhanced MRI**
- the last is the **combining of the previous approaches** by providing the **deposition of the block-copolymer on the surface of the obtained nanocapsules**.

In the first part of the thesis, we developed a novel approach based on the thermodynamics of **Thermally Induced Phase Separation (TIPS) to produce semicrystalline nanocapsules**. Thermally Induced Phase Separation has extensively been used to fabricate various porous biodegradable scaffolds suitable for tissue engineering and drug delivery, even though **it has never been studied neither to produce nanocapsules nor to produce semicrystalline nanocapsules**. Because of the variety of parameters involved in TIPS process, such as types of polymers, polymer concentration, solvent/nonsolvent ratio, and quenching temperature, we individuate in this approach the possibility to create a value added process enables to overcome the issues related to the production of the nanocapsular systems even by preserving fundamental architectural properties.

In this process, we started by a **Poly-L-Lactic Acid (PLLA)**, a biopolymer largely studied by TIPS. PLLA is a Food&Drug Administration Approved polymer and it is biocompatible and biodegradable material which undergoes scission in the body to monomeric units of lactic acid as a natural intermediate in carbohydrate metabolism. The work also investigates **thermodynamic parameters** involved in the process able to induce for the first time simultaneously bending and crystallization of polymeric chain to form a nanocapsule. An explanation of this unusual crystallization phenomenon will be described **in term of**

**nanoscopic confinement** of long flexible chain. Knowledge of the phase behavior of confined long flexible chain is a prerequisite to support the current interest in the construction of nanoscopic devices as so in confinement altering the statistical mechanical properties of DNA.

In the second part of the thesis a **Block copolymers of poly lactic acid (PLA) and polyethylene glycol (PEG)** has been studied. Block copolymer are few of the commonly used polymers with **hydrophilic and hydrophobic** blocks which allows the formation of a stable nano-particulate suspension in an aqueous solvent, where PLA chains predominantly form the core and PEG chains are located outside. A systematic variation in their chemical structure, composition, size, and architecture; block copolymers offer advantages in tuning their shape and functionality in comparison to conventional amphiphiles such as low molecular weight surfactants and lipids. In particular, Diblock PLA-PEG copolymers and triblock **PLA-PEG-PLA copolymers allow modulation of the biodegradation rate, the hydrophilicity, and the mechanical properties of the copolymers**. Herein we present temperature/time-reliant self-assembly driven simple approach for the development of biocompatible nanostructures for MRI. Endeavor of the present research was to develop Gd loaded PLA-PEG-PLA NPs as the molecular MRI contrast agents to efficiently target tumor. A low molecular PLA-PEG-PLA have been designated to prepare **well-**

**demarcated NPs through optimization of kinetics of the self-assembly viz a viz temperature/time/concentration**. The hydrophobic/hydrophilic moieties of block copolymer nanoparticles (BCN) were employed **to adsorb $GD^{+3}$ at the surface of BCNs to achieve multifunctional biodegradable NPs for MRI**. The paramagnetic properties of the BCNs designed here compare sympathetically with Gd-based agents that have previously been reported. For example, while relaxivity of the commercial products, such Magnevist is of 4 $mM_{-1}$ $sec^{-1}$, our micelles can reach relaxivitry of around 30 $mM^{-1}$ $sec^{-1}$ , indicating a relaxivity significantly higher than the common paramagnetic contrast agents.

**Last part of the thesis has been devoted to the combination of the previous obtained structures in order to apply these new nanostructures in the theranostic field**. For this reason only some Caolrimetric studies were performed. Nano-Isothermal Calorimetry (NanoITC) was used to evaluate the deposition of the block on the surface of the nanoparticles while Differential Scanning Calorimetry was used to show the melting properties of the combined system.

## Peer Reviewed Paper

- **Nanocapsules production by Thermally Induced Phase Separation in a nanoconfinement** – Rosaria Aruta, Enza Torino, Paolo Antonio Netti

  Submitted to Biomaterials

- **Aqueous Channel Manifestation amongst Biodegradable nanomaterials for favorable Gadolinium entrapping** – Rosaria Aruta, Pankaj Thakur, Enza Torino, Paolo Antonio Netti

  Submitted to International Journal of Nanomedicine

- **Nanocapsules decoration by tri-block copolymer and study of their behavior in the theranostic field**

  Paper in preparation

## TABLES OF CONTENTS

# CHAPTER I: INTRODUCTION

## NANOPARTICLE FOR THERAPY AND DIAGNOSTIC: ARCHITECTURE AND FEATURES

Theranostic is an emerging and promising field of the nanomedicine that has captured the interest of researchers because its purpose is to diagnose and treat the diseases at their earliest stage, when the diseases are most likely curable or at least treatable[1]. To achieve this, it takes advantage of the high capacity of nanoparticles, submicron sized colloidal particles with sizes ranging from 10-1000 nm in diameter, to ferry cargo and loads onto them both imaging and therapeutic functions. Thus, nanoparticle technologies are significantly impacting on the development of both therapeutic and diagnostic agents for simultaneous drug delivery and molecular imaging.

From the point of view of Drug delivery, nanoparticle objective is the delivery of a medicine to its site of therapeutic action because this is one of the main limitations of pharmaceutical and biotechnology industries[2]. Indeed, most of the drugs are limited by their poor solubility, high toxicity and dosage, aggregation due to poor solubility, nonspecific delivery, in vivo degradation and short circulating half-lives. Thus, nanoparticles have the potential to overcome this limitations and could improve the process of releasing of a bioactive agent at a specific rate and at a specific site, allowing to

exploit thousands of new therapeutics that are limited by a safe and effective drug-delivery system.

Although nanoparticles have been developed for a myriad of important diseases, the thrust of research has been focused on solid tumors, cardiovascular diseases, and immunological diseases. In particular, as drug carriers for chemotherapeutics, nanoparticles can be used to deliver medication directly to the tumor while sparing healthy tissue, by bringing several advantages over conventional chemotherapy[3], because they can:

• Protect drugs from being degraded in the body before they reach their target;

• Enhance drug absorption into tumors and the cancerous cells themselves;

• Allow for better control over the timing and distribution of drugs to the tissue, making it easier for oncologists to assess how well they work;

• Prevent drugs from interacting with normal cells, thus avoiding side effects.

Along with drug delivery researches other studies have been done for diagnostic applications. In particular, for molecular imaging, that allows the characterization of biological processes at the cellular and subcellular levels in intact organism by exploiting specific molecular probes or contrast agents, most of the contrast agents currently in use consist of low molecular weight compounds that are non-specific, thus making the quantification of disease at early stage difficult[4]. So,

the development of nanoparticulate-based contrast agents could offers a platform to enhance tissue specificity and sensitivity required for in vivo molecular imaging with a minimal administration of the contrast agent.

One significant challenge for the successful development of therapeutic nanoparticles is rapid clearance during systemic delivery[5]. When nanoparticles enter the bloodstream, the particle surface may experience nonspecific protein adsorption (opsonization), thereby making them more visible to phagocytic cells. After opsonization, nanoparticles could be rapidly cleared from the bloodstream through phagocytosis by the reticuloendothelial system (RES) in the liver and by spleen filtration. Therefore, the factors that could affect the clearance and biodistribution of nanoparticles, such as particle physicochemical properties and targeting ligand functionalization, should be carefully considered for the optimal design of therapeutic nanoparticles. On the basis of physiological parameters such as hepatic filtration, tissue extravasation/diffusion, and kidney excretion, it is clear that particle size plays a key factor in the long circulation and biodistribution of nanoparticles. Indeed, nanoparticles smaller than 10 nm can be rapidly cleared by the kidneys or through extravasation, while larger nanoparticles may have higher tendency to be cleared by cells of reticuloendothelial system (RES). Moreover, It was observed that nanoparticles <100 nm have a higher potential to circulate in the blood for long periods of time and experience reduced hepatic filtration. Nanoparticle size also

plays a key role in tumor accumulation through the EPR effect (Enhanced Permeability and Retention effect)[6]. This is a phenomenon due to the unique anatomical and pathophysiological characteristics of solid tumor. Namely, in contrast to normal tissues and organs, most solid tumors show a higher vascular density, and tumors blood vessels present defective architecture, such as large gap between endothelial cells (e.g., ~ 1μm), lack of smooth muscle layers, so that macromolecules will have the opportunity to escape from tumor blood vessels and accumulate selectively in tumor tissues, whereas they could not cross normal blood vessels which will result in less side effects. In addition, defected lymphatic function that is important for the recovery of macromolecules in tissues is always found in tumor tissues. Consequently, once macromolecules accumulate in tumor tissues, they will not be cleared from tumor tissues but retain there for long time. Several studies have tried to determine the gap size in the leaky vasculature that depends on the kind of tumor considered. Therefore, to capitalize on the EPR effect and to efficiently escape from the physiological barriers, many studies advocate the optimal nanoparticle size range of approximately 10–250 nm.

It has been established that the surface charge of nanoparticles is another important property because it could affect their uptake by the RES cells[7]. Neutrally charged particles have demonstrated much lower opsonization rates than charged particles. It was found that positively charged nanoparticles generate a higher immune response

compared to neutral or negatively charged nanoparticle formulations. For example, nanoparticles with a primary amine at the surface promote higher rates of phagocytic uptake when compared to those having sulfate, hydroxyl, or carboxyl groups at the surface. Many studies suggest that the optimal range of nanoparticle surface charge should be between −10 and +10 mV for reduced phagocytosis and minimized nonspecific interactions of nanoparticles. Surface modification of nanoparticles with PEG, which has favorable intrinsic physicochemical properties (*e.g.*, high flexibility and hydrophilicity, low toxicity and immunogenicity), was found to reduce nanoparticle accumulation in off-target organs such as liver and spleen[8]. A PEG decoration on the nanoparticle's surface shields hydrophobic or charged particles from being attacked by blood proteins, leading to prolonged circulation half-life compared to non-PEGylated nanoparticles. The length, shape, and density of PEG chains on the nanoparticle surface largely affect its surface hydrophilicity and phagocytosis.

Until now, different architectures of nanoparticles have been developed using a variety of materials including lipids (liposomes), organometallic compound (nanotubes) and polymers (micelles, dendrimers and polymeric nanoparticles)[9].

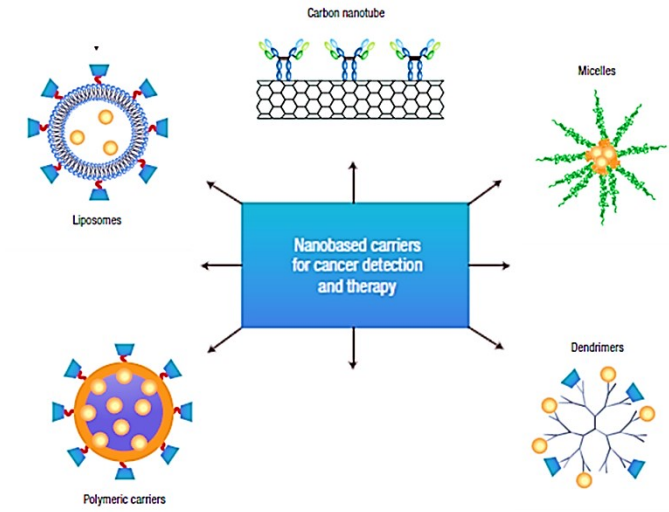


**Figure 1. Different architectures applied in the nanomedicine field**

## Liposomes

Liposomes are artificial, single, or multilaminar vesicles made with bilayered membrane structures with inner aqueous phases, composed of natural or synthetic amphiphilic lipid molecules. They are versatile and tunable vehicles for drug delivery and imaging. Liposomes exhibit several unique properties including favorable safety profiles, long systemic circulation half-life, and ease of surface modifications. Among the clinically validated nanotechnology products, liposomal drugs were the first nanotherapeutics to get FDA approval for clinical use. Upon intravenous injection, these nanoparticles are rapidly cleared from the bloodstream by the reticuloendothelial defence mechanism, regardless of particle composition. Moreover, instability of the carrier and burst drug release, as well as non-specific uptake by the mononuclear

phagocytic system (MPS), provides additional challenges for translating these carriers to the clinic. Other challenges facing the use of liposomes in the clinic include the high production cost, fast oxidation of some phospholipids, and lack of controlled-release properties of encapsulated drugs.

**Micelles**

Micellar nanoparticles are attractive structures for carriers of drug and contrast agents because they can form relatively uniform size structures. They can be prepared by self-assembly of a variety of amphiphilic materials that, in aqueous environments, under certain concentrations and temperature, spontaneously self-assemble into core-shell nanostructure, with a hydrophobic core and a hydrophilic shell. This architecture increases the solubility of hydrophobic molecules, and allows incorporating multiple functionalities into a single structure. Polymeric micelles represent a class of micelles that are formed of block copolymers consisting of a hydrophobic block that forms the micellar core, and a hydrophilic portion that forms the corona. This corona (commonly consisting of PEG or equivalent hydrophilic polymer) confers these micelles with biocompatibility, stealth-like properties, and a platform for functionalization.

**Dendrimers**

Dendrimers are polymeric molecules composed of multiple perfectly branched monomers that emanate radially from the central core,

thus forming a tree-like structure. They consist of three critical architectural domains: (i) the multivalent surface, containing a larger number of potentially reactive sites, (ii) the interior shells (i.e., branch cell layers defined by dendrons) surrounding the core, and (iii) the core to which the dendrons are attached. These three domains can be tailored to serve various purposes, such as dendritic sensors, drug, contrast agent and gene carriers, or themselves as drugs. They have shown promise for biomedical applications because they (1) can be easily conjugated with targeting molecules, imaging agents, and drugs, (2) have high water solubility and well-defined chemical structures, (3) are biocompatible, and (4) are rapidly cleared from the blood through the kidneys, made possible by their small size (<5 nm), which eliminates the need for biodegradability. Furthermore the end groups of dendrimers can also be modulated to alter dendrimers' solubility; for instance, the hydrophilic end groups can make a dendrimer with a hydrophobic core water soluble, whereas hydrophobic peripheral moieties can make a dendrimer with a hydrophilic interior soluble in oil. Although promising, dendrimers are more expensive than other nanoparticles and require many repetitive steps for synthesis, posing a challenge for large-scale production.

**Carbon nanotubes**

Carbon nanotubes (CNTs) consist exclusively of carbon atoms arranged in tubular structure. This novel artificial nanomaterial belongs to the family of fullerenes, the third allotropic form of

carbon . Based on the number of layers, structures of CNTs are classified into two types: single-walled carbon nanotubes (SWCNTs) and multiwalled carbon nanotubes (MWCNTs). SWCNTs consist of a single graphene cylinder with diameter varying between 0.4 and 2 nm, and usually occur as hexagonal close-packed bundles. MWCNTs consist of two to several coaxial cylinders, each made of a single graphene sheet surrounding a hollow core. CNTs are not soluble in aqueous solutions because they have highly hydrophobic surfaces. Surface functionalization is required to solubilize CNTs, and to make them biocompatible and low toxic for their medical applications. They are being investigated as theranostic nanoparticles because of their tunable properties and ability to incorporate multiple functionalities. Many studies have confirmed CNTs to be effective carriers of therapeutics and imaging agent in vitro, however, in vivo studies have led to concerns regarding the associated toxicities. So, the primary barriers that must be overcome include route of biodegradation and reduction of off-target toxicity.

**Polymeric Nanoparticles**

Polymers are the most commonly explored materials for constructing nanoparticles-based drug carriers. Most polymeric nanoparticles are biodegradable and biocompatible, moreover, they exhibit a good potential for surface modification and functionalization with different ligands, provide excellent pharmacokinetic control and are suitable to encapsulate and deliver a plethora of therapeutic agents. The main

advantage of using polymeric nanoparticles for drug-delivery applications is their small size when taken up by cells, which could allow efficient drug accumulation at the target sites. Biodegradable materials used for their formulation allow sustained drug release within the target site over a period of days or even weeks.

For preparation of nanoparticles is possible to use both natural hydrophilic polymer and synthetic hydrophobic polymer. Natural hydrophilic polymers such as proteins (gelatine, albumin, lecithin) and polysaccharides (alginate, dextran, chitosan) are widely used. But these polymers have certain disadvantages such as poor batch-to-batch reproductivity, poor mechanical properties, limited residence time (fast degradation and absorption), and potential antigenicity. Synthetic hydrophobic polymers are characterized by low production costs, and it is possible to design them to obtain the desired chemical-physical properties. They are divided into two groups: The first group includes polyesters (poly (€-caprolactone), poly(lactic acid), poly (lactide-co-glycolide), polystyrene) and the second group includes poly (alkyl cyanoacrylates) (poly (isobutyl cyanoacrylates), poly (butylcyanoacrylates), poly methyl (methcyanoacrylates)).

Nanoparticles can be produced in two different approaches, by polymerization of the monomer or by the preformed polymer. The second case is preferable because the chemical/physical properties of the polymer are already well defined. Depending on the process

used for nanoparticles preparation, we can obtain nanospheres or nanocapsules.

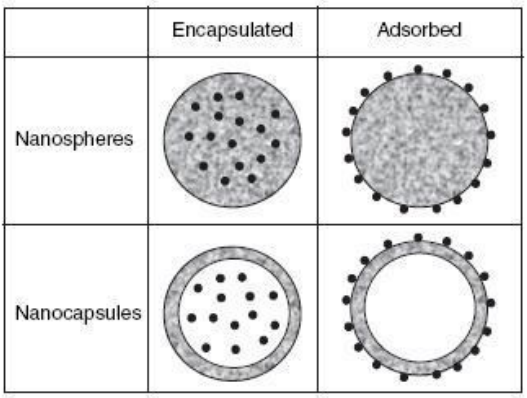


**Figure 2: In this image the difference between nanoparticles and nanospheres as so between drug encapsulation and absorption is showed.**

Nanospheres are matrix particles, i.e., particles whose entire mass is solid and molecules may be adsorbed at the sphere surface or entrapped within the particle matrix. In general, they are spherical, but "nanospheres" with a nonspherical shape are also described in the literature. Nanocapsules are vesicular systems, acting as a kind of reservoir, in which the encapsulated substances are confined to a cavity consisting of a liquid core (either oil or water) surrounded by a solid material shell.

## PRODUCTION OF NANOCAPSULES: METHODS, ADVANTAGES AND DRAWBACKS

Nanocapsules can be defined as nano-vesicular systems that exhibit a typical core-shell structure in which the drug is confined to a

reservoir or within a cavity surrounded by a polymer membrane or coating[10]. The cavity can contain the active substance in liquid or solid form or as a molecular dispersion. Likewise, this reservoir can be lipophilic or hydrophobic according to the preparation method and raw materials used. Also, taking into account the operative limitations of preparation methods, nanocapsules can also carry the active substance on their surfaces or imbibed in the polymeric membrane.

Generally, there are six classical methods for the preparation of nanocapsules: nanoprecipitation, emulsion–diffusion, double emulsification, emulsion-coacervation, polymer-coating and layer-by-layer.

**Nanoprecipitation (Solvent displacement) method**

The nanoprecipitation method is also called solvent displacement[11]. In this method, the nanocapsule synthesis needs both solvent and non-solvent phases. The solvent phase consists of a solution in a solvent or in a mixture of solvents (i.e. ethanol, acetone, hexane, methylene chloride or dioxane) of a film-forming substance such as a polymer (synthetic, semi-synthetic or naturally occurring polymer), the drug, oil and lipophilic surfactants. On the other hand, the non-solvent phase consisting of a non-solvent or a mixture of non-solvents for the film-forming substance, supplemented with one or more naturally occurring or synthetic surfactants. In most cases, the solvent and non-solvent phases are called organic and aqueous phases, respectively. As a general tendency, the solvent is an organic

medium, while the non-solvent is mainly water. However, it is possible to use either two organic phases or two aqueous phases as long as solubility, insolubility and miscibility conditions are satisfied. In the nanoprecipitation method, the nanocapsules are obtained as a colloidal suspension formed when the organic phase is added slowly and with moderate stirring to the aqueous phase.

The key variables of the procedure are those associated with the conditions of adding the organic phase to the aqueous phase, such as organic phase injection rate, aqueous phase agitation rate, the method of organic phase addition and the organic phase/aqueous phase ratio. Likewise, nanocapsule characteristics are influenced by the nature and concentration of their components. Different theories have been developed to explain the mechanism of nanocapsules formation using this technique. The first is based on Sugimoto's theory on polymer precipitation that indicated three stages for the process of particle formation in the nanoprecipitation: nucleation, growth and aggregation. The rate of each step determines the particle size and the driving force of these phenomena is supersaturation, which is defined as the ratio of polymer concentration over the solubility of the polymer in the solvent mixture. The separation between the nucleation and the growth stages is the key factor for uniform particle formation. Ideally, operating conditions should allow a high nucleation rate strongly dependent on supersaturation and low growth rate. The second theory is based on Gibbs–Marangoni effect, that explained rapid

nanoparticle formation as a process due to differences in surface tension, since a liquid with a high surface tension (aqueous phase) pulls more strongly on the surrounding liquid than one with a low surface tension (organic phase solvent). These differences between surface tensions cause interfacial turbulence and thermal inequalities in the system, leading to the continuous formation of eddies of solvent at the interface of both liquids. Consequently, violent spreading is observed due to mutual miscibility between the solvents, the solvent flows away from regions of low surface tension and the polymer tends to aggregate on the oil surface and forms nanocapsules. According to this explanation, nanocapsule formation is due to polymer aggregation in stabilized emulsion droplets, while apparently the nucleation and growth steps are not involved.

**Emulsion-diffusion method**

In emulsion-diffusion method[12] the experimental procedure performed to achieve this requires three phases: organic, aqueous and dilution. In particular, the encapsulating polymer is dissolved in the organic phase that contain a partially water soluble solvent, saturated with water to ensure the initial thermodynamic equilibrium of both liquids, the active substance and oil. The aqueous phase is an aqueous dispersion of a stabilizing agent, prepared using water saturated with solvent, while the dilution phase is usually water.

For preparation of nanocapsules using the emulsion–diffusion method, the organic phase is emulsified under vigorous agitation in the aqueous phase.

The subsequent addition of water to the system causes the diffusion of the solvent into the external phase, resulting in nanocapsule formation. This can be eliminated by distillation or cross-flow filtration depending on the boiling point of the solvent. It has been shown that nanocapsule size is related to the shear rate used in the emulsification process, the chemical composition of the organic phase, the polymer concentration, the oil-to-polymer ratio and the drop size of the primary emulsion. The nanocapsule formation mechanism is based on the theory that each emulsion droplet produces several nanocapsules and that these are formed by the combination of polymer precipitation and interfacial phenomena during solvent diffusion. It is important to note that the interface between organic and aqueous phases was subjected to shear force during the emulsification step. Thus, for the emulsification–diffusion method it might be expected that surface tension gradients can be due to the thermal effects associated with heat transport during organic solvent diffusion. Typically, the thermal Marangoni effect results in fingering instability where the low interfacial tension difference and the drop curvature less than its spontaneous one allow that the flexible drop surface develops multiple undulations generating long fingers as the organic solvent diffuses towards the aqueous medium. In this process, the solvent carries polymer molecules into the aqueous phase. Then, if spontaneous curvature favors an organic phase-in water arrangement, it could be expected that many drops of smaller diameter detach from the fingers and

become dispersed in the aqueous phase. Thus new globules or polymer aggregates (not totally desolvated) are formed and stabilized by the stabilizing agent (protoparticles) which prevents their coalescence and the formation of agglomerates. The submicron particles will be formed after the complete diffusion of the solvent, if the stabilizing agent remains at the liquid–liquid interface during the diffusion process and if its protective effect is adequate. The mean nanocapsule size is always smaller than that of the emulsion droplets, in agreement with the diffusion theory proposed.

This technique presents several advantages, such as high encapsulation efficiencies, no need for homogenization, high batch-to-batch reproducibility, simplicity, and narrow size distribution. Disadvantages are the high volumes of water to be eliminated from the suspension and the leakage of water-soluble drug into the saturated-aqueous external phase during emulsification, reducing encapsulation efficiency.

**Double Emulsification**

Double emulsions[13] are complex heterodisperse systems called "emulsions of emulsions", that can be classified into two major types: water-oil-water emulsion (w/o/w) and oil-water-oil emulsion (o/w/o). Thus the dispersed phase is itself an emulsion and the inner dispersed globule/ droplet is separated from the outer liquid phase by a layer of another phase. Double emulsions are usually prepared in a two-step emulsification process using two surfactants: a hydrophobic one designed to stabilize the interface of the w/o

internal emulsion and a hydrophilic one to stabilize the external interface of the oil globules for w/o/w emulsions. For preparation of nanocapsules, the principle of double emulsion formation, specifically of the w/o/w type, is associated with the principles of both nanoprecipitation and emulsion–diffusion methods. In this case, in the primary w/o emulsion the oil is changed by an organic phase containing a solvent that is totally or partially miscible in water, the film-formed polymer and a w/o surfactant. Then the water containing a stabilizing agent is added to the system to obtain the water in organic in water emulsion. However in this step, particle hardening is obtained through solvent diffusion and polymer precipitation. Water is frequently added to the double emulsion in order to achieve full solvent diffusion. The surfactants play a dual role in emulsions: as a film former and a barrier to drug release at the internal interface, and as a steric stabilizer on the external interface. It was found that drug encapsulation efficiency and average particle size are affected by changing the type and concentration of both the w/o emulsion and the stabilizing agent. In a typical procedure for preparation of nanocapsules by double emulsification, the primary emulsion is formed by ultrasound and the w/o surfactant stabilizes the interface of the w/o internal emulsion.

The second emulsion is also formed by ultrasound and nanocapsule dispersion is stabilized by the addition of the stabilizing agent. Finally, the solvents are removed by evaporation or extraction by vacuum, leaving hardened nanocapsules in an aqueous medium.

**Emulsion-Coacervation method**

The emulsion-coacervation process is mainly presented as a strategy for nanocapsules preparation from naturally occurring polymeric materials. Up to now, sodium alginate and gelatin have been used though synthetic polymeric materials could be used for this purpose. The procedure involves the o/w emulsification of an organic phase (oil, active substance and active substance solvent if necessary) with an aqueous phase (water, polymer, stabilizing agent) by mechanical stirring or ultrasound. Then, a simple coacervation process is performed by using either electrolytes[14], by the addition of a water miscible non-solvent[15] or a dehydration agent or by temperature modification[16]. Finally, the coacervation process is complemented with additional crosslinked steps that make it possible to obtain a rigid nanocapsule shell structure.

Nanocapsule formation by the emulsion-coacervation method uses the emulsion as a template phase and the formation of a coacervate phase that causes polymer precipitation from the continuous emulsion-phase to form a film on the template forming the nanocapsule. Additionally, it can be stabilized by physical intermolecular or covalent cross-linking, which typically can be achieved by altering pH or temperature, or by adding a cross-linking agent. Probably the critical stage in preparation of nanocapsules by the emulsion-coacervation method is coacervate phase formation[17]. In particular, the polymer dissolved in water is enclosed by water molecules that solvate its functional groups, typically through

hydrogen-bonding and van der Waals forces that prevent attraction among chain segments in close proximity by interchain H-bonds, or van der Waals or opposing ionic forces. Thus, the coacervating agents lower the solvation of dissolved polymers and induce thin solvated shell. It may also allow the attraction among contiguous chains via secondary valence bonds to form an entangled network or even non-covalent weak cross-links as the polymer concentration gradually increases in the coacervated phase. The use of electrolytes for polymer desolvation is known as salting-out. On the other hand, in the case where a dehydrating agent is used, the ternary system formed (polymer – dehydrating agent– water) allows the increase of polymer concentration due to solvent–solvation competition process. This results in the desolvation of the polymer chains, leading to phase separation.

**Polymer Coating method**

In polymer coating method different methodological strategies can be used to deposit a thin layer of polymer on the nanoparticle surface. This can be achieved by adsorbing the polymer onto the preformed uncoated nanocapsules when the latter are incubated in polymer dispersion under predetermined stirring and time conditions[18]. Likewise, layer-formed polymer can be added during the final stage of conventional methods for the preparation of nanocapsules such as nanoprecipitation and double emulsification. Thus, these methods have been modified in order to add a layer of polymer to the external aqueous medium and allow to simultaneous

layer formation due to the precipitation of the charged polymer (mainly negatively in nature) and to the diffusion of the solvent. Another way is to prepare a nanoemulsion as template and then coat it by polymer deposition on the water/oil nanoemulsion surface. The polymers are added in the continuous phase and their precipitation onto the nanoemulsion droplets is triggered by solvent evaporation, as opposed to the emulsion coacervation method. For preparation of nanocapsules using this method an organic phase, composed of the active substance, oil, surfactant and solvent, and an aqueous phase containing the stabilizing agent and an aqueous polymer-coating solution are mixed under moderate stirring and the o/w nanoemulsion is formed by solvent displacement. The solvents are subsequently evaporated under vacuum until reaching a specific volume and the nanoemulsion is finally coated by the polymer by simple incubation in the polymer solution. The nanocapsule formation mechanism is mediated by the ionic interaction between surfactant and polymer.

**Layer-by-Layer method**

The layer-by-layer assembly process developed for colloidal particle preparation makes it possible to obtain vesicular particles, called polyelectrolyte capsules, with well-defined chemical and structural properties[19]. To sum up, the mechanism of nanocapsule formation is based on irreversible electrostatic attraction that leads to polyelectrolyte adsorption at supersaturating bulk polyelectrolyte concentrations. This method requires a colloidal template onto which

is adsorbed a polymer layer either by incubation in the polymer solution, subsequently washed, or by decreasing polymer solubility by drop-wise addition of a miscible solvent. This procedure is then repeated with a second polymer and multiple polymer layers are deposited sequentially, one after another. It can be used as a template the solid form of the active substance, as can inorganic particles and biological cells. Likewise, the adsorption of oppositely charged polyelectrolytes can be done on the surface of colloidal particles with subsequent core dissolution. Also emulsion droplets, prepared by high-pressure homogenization, can be used as template.
Once the polyelectrolyte addition had ended, nanocapsule dispersion was again treated by high-pressure homogenization and the dispersion was finally centrifuged. The molecules employed for assembly should have a sufficient number of charged groups to provide stable adsorption on an oppositely charged surface and non-compensated charges exposed to the exterior. Furthermore, this method raises other difficulties such as the formation of counterions aggregates, the separation of the remaining free polyelectrolyte from the particles prior to the next deposition cycle and polyelectrolyte-induced bridging during centrifugation. Close particle–particle encounters may cause unfavorable interactions with the polyelectrolyte films, possibly leading to film destruction and aggregate formation. In addition, another difficulty is the particle sizes obtained which are higher than 500nm. Although these particle

sizes are at submicronic scale, they are obviously larger than the size commonly accepted for nanocapsules.

**Thermally Induced Phase Separation (TIPS)**

As explained in the previous paragraphs, nanocapsules of desired shape, composition and with tailored properties have exhibited potential applications of wide scientific and technological interest in the field of nanomedicine. However, methods applied in nanocapsular structure productions are still limited by several drawbacks, related to their production, such as high polidispersity index, low biocompability, poor feasibility of scaling-up to produce the cost reduction required to target markets, and time consuming procedures not suitable to be industrialized. Thus, the aim of this work is to overcome limitations of methods currently proposed in the fabrication of nanocapsules through several novel approaches.

In particular, most of the work involves Thermally Induced Phase Separation (TIPS) is a process based on the phenomenon that solvent effectiveness decreases when temperature is decreased[20]. Thus, when a homogeneous polymer solution at elevated temperature is cooled down, phase separation occurs, resulting in the formation of a polymer-rich phase and a polymer-lean phase. During the TIPS process the phase transitions may proceed in combinations with liquid–liquid phase separation and solidification such as vitrification, crystallization of the polymer, or freezing of the solvent. In most cases these solidifications are useful for fixing the structure of the solution at a certain stage during liquid–liquid phase separation. Afterwards, the solvent can be removed by evaporation, freeze

drying, and extraction with non-solvents or critical point drying. The final morphology of the solution is determined by the extent of the liquid–liquid phase separation before solidification.

A typical phase diagram for a binary polymer solvent system is schematically represented in Fig .

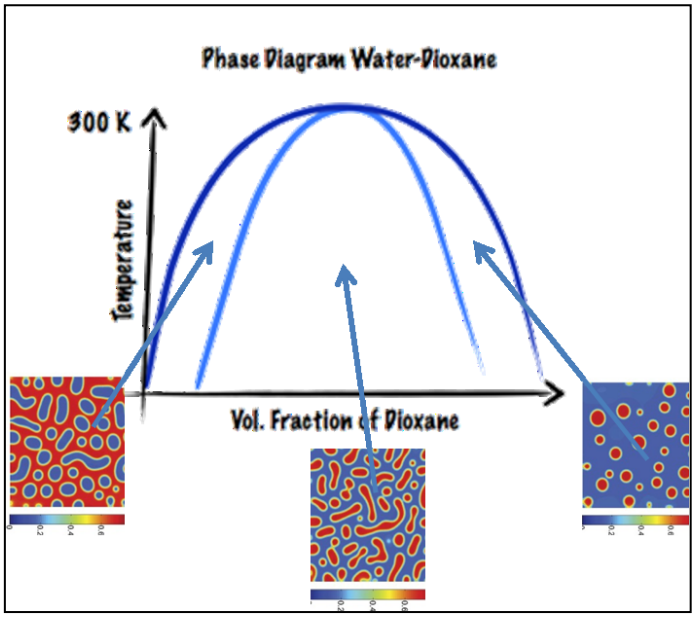


**Figure 3: A schematic representation of a binary phase diagram of a polymer solution showing a liquid-liquid demixing gap. In addition, the possible structure formation in the different parts of the liquid-liquid demixing gap is indicated: nucleation and growth of polymer rich phase (left picture), bicontinuous morphology due tospinodal decomposition (middle picture) and nucleation of a polymer poor phase (right picture).**

In the figure the temperature is plotted as function of the polymer concentration. At higher temperatures the solution is still homogeneous, at lower temperatures liquid-liquid phase separation can take place. The miscibility gap can be divided into three areas. The border of the miscibility gap is called the binodal, the dashed line is called the spinodal. Examples of compositions that are in

equilibrium are given by horizontal lines called tie lines. The point where the binodal and spinodal touch is called the critical point. At the critical point the polymer rich phase and the polymer poor phase have the same compositions. Compositions located between the binodal and the spinodal are metastable, this means that solutions are stable with respect to small composition fluctuations. However when the composition fluctuations are large enough phase separation will take place by nucleation and growth of a polymer poor phase in case the original composition of the solution is located at polymer concentrations lower than the critical point, resulting in a globular microporous structure. Likewise, the phase separation take place nucleation and growth of the polymer rich phase in case the polymer concentration is higher than the polymer concentration of the critical point, resulting in a cell-tunnel microporous structure. Solutions quenched into the area enclosed by the spinodal are unstable. Any composition fluctuation can trigger a wave of composition fluctuations through the solution. The amplitude of the fluctuations will increase because the molecules of both components will move from low concentration regions to high concentration regions. In this case demixing usually yields network structures, in which both the polymer rich phase and the polymer poor phase are completely interconnected, forming a continuous structure. The spinodal area can only be entered directly at the critical point. In all other cases, the metastable area must first be passed. High cooling rates can be used to prevent demixing in the metastable area.

Up to now, Thermally Induced Phase Separation has extensively been used to fabricate foams, membranes and various porous biodegradable scaffolds suitable for tissue engineering and drug delivery. Here in, we demonstrate that by performing TIPS within nanoconfinement[21] a transition to semicrystalline vesicular morphology can be observed for the first time and the formation of the uniform nanocapsules with controllable size and shell thickness can be obtained. This kind of architecture presents crystal properties, important features in the design and behavior of biocompatible, biodegradable and functionalized vectors, opening the way to the role of *surface* crystallinity of nanocapsular structures on several physicochemical aspects of interaction with a biological system. In particular, for this purpose we focused our research on Poly-L-Lactic Acid (PLLA), because it is a biopolymer largely studied by TIPS[22; 23], generally producing two main types of morphology: *globular-like* and *membrane-like*. In our case, a mixture of dioxane and water was used for a binary composition of solvent and antisolvent respectively of the polymer. In particular, the ternary system PLLA/Dioxane/Water is a well-known UCST (Upper Critical Solution Temperature) system, for which several cloud point studies have already been reported in literature. Its binodal-spinodal diagram shows that the fundamental condition to perform our experiment is at low polymer concentration, where a solvent rich phase formation, as well as globular-like morphology, is favorite by decreasing temperature.

## AIM OF THE WORK

In my PhD project I have focused my attention on Poly Lactic Acid because it is a synthetic polymeric material, already approved by The Food & Drug Administration on the basis of its good properties of non-toxicity, absolute biodegradability, adjustable degradation rate, and good biocompatibility[24]. In the first part of my work, I tried to take advantages by the Thermally Induced Phase Separation in order to control PLLA crystallization properties and to obtain for the first time nanocapsular morphology. Results were obtained by inducing phase transition of polymer chain in a nanoconfined domain. Later, I focused my attention on the tri-block copolymer made by PLA-PEG-PLA and I studied their micellization behavior in order to encapsulate contrast agents for Enhanced MRI. Last efforts were devoted to the combining of the previous processes to obtain nanostructures for application in the theranostic field. We envision polymer nanocapsules with cancer drug entrapped within the core, protected by a soft shell made by triblock copolymer containing contrast agents.

## References


[1] JANIB, S. M.; MOSES, A. S.; MACKAY, J. A. Imaging and drug delivery using theranostic nanoparticles. **Advanced Drug Delivery Reviews,** v. 62, n. 11, p. 1052-1063, Aug 30 2010. ISSN 0169-409X. Disponível em: < <Go to ISI>://WOS:000285225200005 >.

[2] CHO, K. et al. Therapeutic nanoparticles for drug delivery in cancer. **Clinical Cancer Research,** v. 14, n. 5, p. 1310-1316, Mar 1 2008. ISSN 1078-0432. Disponível em: < <Go to ISI>://WOS:000253565000007 >.

[3] PEER, D. et al. Nanocarriers as an emerging platform for cancer therapy. **Nature Nanotechnology,** v. 2, n. 12, p. 751-760, Dec 2007. ISSN 1748-3387. Disponível em: < <Go to ISI>://WOS:000251456500010 >.

[4] BAO, G.; MITRAGOTRI, S.; TONG, S. Multifunctional Nanoparticles for Drug Delivery and Molecular Imaging. **Annual Review of Biomedical Engineering, Vol 15,** v. 15, p. 253-282, 2013 2013. ISSN 1523-9829. Disponível em: < <Go to ISI>://WOS:000323896000012 >.

[5] SWAMI, A. et al. Nanoparticles for Targeted and Temporally Controlled Drug Delivery. **Multifunctional Nanoparticles for Drug Delivery Applications: Imaging, Targeting, and Delivery**, p. 9-29, 2012 2012. Disponível em: < <Go to ISI>://WOS:000303542200002 >.

[6] BAE, Y. H.; PARK, K. Targeted drug delivery to tumors: Myths, reality and possibility. **Journal of Controlled Release,** v. 153, n. 3, p. 198-205, Aug 10 2011. ISSN 0168-3659. Disponível em: < <Go to ISI>://WOS:000295353800002 >.

[7] HE, C. et al. Effects of particle size and surface charge on cellular uptake and biodistribution of polymeric nanoparticles. **Biomaterials,** v. 31, n. 13, p. 3657-3666, May 2010. ISSN 0142-9612. Disponível em: < <Go to ISI>://WOS:000276254100027 >.

[8] JOKERST, J. V. et al. Nanoparticle PEGylation for imaging and therapy. **Nanomedicine,** v. 6, n. 4, p. 715-728, Jun 2011. ISSN 1743-5889. Disponível em: < <Go to ISI>://WOS:000292994300019 >.

[9] DE JONG, W. H.; BORM, P. J. A. Drug delivery and nanoparticles: Applications and hazards. **International Journal of Nanomedicine,** v. 3, n. 2, p. 133-149, 2008 2008. ISSN 1176-9114. Disponível em: < <Go to ISI>://WOS:000257848000002 >.

[10] MORA-HUERTAS, C. E.; FESSI, H.; ELAISSARI, A. Polymer-based nanocapsules for drug delivery. **International Journal of Pharmaceutics,** v. 385, n. 1-2, p. 113-142, Jan 29 2010. ISSN 0378-5173. Disponível em: < <Go to ISI>://WOS:000274234100017 >.

[11] _____. Influence of process and formulation parameters on the formation of submicron particles by solvent displacement and emulsification-diffusion methods Critical comparison. **Advances in Colloid and Interface Science,** v. 163, n. 2, p. 90-

122, Apr 14 2011. ISSN 0001-8686. Disponível em: < <Go to ISI>://WOS:000290704600002 >.

12 QUINTANAR-GUERRERO, D. et al. Preparation and characterization of nanocapsules from preformed polymers by a new process based on emulsification-diffusion technique. **Pharmaceutical Research,** v. 15, n. 7, p. 1056-1062, Jul 1998. ISSN 0724-8741. Disponível em: < <Go to ISI>://WOS:000074897300017 >.

13 GARTI, N. Double emulsions - Scope, limitations and new achievements. **Colloids and Surfaces a-Physicochemical and Engineering Aspects,** v. 123, p. 233-246, May 15 1997. ISSN 0927-7757. Disponível em: < <Go to ISI>://WOS:A1997XG19000022 >.

14 LERTSUTTHIWONG, P. et al. Preparation of alginate nanocapsules containing turmeric oil. **Carbohydrate Polymers,** v. 74, n. 2, p. 209-214, Oct 16 2008. ISSN 0144-8617. Disponível em: < <Go to ISI>://WOS:000258586700007 >.

15 KRAUSE, H. J.; ROHDEWALD, P. Preparation of gelatin nanocapsules and their pharmaceutical characterization. **Pharmaceutical research,** v. 2, n. 5, p. 239-43, 1985-Sep 1985. ISSN 0724-8741. Disponível em: < <Go to ISI>://MEDLINE:24272844 >.

16 LUTTER, S. et al. Formation of gold nanoparticles in triblock terpolymer-modified inverse microemulsions. **Colloids and Surfaces a-Physicochemical and Engineering Aspects,** v. 329, n. 3, p. 169-176, Nov 5 2008. ISSN 0927-7757. Disponível em: < <Go to ISI>://WOS:000260703400008 >.

[17] ISHII, F.; TAKAMURA, A.; ISHIGAMI, Y. PROCEDURE FOR PREPARATION OF LIPID VESICLES (LIPOSOMES) USING THE COACERVATION (PHASE-SEPARATION) TECHNIQUE. **Langmuir,** v. 11, n. 2, p. 483-486, Feb 1995. ISSN 0743-7463. Disponível em: < <Go to ISI>://WOS:A1995QH98400020 >.

[18] CALVO, P.; VILAJATO, J. L.; ALONSO, M. J. Evaluation of cationic polymer-coated nanocapsules as ocular drug carriers. **International Journal of Pharmaceutics,** v. 153, n. 1, p. 41-50, Jul 16 1997. ISSN 0378-5173. Disponível em: < <Go to ISI>://WOS:A1997XL40100004 >.

[19] SUKHORUKOV, G. B. et al. Layer-by-layer self assembly of polyelectrolytes on colloidal particles. **Colloids and Surfaces a-Physicochemical and Engineering Aspects,** v. 137, n. 1-3, p. 253-266, Jun 15 1998. ISSN 0927-7757. Disponível em: < <Go to ISI>://WOS:000074263400025 >.

[20] VANDEWITTE, P. et al. Phase separation processes in polymer solutions in relation to membrane formation. **Journal of Membrane Science,** v. 117, n. 1-2, p. 1-31, Aug 21 1996. ISSN 0376-7388. Disponível em: < <Go to ISI>://WOS:A1996UZ77500001 >.

[21] BINDER, K. et al. Confinement effects on phase behavior of soft matter systems. **Soft Matter,** v. 4, n. 8, p. 1555-1568, 2008 2008. ISSN 1744-683X. Disponível em: < <Go to ISI>://WOS:000260376800001 >.

[22] TANAKA, T.; LLOYD, D. R. Formation of poly(L-lactic acid) microfiltration membranes via thermally induced phase separation. **Journal of Membrane Science,** v. 238, n. 1-2, p.

65-73, Jul 15 2004. ISSN 0376-7388. Disponível em: < <Go to ISI>://WOS:000222290900007 >.

[23] CHEN, J.-S.; TU, S.-L.; TSAY, R.-Y. A morphological study of porous polylactide scaffolds prepared by thermally induced phase separation. **Journal of the Taiwan Institute of Chemical Engineers,** v. 41, n. 2, p. 229-238, Mar 2010. ISSN 1876-1070. Disponível em: < <Go to ISI>://WOS:000276005400016 >.

[24] GARLOTTA, D. A literature review of poly(lactic acid). **Journal of Polymers and the Environment,** v. 9, n. 2, p. 63-84, Apr 2001. ISSN 1566-2543. Disponível em: < <Go to ISI>://WOS:000177985700003 >.

# CHAPTER II: NANOCAPSULES PRODUCTION BY THERMALLY INDUCED PHASE SEPRATION IN A NANOCONFINEMENT

## INTRODUCTION

Nanostructures were obtained through a novel approach based on Thermally Induced Phase Separation (TIPS) in nanoconfinement, that allows to obtain semicrystalline nanocapsules (down to 50 nm).Indeed, PLA is a slow-crystallizing material, and it is a hard challenge to succeed in inducing its crystallization in a TIPS process through the control of the main operating parameters. However, it is even more difficult to induce a nanoconfinement to produce semicrystalline PLLA nanocapsules by TIPS. Indeed, the prerequisites for a successful traditional TIPS process are (a) the complete miscibility between the liquid solvent and the antisolvent and (b) the insolubility of the solute in the antisolvent. So, in the approach that we are proposing, the idea was to follow the thermodynamic equilibrium of a standard ternary system with the peculiarity to induce the quenching phenomenon not in a macroscopic environment but in a single emulsion droplet, that we have called flexible nanoconfinement. For this purpose, we developed a new manufacturing process that takes advantages on the use of the innovative technology of High Pressure Homogenizer to produce very fine and more stable emulsions. Furthermore, this new process allows

producing stable, nanosized, biopolymer nanocapsules working in a continuous mode, with high throughput and in a cost effective way.

## MATERIALS

**Poly,L-lactic acid** (PLLA, Product name "Resomer$^{TM}$L 209 S", with $M_w$ = 12.5 KDa), was purchased by Evonik Industries.

**Diethylene dioxide** (1,4 – dioxane, anhydrous, purity 99.8%; density 1,034 g/ml at 25°C (lit.); molecular formula $C_4H_8O_2$; $M_w = 88{,}11\ g\ mol^{-1}$), **Polyvinyl alcohol** (PVA, linear formula [-$CH_2CHOH$-]$_n$, $M_w = 13000 - 23000\ g\ mol^{-1}$), **Pluronic F127** (PF127, powder, non-ionic, cmc: 950-1000 ppm ), **Rhodamine B** (molecular formula $C_{28}H_{31}ClN_2O_3$; $M_w = 479.01\ g\ mol^{-1}$, powder, purity≥95% (HPLC)), **Gadolinium (III) Chloride** (anhydrous, powder, 99.99% trace metals basis), **Threalose dehydrate** (molecular formula $C_{12}H_{22}O_{11} \cdot 2H_2O$; $M_w = 378.33\ g\ mol^{-1}$) were purchased by Sigma-Aldrich. **Chromeo 488 Carboxylic Acid** (molecular formula $C_{30}H_{31}NO_7$; $M_w = 517.58\ g\ mol^{-1}$**,** reagent color: yellow-orange) was purchased by Active Motif.

The water, used as antisolvent for the polymer, was purified by distillation, deionization, and reserve osmosis (Milli–Q PLUS water purification system).

### Poly - Lactic Acid (PLA)

Poly(lactic acid) (PLA) belongs to the family of aliphatic polyesters[1; 2; 3]. It can be produced by condensation polymerization directly from its basic building block lactic acid. The chiral nature of lactic acid results in

distinct forms of polylactide, namely, poly(L-lactide) (PLLA), poly(D-lactide) (PDLA), and poly(DL-lactide) (PDLLA), which are synthesized from the L-, D-, and DL-lactic acid monomers, respectively. The polymerization of racemic (D,L)-lactide however, results in the formation of amorphous polymers. Commercial PLA is usually prepared from L-lactide (LLA), because the resulting poly(L-lactic acid) (PLLA) is semicrystalline (~ 37% crystallinity) with a relatively high melting (175°C) and glass transition temperature (Tg = 60-65°C). The monomer LLA can be prepared with relatively high enantiopurity from corn starch fermentation. PLLA is a versatile, degradable polymer having excellent mechanical properties, good biocompatibility, and low toxicity, and is FDA approved. It has been used in a variety of applications in the pharmaceutical and biomedical fields, as well as used as a degradable plastic for disposable consumer products.

Processing, crystallization, and degradation behavior of PLA all depend on the structure and composition of the polymer chains, in particular on the ratio of the L- to the D-isomer of lactic acid[4]. PLLA is degraded by simple hydrolysis of the ester bond and does not require the presence of enzymes to catalyze this hydrolysis.

## METHODS

### PROTOCOL FOR PLLA NANOCAPSULES PRODUCTION

Semicrystalline PLLA nanocapsules were produced in a cost effective and large quantity through an innovative Thermally Induced Phase

Separation (TIPS) approach starting by a preformed emulsion. Process has been performed in a continuous mode for preparing stable, dispensable, nanosized, biopolymer nanocapsules. A ternary solution of PLLA/water/Dioxane at a selected temperature ranging from 30 to 70°C was prepared. The components are added in an Erlenmeyer bulb, immersed in a silicone oil bath on a stirring hot plate, with a thermocouple used to control the oil bath temperature, set at 116°C, in order to allow the polymer to dissolve in the dioxane/water mixture. The system is maintained at this temperature for at least 3 hours (depending on the polymer concentration) in continuous stirring (300 – 350 rpm), to facilitate the dissolution of the solid polymer pellets in solution and to keep the system homogeneity. The temperature of 116°C is higher than both the boiling points of dioxane (101°C) and water (100°C), so, during the dissolution of the polymer, evaporation of the low molecular weight species is expected, with consequent undesired change in system composition. To avoid this drawback, a glass Liebig condenser is installed on the top of the Erlenmeyer bulb containing the solution allowing condensing the vapors generated from heating the system, restoring the desired solution composition. After several hours, when the solution appears transparent, without stopping stirring, the system temperature is finally lowered at the preferred temperature and maintained at this value for at least one hour before starting the experiment, in order to stabilize the homogeneous solution obtained. The preformed solution was added to a continuous phase

containing a selected surfactant at the same temperature, with a surfactant concentration ranging from 0,5 to 3wt%, as required. This pre-emulsion was treated by ultrasonication (Branson Sonifier 450 cell disruptor) for 5 minutes at constant Temperature, controlled by a thermocouple. Then, the pre-emulsion is directly flowed in the High Pressure Homogenizer (Microfluidics M110P) with a Pressure ranging from 1000 to 2000 bar. After recirculating the emulsion for 10 minutes at high shear rate, the cooling steps has been performed. The emulsion was unloaded and kept under stirring at the same temperature, then directly injected in a custom-made hydrodynamic flow focusing system obtained by cold water at 5-6 °C. Inlet and outlet temperature were measured by a thermocouple. The obtained capsules were kept at 7-8 °C for at least 15 minutes up to 30.

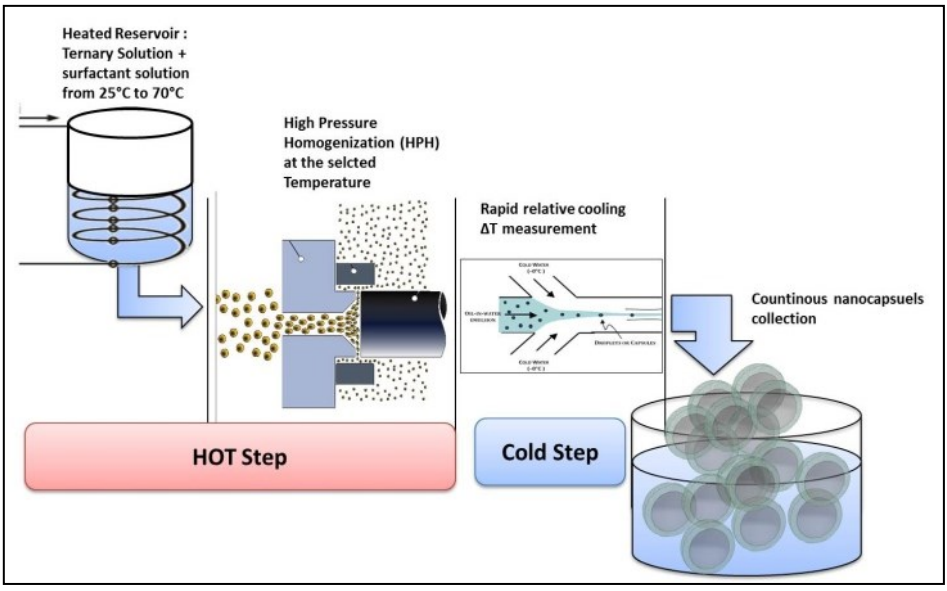


**Figure 1: Schematic representative of the process.**

**METHOD TO AVALUATE THE EFFECT OF COOLING RATE AND CONDITIONS ON THE SYSTEM**

In order to evaluate the influence of quenching step, different kind of cooling methods have been applied on polymer solution, on pre-emulsion processed by ultrasonicator and on emulsion obtained by HPH, and different obtained morphologies have been observed. Protocols performed are listed below.

- **Polymer solution:**
  - **Method I. Cooling at room temperature**

    Starting from the polymer solution at fixed polymer concentration, keeping ratio dioxane/water constantly at 87:13, cooling step has been performed by inducing the decreasing of the temperature leaving it at room temperature. The polymer solution temperature before the cooling step was always kept at 80°C.
  - **Method II. Cooling by water at room temperature**

    Starting from the polymer solution at fixed polymer concentration, keeping ratio dioxane/water constantly at 87:13, cooling step has been performed by inducing the decreasing of the temperature leaving it at room temperature and then injecting it in water at room temperature. The polymer solution temperature before the cooling step was always kept at 80°C.
  - **Method III. Cooling by cold water**

Starting from the polymer solution at fixed polymer concentration, keeping ratio dioxane/water constantly at 87:13, cooling step has been performed by inducing the decreasing of the temperature injecting the solution in cold water. The polymer solution temperature before the cooling step was always kept at 80°C.

- **Method IV. Cooling at room temperature starting from different temperatures**

  Starting from the polymer solution at fixed polymer concentration, keeping ratio dioxane/water constantly at 87:13, cooling step has been performed by inducing the decreasing of the temperature leaving it at room temperature, starting from different temperatures.

- **<u>Pre-emulsion</u>:**
  - **Method I. Cooling by liquid nitrogen bath**

    Starting from the pre-emulsion at fixed polymer concentration, keeping ratio polymer/surfactant constantly at 1:2, cooling step has been performed by inducing the decreasing of the temperature immersing the pre-emulsion in a nitrogen bath. Temperature was monitored at the beginning and at the end. The pre-emulsion temperature before the injection was always kept at 80°C.
  - **Method II. Cooling by by Flow focusing**

Starting from the pre-emulsion at fixed polymer concentration, keeping ratio polymer/surfactant constantly at 1:2, a cooling step has been performed by a custom-made hydrodynamic flow focusing obtained by cold water at ~5°C. Temperature was monitored at the inlet and outlet of the system and the pre-emulsion temperature before the injection was always kept at 80°C.

- **<u>Emulsion</u>:**
  - **Method I. Cooling by Flow focusing**

    Starting from our standard emulsion at fixed polymer concentration, keeping ratio polymer/surfactant constantly at 1:2, a cooling step has been performed on by a custom-made hydrodynamic flow focusing obtained by cold water at ~5°C. Temperature was monitored at the inlet and outlet of the system and the emulsion temperature before the injection was always kept at 80°C.
  - **Method II. Cooling by iced water jacket**

    Starting from our standard emulsion at fixed polymer concentration, keeping ratio polymer/surfactant constantly at 1:2, a cooling step has been performed by letting the emulsion through a silicon coil pipe covered with fine milled ice. Temperature was monitored at the inlet and outlet of the system

and the emulsion temperature before the injection was always kept at 80°C.

- **Method III. Cooling by liquid nitrogen vapors**

  The same procedure as above was performed, with the difference that the silicon coil pipe is invested by liquid nitrogen vapors. Temperature was monitored at the inlet and outlet of the system and the emulsion temperature before the injection was always kept at 80°C.

- **Method IV. Cooling by liquid nitrogen bath**

  Starting from our standard emulsion at different polymer concentration, keeping ratio polymer/surfactant constantly at 1:2, a cooling step has been performed by inducing the decreasing of the Temperature immersing the emulsion in a nitrogen bath. Temperature was monitored at the beginning and the end of the cooling. The emulsion temperature before the injection was always kept at 80°C.

## MORPHOLOGICAL AND STRUCTURAL CHARACTERIZATION

### Nanocapsules characterization

Hydrodynamic diameter, zeta potential, and polydispersity index of the PLLA nanoparticles are measured using a particle sizer (Nano-Zeta-sizer S90, Malvern Instruments, UK).In order to study their morphology, obtained nanocapsule's suspension is often submitted to ultrafiltration under vacuum on a polycarbonate isopore membrane (cut-off 50 nm) to remove the residual water or surfactant. In a different purification step, the suspension isalso centrifuged at 55.000-80.000 rpm for 45 min 4°C by Ultracentrifuge Optima MAX-XP by Beckman Coulter. The morphology of the nanoparticles is observed under a Field Emission - Scanning Electron Microscope (FE-SEM) Ultraplus Zeiss – EHT max 30 KV. To improve conductivity, SEM samples are indifferently coated with a thin layer of metal gold, chrome or platinum-palladium ranging from 3 to 7 nm.

The lyophilization of nanocapsules is performed using a freeze-dryer Christ, 1-4LSC. Briefly, a Freezing step for 3 h at 80°C with a cooling profile of 1°C/min is applied, sublimation at a shelf-temperature of 6° C and pressure of 0,85mbar for at least 24 h and finally, secondary drying at 25 °C and 0,03 mbar for 5-6 h. Trehalose or sucrose ranging from 1-3wt% is added as cryoprotector if necessary. Dried particles are observed by Field Emission-SEM.

The conventional transmission Electron Microscope (TEM) images are obtained at 80 and 200 kV with a FEI Tecnai 200T at a magnification

from 25 000 to 80.000 under low-dose conditions. Nanocapsular structures are also observed by CRYO-TEM under liquid Nitrogen and CRYO- Tomography on the same instrument. Cryo section of the instrument has been purchased by GATAN Inc. For cryo-TEM experiments in the TEM, commercially available lacey carbon membranes on 300-mesh copper grids are used. A sample of the dilute nanocapsule solution is applied to the grid, blotted to a thin film with filter paper, and immediately plunged into liquid propane/ethane (-186 °C) using a vitrifrication system Vitrobot purchased by FEI. A Gatan model 626 cryo-transfer station and cryo-holder are used to transfer the grid containing the vitrified suspension into a TEM Tecnai FEI 200 kV.

**Calorimetric studies**

Thermal properties of PLLA semicrystalline NCs are studied by using differential scanning calorimetry (DSC) (TA Instruments) at a heating rate of 3-5 °C/min under nitrogen atmosphere.

Glass transition temperature ($T_g$) is determined as the point of half $C_p$ (heat capacity) extrapolated while the melting temperature ($T_m$) is determined as the peak temperature. The degree of crystallinity ( Xc ) of the PLLA nanocapsules is calculated as

$$X_c = \frac{\Delta H_m}{\Delta H_m^0}$$

where $\Delta H_m$ is an enthalpy of melting of PLLA and $\Delta H_m^0$ is the enthalpy of melting of 100% crystalline PLLA. The melt enthalpy estimated for an

enantiopure PLA of 100% crystallinity ($\Delta H_m^0$) is 93 J/g; it is the value most often referred to in the literature although higher values (up to 148 J/g) also have been reported.

**X-ray diffraction studies**

X-ray diffraction data have been collected at room temperature from a PLLA nanocapsule's suspension deposited onto Si zero-background substrates as well as from PLLA in powder.

XRD measurements were performed with a D8 Discover-Bruker diffractometer equipped with a Cu source ($\lambda_{K\alpha1}$= 1.54056 Å and $\lambda_{K\alpha2}$= 1.54439Å), a Goebel mirror, an Eurelian cradle goniometer, and a scintillator detector. XRD patterns were collected under ambient atmosphere at a fixed incident angle of 5° while moving the detector over the 10-60° range with a step size of 0.05. In this context we use X-Ray diffraction to identify the crystalline/amorphous nature of PLLA nanocapsules and the extent of crystallinity present in the samples.

The ratio between the integrated intensity under the diffraction peaks (crystalline contribution) and the whole area under the entire XRD pattern (crystalline and amorphous contribution) was evaluated to determine the crystallinity degree. No additional background is present due to the zero contribution of the Si substrate. The results are reported in Figure 2 .

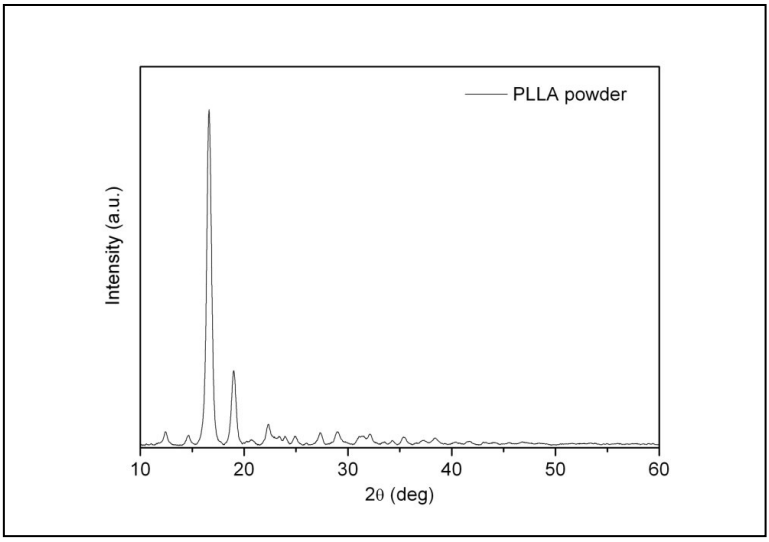


**Figure 2: XRD pattern of PLLA powder.**

## Fourier Transform Infrared Spectroscopy

PLLA nanocapsules suspension is frozen in liquid nitrogen and then freeze dried to obtain a powder for IR measurements. PLLA powder for IR measurements is cast on a germanium window of a Nicolet 6700 FT-IR Spectrometer. All the IR spectra of the specimen were collected at 0.09 cm-1 resolution with 2 min interval.

Several important papers have been published concerning the infrared spectra of PLA, and on structural changes and crystallization of PLLA. In some of these works, characteristic peaks of both amorphous and crystalline phase of PLLA were obtained. In particular, among the crystalline sensitive bands, the 1458 $cm^{-1}$ band has been assigned to the structural order of the $CH_3$ group, while the band at 1109 $cm^{-1}$ relates to the C-O-C trans conformation in the crystalline phase of PLLA. In addition, the band at 1193 $cm^{-1}$ is sensitive not only to the structural

adjustment of C-O-C but also to the structural order of $CH_3$ group in the crystalline phase. Moreover the 1762 $cm^{-1}$ band has been assigned to the ν(C=O) in the crystalline phase and the 1749 $cm^{-1}$ band to the ν(C=O) in the amorphous phase. In literature have been reported also two bands that are related to the crystalline and the amorphous phase of PLA, at 755 $cm^{-1}$ and 869 $cm^{-1}$ respectively[5], and the band at 923 $cm^{-1}$, that was found in all the samples containing α crystals, assigned to the coupling of C-C backbone stretching with the $CH_3$ rocking mode, and the band at 912 $cm^{-1}$, assigned to the $CH_3$ rocking mode for β crystals[6].

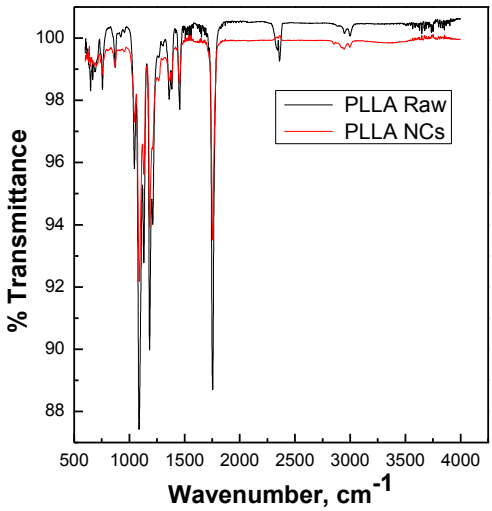


**Figure 3: IR spectrum of PLLA and PLLA NCs, plotted as transmission.**

## Estimation of Drug Content

10 milligrams of drug-loaded nanoparticles of each batch are dispersed in 1 ml of water and 200 microliter of Dichloromethane (DCM). After DCM evaporation, next the resultant solution is centrifuged, the

supernatant liquid is collected, and the absorbance is determined using an ultraviolet (UV) spectrophotometer at 556 nm, with water as a blank. Drug content in the nanoparticles is calculated using the following formula:

**In Vitro Drug Release Studies**

Drug content (%w/w)*(Mass of drug in nanocapsules / Mass of nanoparticles) X 100, :* The dialysis bag diffusion technique was used to study the in vitro drug release of nanoparticles. The prepared nanoparticles were placed in the dialysis bag and immersed into 50 ml of Phosphate buffer pH (7.4). The entire system was kept at 37±0.5°C, with continuous magnetic stirring. The samples were withdrawn from the receptor compartment at predetermined intervals of 30 minutes and replaced by fresh medium. The samples were withdrawn and diluted to 10 ml with Phosphate buffer pH (7.4) and the amount of drug dissolved was analyzed by a UV-Spectrophotometer. All experiments were repeated in triplicate. When metal compounds were encapsulated, loading capability was measured for than measure by Induced Coupled Plasma-Mass (ICP-MS NexIon 300 by Perkin Elmer).

## RESULTS

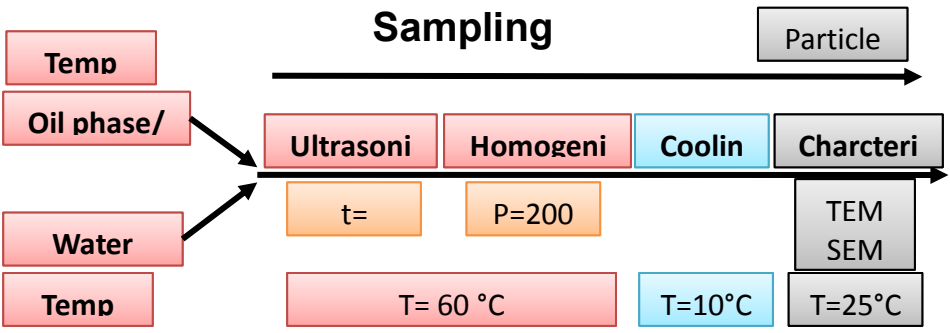


**Figure 4: Flow sheet of the steps performed to produce nanocapsules by TIPS in a nanoconfinement.**

## OPTIMIZATION OF ULTRASONICATION PARAMETERS

As showed in Figure 4, the first step to be performed in our process is the ultrasonication. Optimization of the ultrasonication conditions needed before proceedings with the next steps. Stability, size, surfactant concentration and time of sonication as well as Amplitude have been studied. Table 1 shows all the data related to this optimization.

| Ultrasonicator | Time of Homogenization | Pre-emulsion Temperature | DLS | |
|---|---|---|---|---|
| **Amplitude** | **Time (min)** | **TEMPERATURE (°C)** | **Size (nm)** | **PDI** |
| 20% | 5,10,15* | 30 | 800,7 | 0,910 |
| 40% | 5,10,15* | 40 | 338,7 | 0,798 |
| 60% | 5,10,15* | 65 | 218,4 | 0,77 |

Table1: **Optimization of ultrasonication parameters.** ***Data obtained at 10 and 15 minutes haven't been reported because in all cases a strong solvent evaporation was observed**.

This table reports only some conditions of the pre-emulsion used to obtain the nanocapsules. Several parameters were tested such as Amplitude and Ultrasonication time, in addition surfactant concentration were also studied. However, only in some cases has been possible to reach the desired Temperature and the desired droplet size (nanoconfined domain) and in no case has been possible to obtain the nanocapsules without the High Pressure Homogenization.

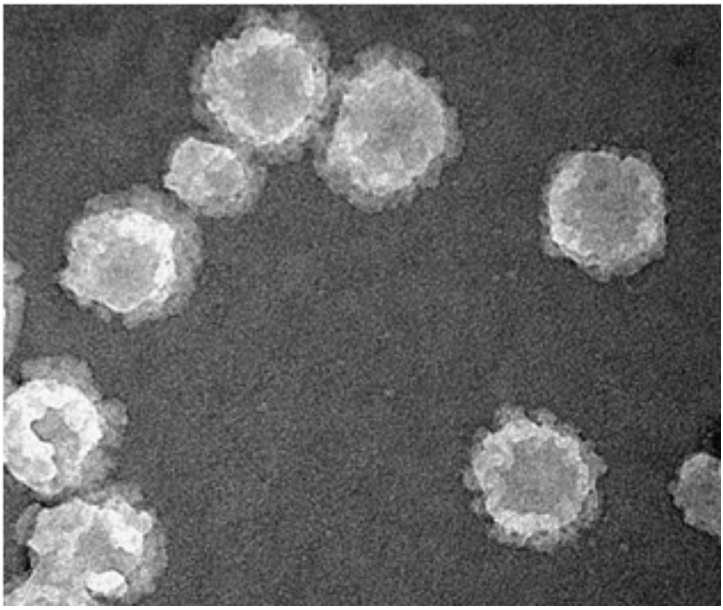

**Figure 5: SEM Image of morphology obtained by TIPS performed only after the ultrasonication without High Pressure Homogenization**

## EFFECT OF HIGH PRESSURE HOMOGENIZATION

Ours experimental results showed that nanocapsular hollow semicrystalline PLLA structures are only obtained when the mean droplet diameter of the primary emulsion is below 500 nm with a polydispersity index measured by DLS of about 0.15. In contrast, when the mean droplet diameter of the primary emulsion is higher than 500 nm, not-hollow nanoparticles are obtained. Thus, a High Pressure Homogenizer (HPH, Microfluidics M110P) has been employed, because it is particularly suitable for the production of the finely dispersed emulsion that we want to realize. To demonstrate that passing from Ultrasonication to High Pressure Homogenizer we attain a finer emulsion we carried out measurements by DLS on nanocapsules

suspension, at a fixed formulation of emulsion (in terms of concentration of polymer, concentration of surfactant and ratio discontinuous phase/continuous phase).The results achieved are shown in the Figure 6a, in which we can observe the reduction of mean droplet size of emulsion. Therefore, we reported also experiments conducted on emulsion optimization, by tuning HPH parameters, like homogenization time (number of passes) and pressure, and emulsion formulation. In particular, in Figure 6b is shown the optimization of homogenization time, from which we can derive that by increasing the number of passes of the whole emulsion volume inside the homogenizer valve, we can obtain a further decreasing of emulsion droplet size, and that the optimal number of passes corresponds to the point at which the plateau is reached.

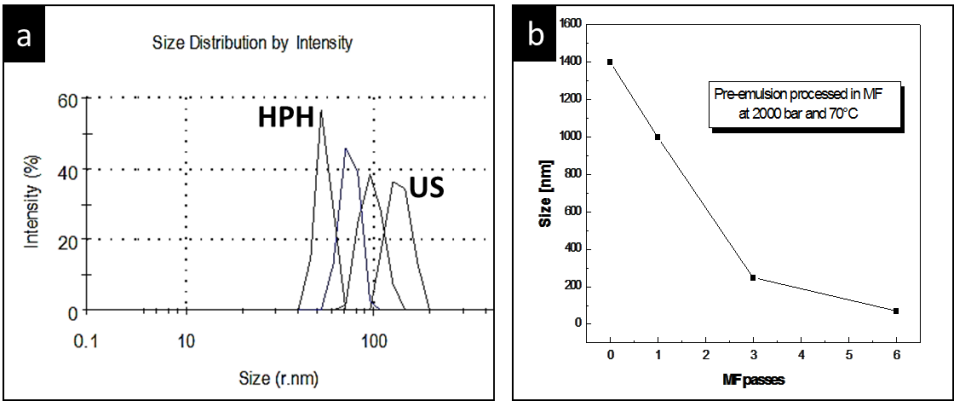


**Figure 6: Size Measurement by DLS of emulsion droplet size, a) size reduction obtained by passing from Ultrasonication to High pressure homogenization; b) size reduction obtained by increasing number of passes in the homogenizer valve.**

Afterwards, we have evaluated the influence of homogenization pressure on emulsion mean droplet diameter. The results are reported

in the following Figure 7, where we can observe that the emulsion droplet size decrease when homogenization pressure increase. This is completely in agreement with theories on Microfluidizer reported in literature, that correlate the emulsion droplet size with the energy required for droplets disruption

$$x = C \cdot E_V^{-b} = C \cdot (P_V \cdot t_{res})^{-b} = C \cdot (\Delta_{p_H})^{-b}$$

that corresponds to the pressure difference operating at the nozzle.

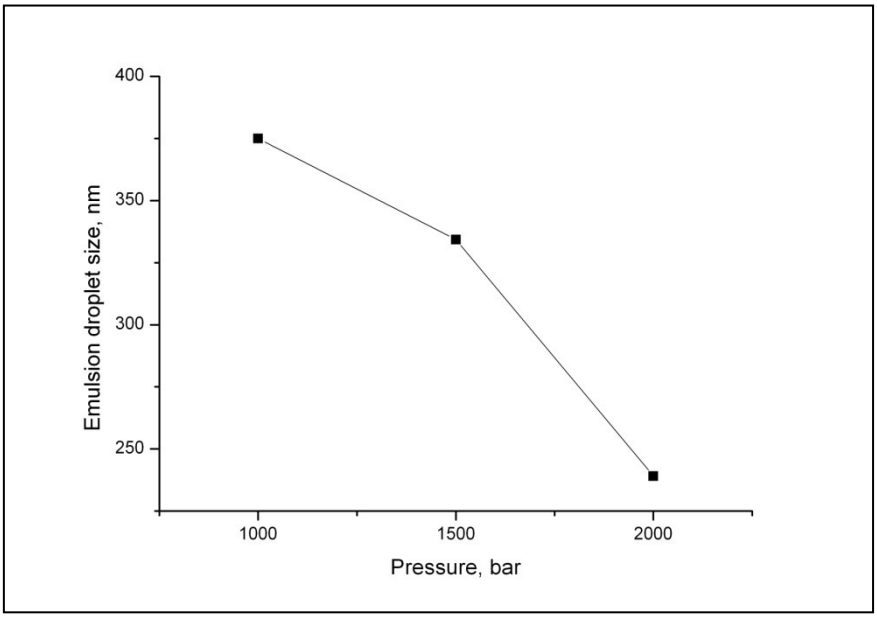


**Figure 7: Size Measurement by DLS of emulsion droplet size as function of homogenization pressure.**

Another important point on which we can play for emulsion optimization is its formulation. Thus, we carried out tests by changing the concentration of surfactant and the type of surfactant in the continuous phase of emulsion. The results obtained are reported in the following Figure 8, where we can observe that emulsion droplet size

decrease when surfactant concentration increase, in agreement with the theory on Microfluidizer reported in literature, that correlate the emulsion droplet size with viscosity of continuous phase

$$x = C \cdot \eta_c^b = C \cdot \eta_c^{-0.02}$$

that increase when surfactant concentration increase.

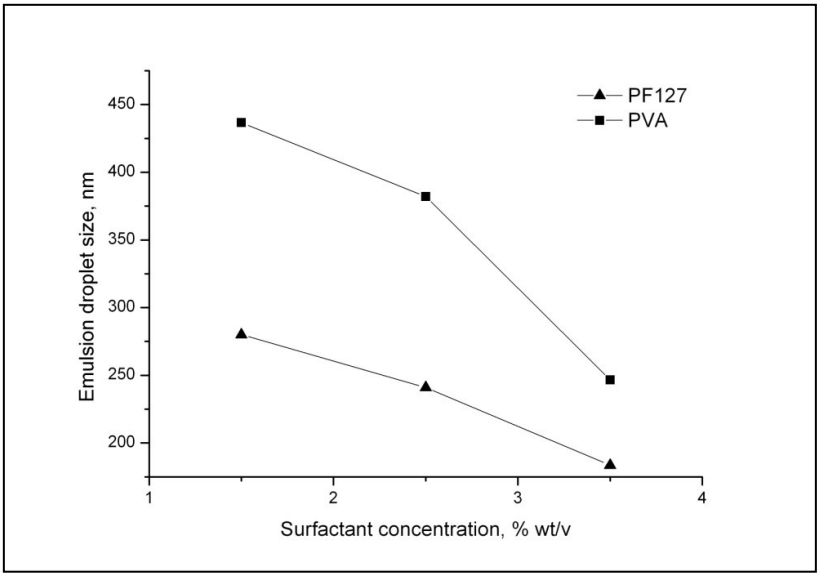


**Figure 8: Size Measurement by DLS of emulsion droplet size as function of surfactant concentration and of kind of surfactant.**

Moreover, we can also observe that better results are obtained with Pluronic F127.

## EFFECT OF COOLING RATE ON THE FINAL MORPHLOGY

In order to evaluate the influence of cooling on the final morphology of our nanocapsules we performed different kind of experiments on polymer solution, pre-emulsion processed by ultrasonicator and

emulsion obtained by HPH, by changing the cooling method and rate. The results obtained for each case are presented below.

**Polymer solution:**

- **Method I. Cooling at room temperature**

The polymer solution at 80°C has been cooled by leaving it at room temperature, in order to simulate a slow cooling rate. The result is showed in the following Figure 9. Because of lack in temperature control the system is subjected to local fluctuation, resulting in the formation of both globular (**a** and **c**) and bicontinuous (**b**) morphologies, as showed in the following SEM images.

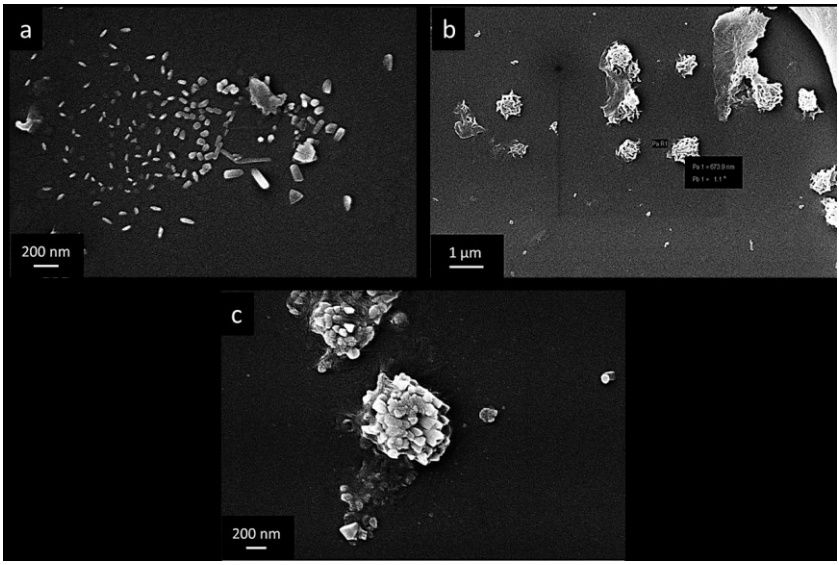


**Figure 9: : Electron Microscope images showing the morphology obtained by cooling polymer solution (with 0.5% of PLLA in Dioxane/ H2O=87/13) at room temperature.Because of lack in temperature control the system is subjected to local fluctuation, resulting in the formation of both globular (a and c) and bicontinuous (b) morphologies.**

- **Method II. Cooling by water at room temperature**

The polymer solution at 80°C has been cooled by leaving it at room temperature and then injecting it in water at room temperature, in order to evaluate not only the effect of a slow cooling rate but also that of extraction of dioxane in water. The result is showed in the following Figure 10. In this case, from SEM images (**a** and **b**) can observe the formation of globular morphologies fused together.

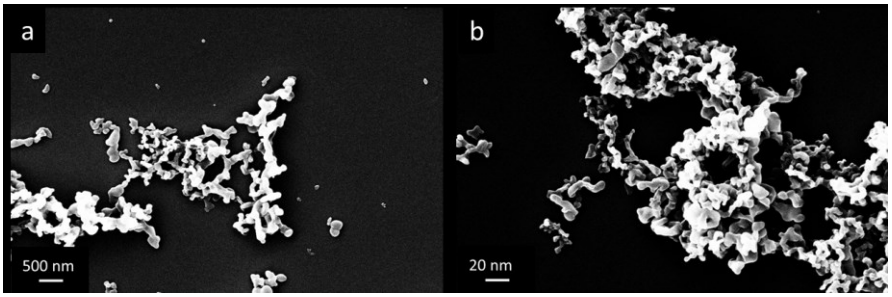


**Figure 10: : Electron Microscope images showing the morphology obtained by cooling polymer solution (with 0.5% of PLLA in Dioxane/ H2O=87/13) at room temperature and injecting it in water at the same temperature. Both images (a and b) show the formation of globular morphologies fused together.**

- **Method III. Cooling by cold water**

The polymer solution at 80°C has been cooled by injecting it in cold water, in order to simulate a fast cooling rate. The result is showed in the following Figure 11. From SEM images (**a** and **b**) we can observe the formation of globular morphologies.

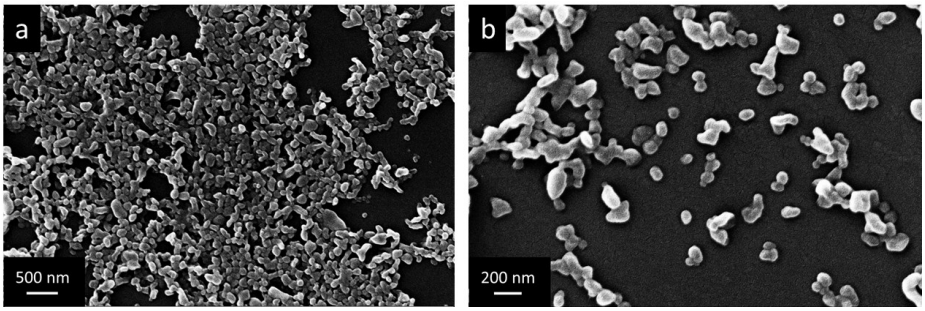


**Figure 11: Electron Microscope images showing the morphology obtained by cooling polymer solution (with 0.5% of PLLA in Dioxane/ H2O=87/13)by injection in cold water. Both images (a and b) show the formation of globular morphologies.**

- **Method IV. Cooling at room temperature starting from different temperatures**

The polymer solution has been cooled starting from different temperatures (80, 35, 30, 25, 15°C) by leaving it at room temperature, in order to evaluate not only the effect of a slow cooling rate but also that of different quench dept. The result is showed in the following Figure 12. In particular, we can observe from SEM images the formation of: an homogeneous polymer layer starting from a polymer solution at 80°C (**a**); connected polymer branches starting from a polymer solution at 35°C (**b**); connected polymer branches and globular morphologies starting from a polymer solution at 30°C(**c**); polymer branches and globular morphologies starting from a polymer solution at 25°C (**d**); globular morphologies starting from a polymer solution at 15°C (**e**).

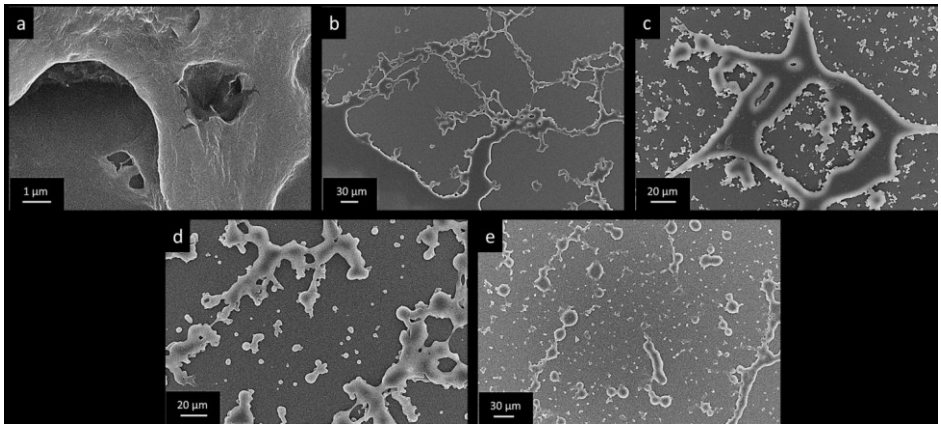


**Figure 12: Electron Microscope images showing the morphology obtained by cooling polymer solution (with 0.5%of PLLA in Dioxane/ H2O=87/13) at room temperature, starting from different initial temperatures. We observe: at 80°C (a) an homogeneous polymer layer; at 35°c (b) connected polymer branches; at 30°C (c) connected polymer branches and globular morphologies; (d) at 25°C polymer branches and globular morphologies; (e) at 15°C globular morphologies.**

## Pre-emulsion:

- **Method I. Cooling by liquid nitrogen bath**

The pre-emulsion at 80°C, obtained by Ultrasonication, has been cooled by immersing it in a nitrogen bath, in order to evaluate the effect of fast cooling rate. The result is showed in the following Figure 13. From SEM images we can observe the formation of slices of polymer (**a**) and (**b**) globular morphologies.

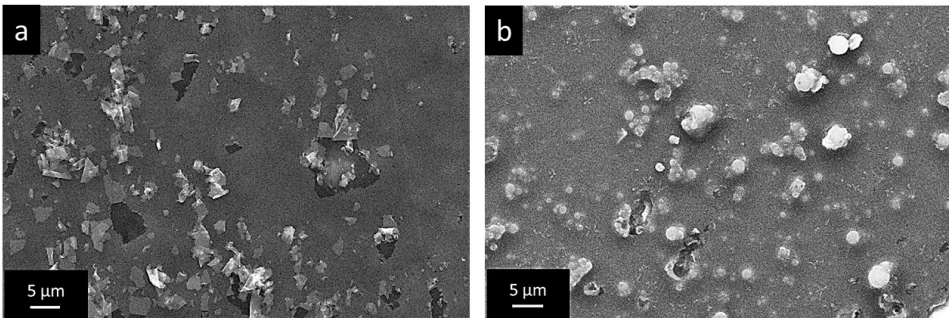


**Figure 13: Electron Microscope images showing the morphology obtained by cooling pre-emulsion (with Polymeric solution: 1% of PLLA in Dioxane/ H2O=87/13; Continuous phase: 3.5% of PF127 in H2O) in a liquid nitrogen bath. We observe the presence of slices of polymer (a) and (b) globular morphologies.**

- **Method II. Cooling by Flow focusing**

The pre-emulsion at 80°C, obtained by Ultrasonication, has been cooled by a custom-made hydrodynamic flow focusing obtained by cold water at ~5°C, in order to evaluate the effect of a cooling rate slower than the previous method, but still fast, and to obtain a more controlled cooling. The result is showed in the following Figure 14. From SEM images (**a** and **b**) we can observe the formation of well-defined micro and nanoparticles.

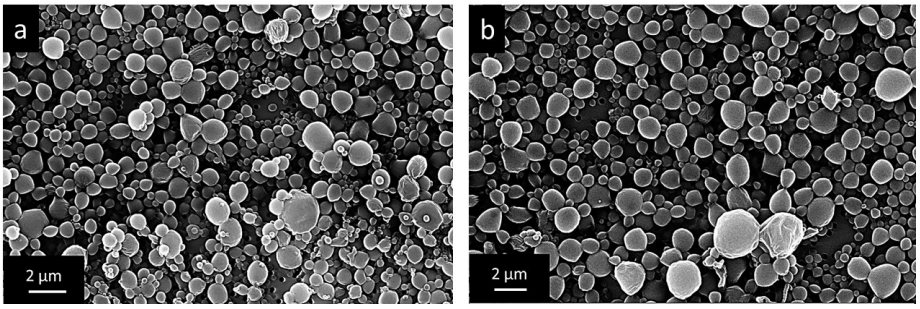


**Figure 14: morphology obtained by cooling pre-emulsion (with Polymeric solution: 1% of PLLA in Dioxane/ H2O=87/13; Continuous phase: 3.5% of PF127 in H2O) in a liquid nitrogen bath. In both images (a and b) we observe well defined micro and nanoparticles.**

**Emulsion:**

- **Method I. Cooling by iced water jacket**

The emulsion at 80°C, obtained by High Pressure Homogenization, has been cooled by letting it through a silicon coil pipe covered with fine milled ice, in order to evaluate the effect of a medium fast cooling rate. The result is showed in the following Figure 15. From SEM images (**a** and **b**) we can observe the formation of well-defined micro and nanoparticles.

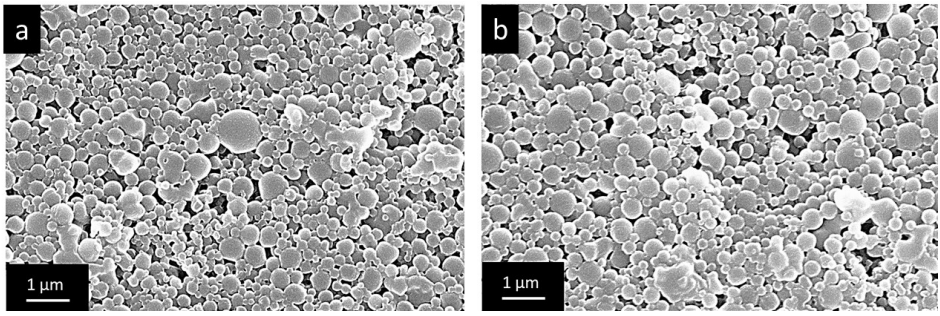


**Figure 15: Electron Microscope images showing the morphology obtained by cooling the emulsion (with Polymeric solution: 0.5% of PLLA in Dioxane/ H2O=87/13; Continuous phase: 1% of PVA in H2O), processed in HPH, letting through a silicon pipe coil covered with fine milled ice. In both images (a and b) we observe well defined micro and nanoparticles.**

- **Method II. Cooling by liquid nitrogen vapors**

The same procedure as above was performed, with the difference that the silicon coil pipe is invested by liquid nitrogen vapors, in order to evaluate the effect of a medium fast cooling rate. The result is showed

in the following Figure 16.From SEM images (**a** and **b**) we can observe the formation of well-defined micro and nanoparticles.

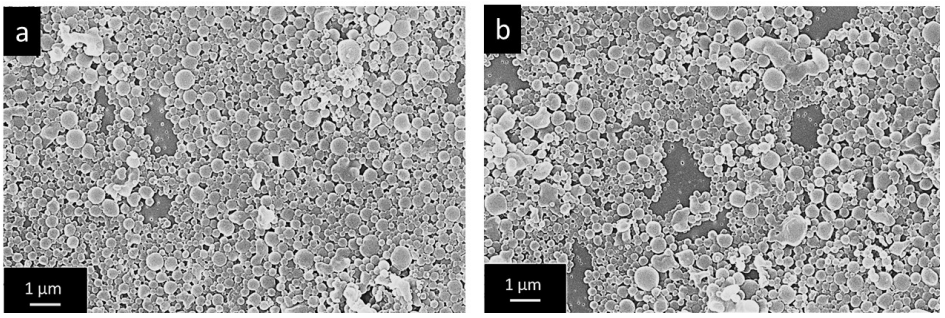


**Figure 16: Electron Microscope images showing the morphology obtained letting the emulsion (with Polymeric solution: 0.5% of PLLA in Dioxane/ H2O=87/13; Continuous phase: 1% of PVA in H2O), processed in HPH, in a silicon pipe coil cooled by liquid nitrogen fumes. In both images (a and b) we observe well defined micro and nanoparticles.**

- **Method III. Cooling by liquid nitrogen bath**

The emulsion at 80°C, obtained by High Pressure Homogenization, has been cooled by immersing it in a nitrogen bath, in order to evaluate the effect of a fast cooling rate. The result is showed in the following Figure 17. From SEM images (**a** and **b**) we can observe the formation of well-defined micro and nanoparticles.

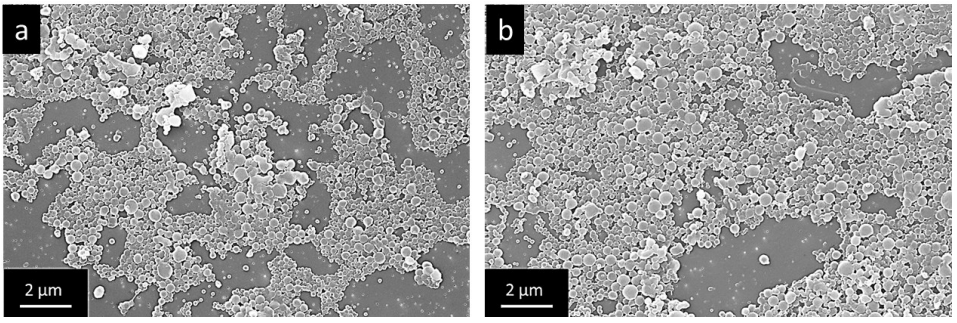


**Figure 17: Electron Microscope images showing the morphology obtained by immerging the emulsion (with Polymeric solution: 0.5% of PLLA in Dioxane/ H2O=87/13; Continuous phase:**

**1% of PVA in H2O), processed by HPH, in a liquid nitrogen bath. In both images (a and b) we observe well defined micro and nanoparticles.**

- **Method IV. Cooling by Flow focusing**

The emulsion at 80°C, obtained by High Pressure Homogenization, has been cooled by a custom-made hydrodynamic flow focusing obtained by cold water at ~5°C, in order evaluate the effect of a medium fast cooling rate and to obtain a more controlled cooling. The result is showed in the following Figure 18. SEM images (**a** and **b**) we can observe the formation of well-defined nanoparticles.

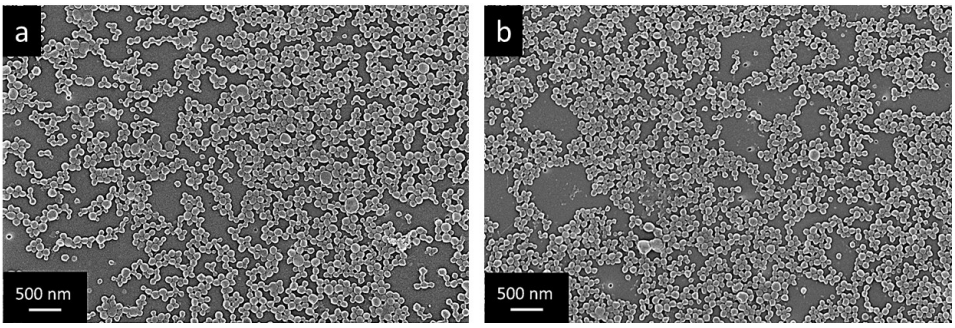


**Figure 18: Electron Microscope images showing the morphology obtained by cooling the emulsion (with Polymeric solution: 0.5% of PLLA in Dioxane/ H2O=87/13; Continuous phase: 1% of PVA in H2O), processed by HPH, by flow focusing. In both images (a and b) we observe well defined nanoparticles.**

## PURIFICATION AND RECOVERY

### ULTRAFILTRATION

Vacuum filtration was used to collect nanocapsules for a better characterization by SEM. Indeed, SEM characterization could be done on a droplet of nanocapsules suspension, left to dry on a glass. In this way, however, we would get an unclear image because of the impurities

present in the system. Vacuum filtration allows to come away impurities, leaving almost cleaned nanocapsules on the surface of the membrane, as can be seen in the following Figure 19.

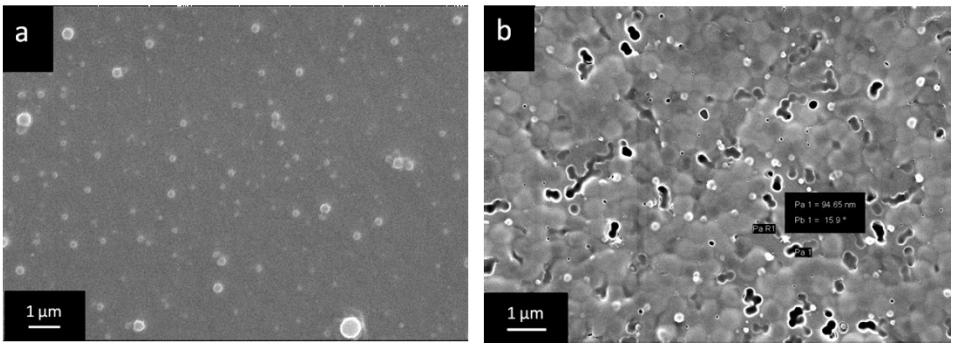


**Figure 19: Collection of nanocapsules by Ultrafiltration: a, SEM image of dried nanocapsules on a glass; b, SEM image of nanocapsules collected by Ultrafiltration on a membrane.**

## MEMBRANE DYALISIS METHOD

In this work, this technique has been employed to remove the excess of dye used in loading tests and to purify nanocapsule suspension from surfactant present in the formulation for the production. In the first case, to assess cleaning of the suspension, we carried out spectrofluorimetric tests. Indeed, in the second case, to prove the purification, we made IR measurements, on the suspension before and after the dialysis, as reported in the following images.

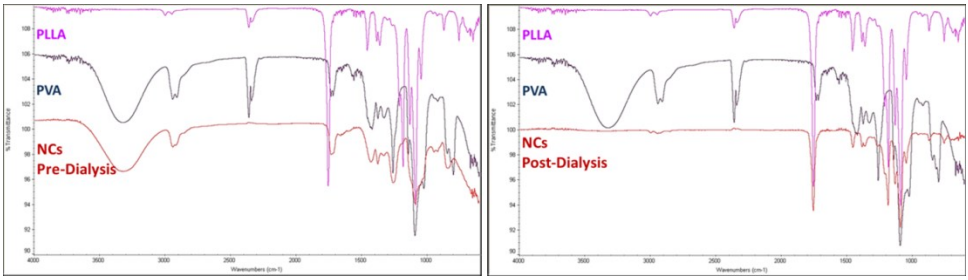


**Figure20: Purification of nanocapsules by Membrane Dialysis method: a, IR measurement on dried nanocapsules before dialysis; b, IR measurement on dried nanocapsules after dalysis.**

As we can see from Figure 20, before dialysis the IR spectrum of surfactant completely cover that one of PLLA nanocapsules, whereas the latter results more evident after the purification.

## ULTRACENTRIFUGE

Ultracentrifuge has been employed, at first, to collect produced nanocapsules from our suspension. As can be seen in the following image (Figure 21), the protocol developed for this purpose was found to be effective, as nanocapsules are present for almost the totality in the pellet.

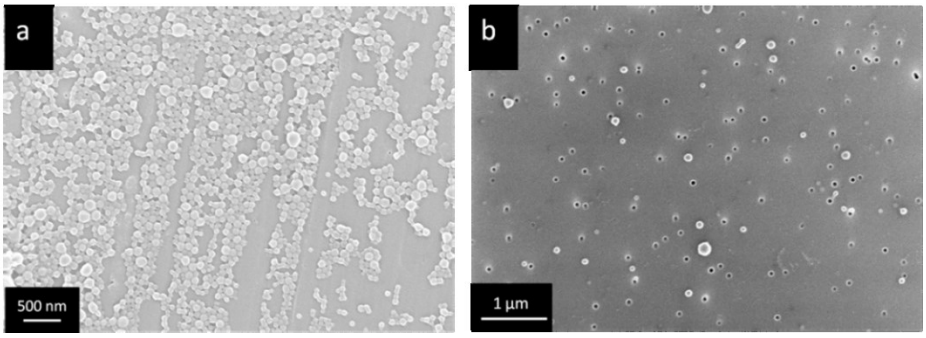


**Figure 21: Collection of nanocapsules by Ultracentrifuge: a, SEM image of nanocapsules collected in the pellet by Ultracentrifuge; b SEM image of nanocapsules collected in the supernatant by Ultracentrifuge.**

Moreover, this technique has also allowed us to purify nanocapsules from surfactant present in the formulation for the production. To prove this, we carried out IR measurements on supernatant and on pellet obtained after the Ultracentrifuge, which shows also this result, as reported in Figure 22.

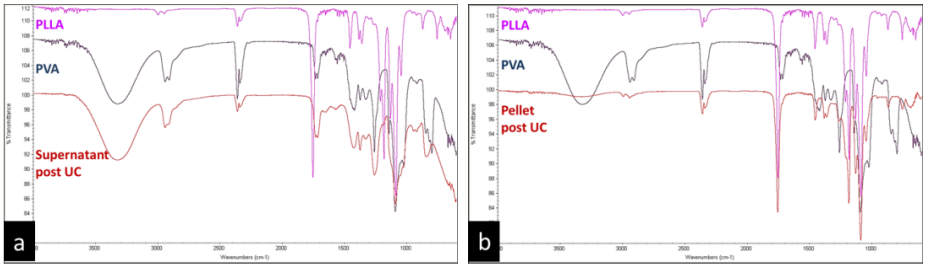


**Figure 22: Purification of nanocapsules by Ultracentrifuge: a, IR measurement of nanocapsules collected in the pellet by Ultracentrifuge; b IR measurement of nanocapsules collected in the supernatant by Ultracentrifuge.**

**FREEZE DRYING**

Freeze-drying has been used to completely remove water from the frozen nanocapsules suspension by sublimation and desorption under vacuum. Generally, protectants are added to the formulation to protect the nanoparticles from freezing and desiccation stresses. In particular, for our nanocapsules trehalose as cryo-protectant was used, with a ratio 1:1, because in literature has been reported to be a preferable cryo-protectant for biomolecules. It has many advantages in comparison with the other sugars as: less hygroscopicity, an absence of internal hydrogen bounds which allows more flexible formation of hydrogen bonds with nanoparticles during freeze-drying, very low chemical reactivity and

finally, higher glass transition temperature. The results are noticeable, as reported in the following Figure 23 which show clearly that without the cryo-protectant nanocapsules tend to merge with each other, while using trehalose they retain their structure downstream the process.

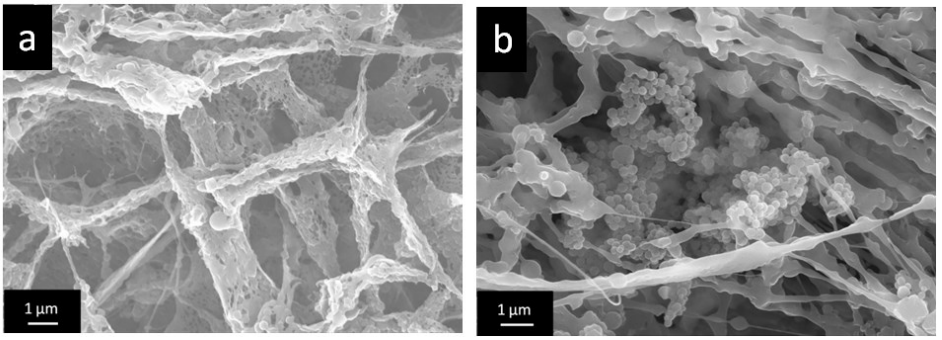


**Figure 23: Freeze Drying of nanocapsules: a, SEM image of freeze-dried nanocapsules without cryo-protectant ; b SEM image of freeze-dried nanocapsules with Trehalose.**

## MORPHOLOGICAL CHARACTERIZATION OF NANOCAPSULES

The production of semicrystalline PLLA nanocapsules was attained modifying a standard TIPS process, in order to control the extent of PLLA crystallization. In particular, the production process consists in the preparation through High pressure homogenization of a primary emulsion, where the disperse phase is a ternary system polymer/solvent/antisolvent, whereas the continuous phase is made by an aqueous solution containing a high concentration of surfactant. PLLA phase separation is induced by cooling the emulsion by cold water at 5°C, which cause the rapid decrease of the emulsion temperature from 5 to 9°C on dependence of the cooling flow rate. In Figure 24a, Scanning Electron Microscope (SEM) images of the produced nanoparticles obtained at 2000 bar and PLLA concentration of 0.1 wt/v% with a mean

particle diameter of 70 nm are shown whereas the data of their mean particle size are reported in Figure 24b as a function of the main operating conditions (pressure, polymer concentration, temperature and homogenization time).

In particular, polymer concentration, as so pressure and homogenization time, significantly influence the droplet size distribution of the primary emulsion and therefore the formation of hollow capsules (Figure 24c) as well as the regulation of their size and shell thickness. More specifically, experimental results clearly showed that by reducing the polymer concentration from 1.5 to 0.1 %wt/v a decreasing in nanocapsules mean diameter and standard deviation is obtained.

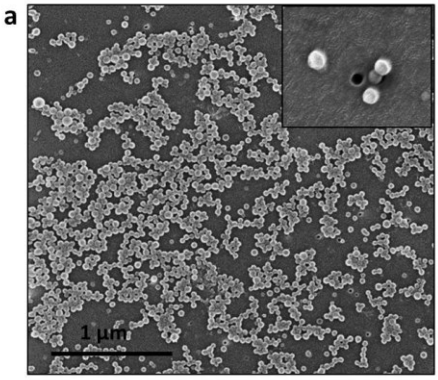


b

| Pressure, bar | C, %wt/V | Mean Diameter, nm | SD (±) | PDI |
|---|---|---|---|---|
| 2000 | 0,1 | 50 | 2,375 | 0,095 |
| 2000 | 0,5 | 70 | 3,85 | 0,11 |
| 2000 | 1 | 110 | 6,6 | 0,12 |
| 2000 | 1,5 | 250 | 16,25 | 0,13 |
| 1500 | 0,1 | 55 | 2,6125 | 0,095 |
| 1500 | 0,5 | 82 | 4,92 | 0,12 |
| 1500 | 1 | 180 | 16,2 | 0,18 |
| 1500 | 1,5 | 227 | 34,05 | 0,3 |
| 1000 | 0,1 | 70 | 8,75 | 0,25 |
| 1000 | 0,5 | 115 | 15,525 | 0,27 |
| 1000 | 1 | 247 | 39,52 | 0,32 |
| 1000 | 1,5 | 320 | 51,2 | 0,32 |

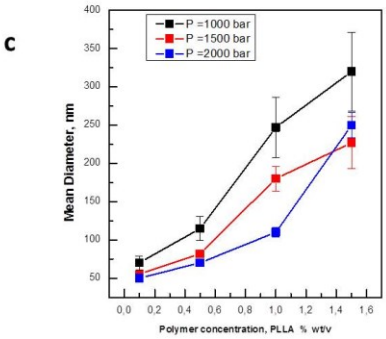


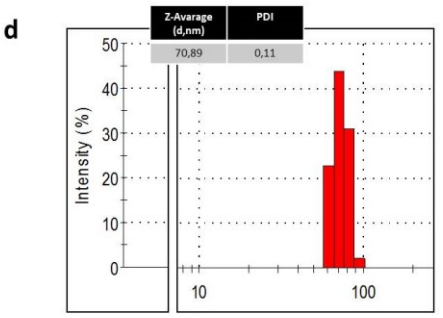


**Figure 24: Size and Shape of PLLA Semicrystalline Nanocapsules by SEM and DLS results. a, Scanning Electron Microscope images showing the morphology of Nanocapsules obtained by TIPS (PLLA NCs Mean Diameter: 70 nm); b, Table reporting details about the conducted experimental campaign and the related mean diameter. Last columns within the table show Standard Deviation (SD) and Polydispersity Index (PDI) as obtained by Dynamic Light Scattering results. All the experiments have been performed at same conditions of Temperature and cooling rate; c, the effect of polymer concentration on the mean diameter is plotted on the graph; d, Detail of a Particle Size Distribution obtained for experiments conducted at 2000 bar and PLLA concentration of 0,5% wt/v.**

The hollow structure of the produced nanocapsules is evident from Transmission Electron Microscopy (TEM) images, shown in Figure 25. In particular, Figure 25a shows the nanocaspules formation for a low PLLA concentration (1%wt/v). Figures 25b instead shows that an increase in PLLA concentration (1.5%wt/v) causes an increase in capsule size. Figure 25c shows an enlargement of the semi-crystalline nanocapsule,

highlighting the organization between crystalline phase and amorphous phase.

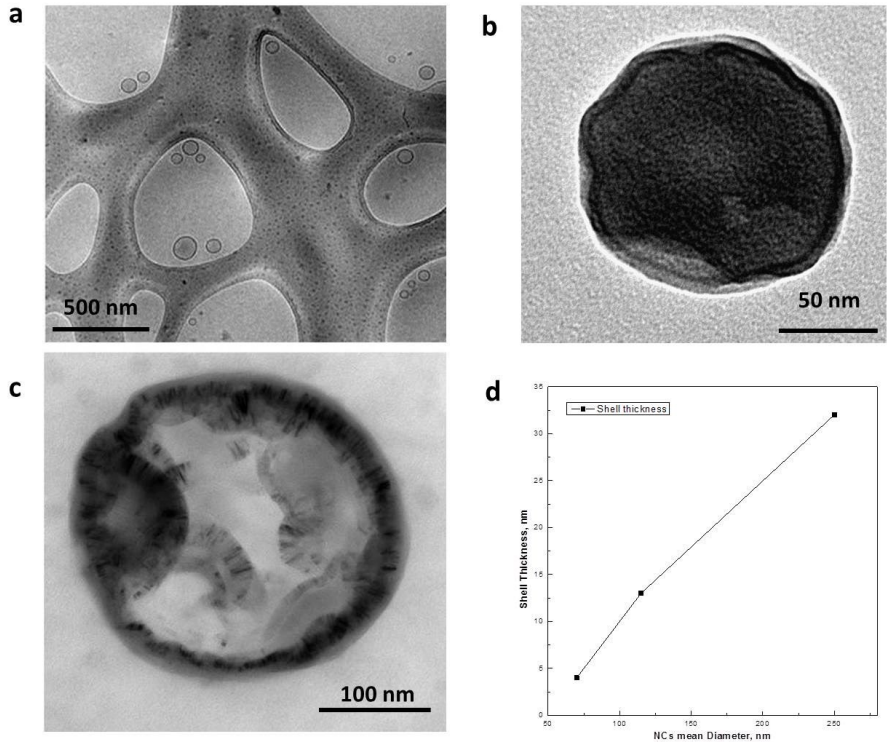


**Figure 25: Analysis of shell thickness by TEM results. a-c, Cryo –TEM and TEM nanocapsules obtained by Thermally Induced Phase Separation in a nanoconfinement by changing the polymer concentration from 0,5 to 1,5wt%, respectively; d, Graph showing the reduction of shell thickness as a function of the NCs mean diameter**

Figure 25d reports the dependence of shell thickness, evaluated from TEM images, on the mean particle size of the hollow capsules, the latter derived from DLS measurements. As it is possible to observe, the reduction in polymer concentration in the disperse phase of the primary emulsion causes a decrease of size as well as of shell thickness of the produced nanocapsules. Reported results are obtained at constant

pressure and homogenization time. Related to their mean diameter, the produced semi-crystalline PLLA nanocapsules (NCs) exhibited a shell thickness of maximum 32 nm. The release mechanism is also modified by this interesting morphology.

Shell thickness of nanocapsules should dictate the mechanical strength and the permeability of the shell even if these peculiar characteristic required further investigations. However, even if the observed shell thickness of the produced NCs is relatively low, they, because of their semi-crystalline nature, should exhibit a compact structure with a low permeability value not reported until now in capsules with thinner shell[7; 8; 9].

## CRYSTALLINITY BEHAVIOR OF THE PRODUCED NANOCAPSULES

Among commercial biopolymers, poly-L-lactic acid (PLLA) exhibits adequate characteristics in terms of crystal polymorphism due to a chiral center in its molecular structure. Despite extensive studies, its crystallization behavior, crystal structure, and melting behavior are still not completely understood. For all these reasons, PLLA crystallization from a solution in a nanoconfined environment, compared to that in a macroscopic one, offers the potential to control the crystallization degree and to reduce time of crystal formation process, thus extending its range of applications, especially in biomedical and pharmaceutical devices by designing new polymer architectures and expanding their industrial utilizations.

To date, three crystalline forms (α, *β*, and *γ*) have been reported for PLLA upon changing the preparation conditions[6; 10; 11; 12]. Crystallization from the melt or from solution leads to α crystal form, which is the most common polymorph. In α form, two antiparallel chains with a left-handed $10^3$ helical conformation are packed into an orthorhombic unit cell with dimensions of *a*=10.7 Å, *b*=6.45 Å, and *c*=27.8 Å (along fiber axis). The *β* form is obtained by hot drawing the melt-spun or solution-spun PLLA fibers under high drawing conditions and high drawing temperatures and it is considered to have a frustrated structure, containing three $3_1$ helix chains in a trigonal unit cell with *a*=*b*=10.52 Å and *c*=8.8 Å. This frustrated structure appears to be formed to accommodate the random orientation of neighboring chains associated with the rapid crystallization during stretching. As for the transition between α- and *β*-crystalline phases, it was found that α-to-*β* crystalline phase transition in PLLA proceeded more rapidly with an increase in the draw ratio, draw temperature or extrusion pressure. The α-structure with a $T_m$ of 185°C is more stable than the *β*-structure with a $T_m$ of 175°C[1]. A new crystal modification, *γ* form, has been recently observed via epitaxial crystallization on hexamethylbenzene (HMB) substrate. Two antiparallel helices were packed in an orthorhombic unit cell of parameters a=0.995 nm, b=0.625 nm, and c=0.880 nm. HMB appeared to be a versatile substrate, but the detailed mechanism of formation and thermal properties of the *γ* -form crystals are yet to be determined[13].

Crystallinity changes of semi-crystalline PLLA depend not only on the preparation conditions, but also on the cooling rate, as generally observed by DSC analysis. Typically in TIPS processes, as well as in injection molding, the crystalline phase of PLLA is only obtained at low cooling rate[14]. In contrast, at high cooling rate, amorphous products are formed[15]. Instead, in the approach that we have developed, a semicrystalline morphology is obtained at very high cooling rates, in excess of 40°C/min, proving that a different phenomenon is interfering with the thermodynamic involved in the nanocapsules formation.

The DSC curves obtained for the produced nanocapsules are showed in Figure 26a, whereas the thermal results are listed in Figure 26b. The average glass transition temperature ($T_g$) of PLLA NCs ranged from about 50°C to 55°C and different $T_m$ peaks are showed by changing experimental parameters. More specifically, Figure 26a shows the melting behavior of untreated raw PLLA in comparison with the PLLA nanocapsules produced by nanoconfined TIPS. The raw PLLA DSC curves exhibit a single and sharp melting peak at 183.9 °C, whereas dried PLLA nanocapsules, obtained at different processing conditions, always exhibit a complex melting behavior, with multiple endothermic peaks at different temperatures. In details, two endothermic peaks appear in the DSC curve of NCs at 0.1%wt/v (red curve in Figure 26a), which can be assigned as low and high melting temperatures (respectively, L and H in Figure 26a). At increasing polymer concentration, the peak at low melting temperature and its peak area decrease, whereas the peaks at

high temperature increase gradually up to temperatures higher than those usually observed for PLLA concentration of 1.5 %wt/v. The low (L)- and high (H) -temperature endothermic peaks appear when the rate of melting overwhelms that of the recrystallization.

A double melting peak is a common phenomenon for polymers and can drive to different interpretations. It can be due to the presence of two distinct crystal forms or morphological structures in the original sample, but often, it is the results of annealing occurring during DSC scans whereby less perfect crystals have time to recrystallize a few degrees above and to remelt[16; 17; 18]. This so called melt-recrystallization model suggests that the low-temperature and high-temperature peaks in the DSC melting curve are attributed to the melting of some amount of original crystals and as well as to the melting of crystals formed through the melt-recrystallization process during a heating scan. Then, the exothermic dip between the two endothermic peaks is attributed to recrystallization. That is, the melting proceeds through the process of the melting of original crystals, and then to recrystallization and melting of recrystallized and perfected crystals.

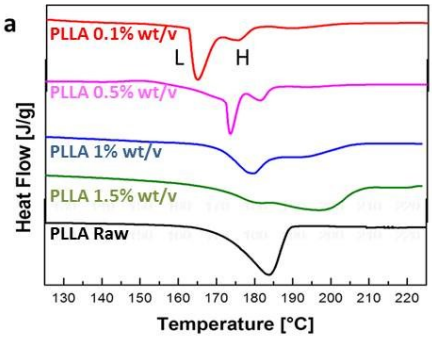


b

| Sample | Tg [°C] | Tm(L) [°C] | Tm(H) [°C] | Xc [%] |
|---|---|---|---|---|
| PLLA 0,1%wt/V | 52,93 | 164,3 | 174,5 | 35,7 |
| PLLA 0,5%wt/V | 51,64 | 179,5 | 191,6 | 32,3 |
| PLLA 1%wt/V | 54,59 | 179,6 | 192,8 | 35,7 |
| PLLA 1,5 %wt/V | 54,57 | 182,1 | 196,46 | 32,1 |
| PLLA Raw | 55 | 183,90 | n.A | 55,7 |

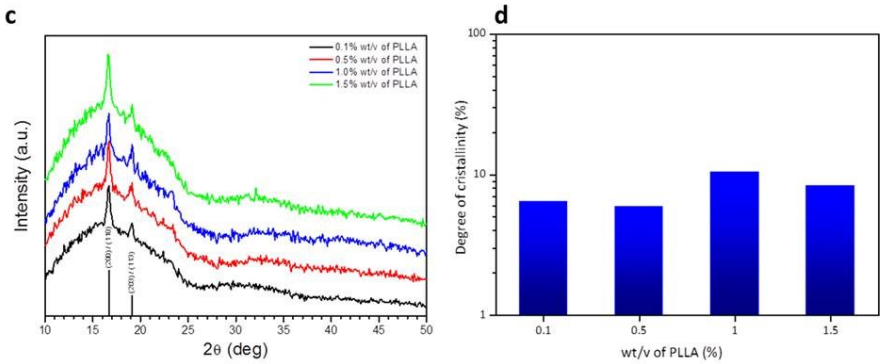


**Figure 26: Crystallinity grade analysis by DSC and XRD. a, DSC heating curves of PLLA nanocapsules at different polymer concentration, from the top: 0,1- 0,5- 1- 1,5 %wt/v – PLLA Raw; b, Table reports DSC data in detail and the crystallinity grade, showing how the polymer concentration can influence crystallization phenomena (DSC heating rate: 5°C/min); c, XRD patterns at different PLLA concentration from 0.1 wt/v % to 1.5wt/v%; d, degree of crystallinity versus PLLA concentration.**

Indeed, the melt-recrystallization model suggests that small and/or imperfect crystals change successively to more stable crystals through melt-recrystallization process leading to a competitive process between melting and recrystallization.

In addition, another model reported to explain this crystallization behavior is dual lamellae population model[19]. In particular, lamellar structures, due to the melting procedure and polymeric material, can range from hundred angstroms to several hundred of angstroms and the

extreme thinness of these lamellar crystals causes their melting point to be depressed below the typical melting temperature. In particular, samples that are crystallized by quenching or slow cooling from melt to room temperature will have crystallized to a considerable extent at high degree of undercooling from their typical melting temperature. Since crystallization at low growth temperatures produces very thin lamellae, such samples contain large fraction of low melting crystals that cause melting depression.

However, even if these observations have been reported for crystallization from a melted polymer they could be considered valid, taking into account the intrinsic differences existing for our nanocapsular system obtained by cooling a polymeric solution. The overall results hence suggest that the TIPS process can be dramatically modified in a nanoconfined system up to induce crystallization. Indeed, in our system, differently from conventional TIPS processes, crystallization appears to be controlled not only by cooling rate but also by the presence of the antisolvent and of the geometrical nanoconfinement due to constrain of the polymer within the primary emulsion droplets, both energetically reducing the mobility of the polymer and increasing polymer-polymer interactions in solution. Thus, this evidence shows that by inducing TIPS of a selected ternary solution within a nanoconfinement, the formation of the polymer chain can still occur leading to a high crystallization behavior and, in some cases, to a

less stable α crystal or thinner lamellae, compared to those obtained by traditional TIPS.

A further confirmation that the crystallization phenomenon is induced by the polymer nanoconfinement in the primary emulsion droplet can be derived when considering the behavior previously observed in twisted and curved crystals and to the different interpretations proposed. Indeed, our results clearly show the curved shape of the nanocapsular shell, presuming the coexistence of curved crystals within the shell. In this case, explanations of crystallization behavior belonging to the produced nanocapsules can be again associated to the crystal grow in a confined and curved volume of a droplet, where a TIPS process occurring at curved liquid/liquid-droplet interface can bring to an unusual polymer solution crystallization.

In order to explore the crystalline structure of PLLA nanocapsules, we performed X-ray diffraction analysis. Figure 26c shows the X-ray diffraction patterns obtained from PLLA at different polymer concentrations, when the primary emulsion is processed at fixed pressure of P=2000 bar. The two main peaks at $2\theta$~16.60° and $2\theta$~19.00° match with the same reflections of the PLLA powder (Figure 27) and allow us to index them as the (200)/(110) and (203)/(113) of the optical pure PLLA α crystalline form, respectively[1].

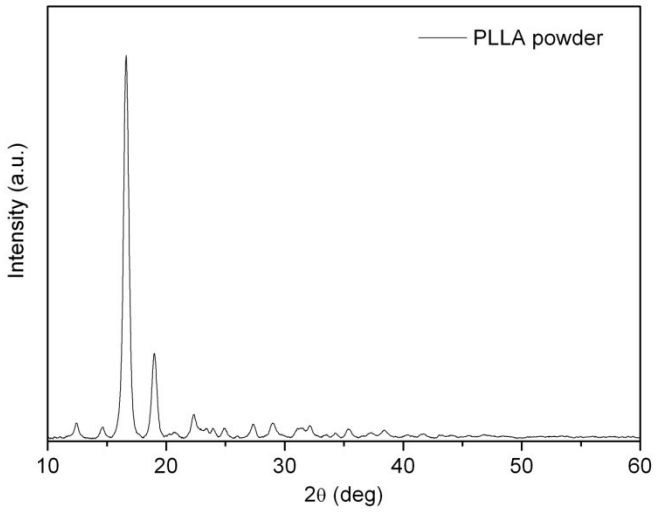


**Figure 27: XRD pattern of PLLA powder.**

By changing the PLLA concentration from 0.1 wt/v % to 1.5wt/v% no changes in the position of the main peaks are observed. It is important to point out that, at a melting temperature $T_m$ of 165°C, other different crystal forms could have been induced. However, XRD patterns reported in Figure 26c only show peaks related to α crystalline form, excluding definitely the presence of different crystalline phases.

Further investigations on crystallinity grade of PLLA nanocapsules were obtained with IR measurements. In particular, PLLA nanocapsules suspension is frozen in liquid nitrogen and then freeze dried to obtain a powder for IR measurements.

As reported in the graph below (Figure 28), characteristics peaks of amorphous and crystalline phase of PLLA at 870.75 cm-1 and 756.06 cm-1 respectively, are observed in our nanocapsules. Moreover, presence of

peak at 1755.56 cm-1 assigned to the carboxyl stretching vibration, at 1453.2 cm-1 related of asymmetric $CH_3$ bending mode, and at 1382.54 cm-1 for $CH_3$ symmetric and asymmetric stretching mode were found and assigned to amorphous phase. In addition, peak related to C-O-C stretching mode and $CH_3$ rocking mode are assigned to crystalline region and observed at 1184.26 cm-1. Finally, the peak at 1088.92, of C-O-C stretching mode is related to both amorphous and crystalline regions while, again, at 1045.75 cm-1 peak of C-$CH_3$ stretching mode and $CH_3$ rocking mode are observed.

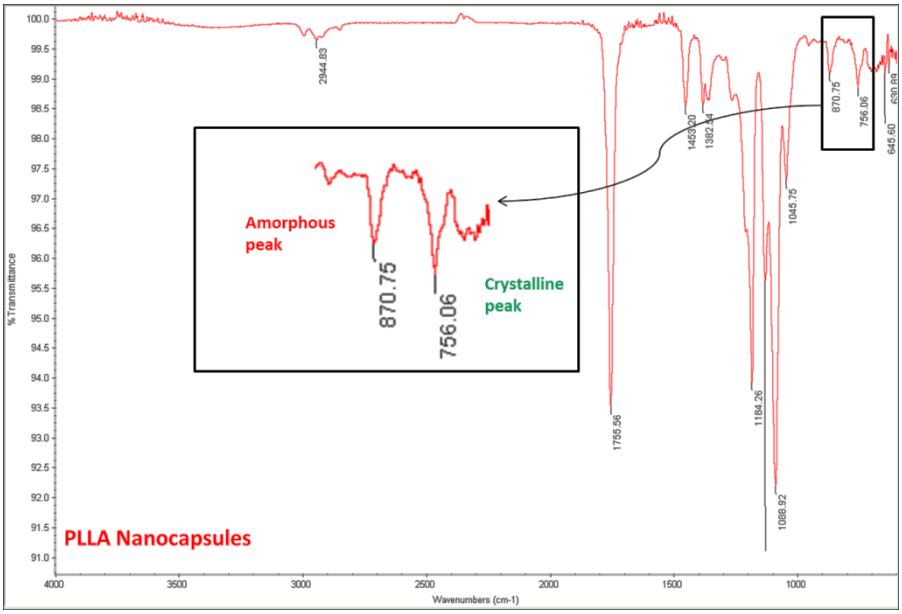


**Figure 28: IR spectra of PLLA powder and PLLA nanocapsules.**

## LOADING CAPABILITY AND RELEASE MECHANISM

Loading capability and release mechanism of the produced nanocapsules were investigated and fluorescent capability were

demonstrated, as reported in Figure 29a-c, where nanocapsules having different diameter were observed by Stimulated Emission Depletion (STED). Peculiar behavior of release mechanism is showed in Figure 29d.

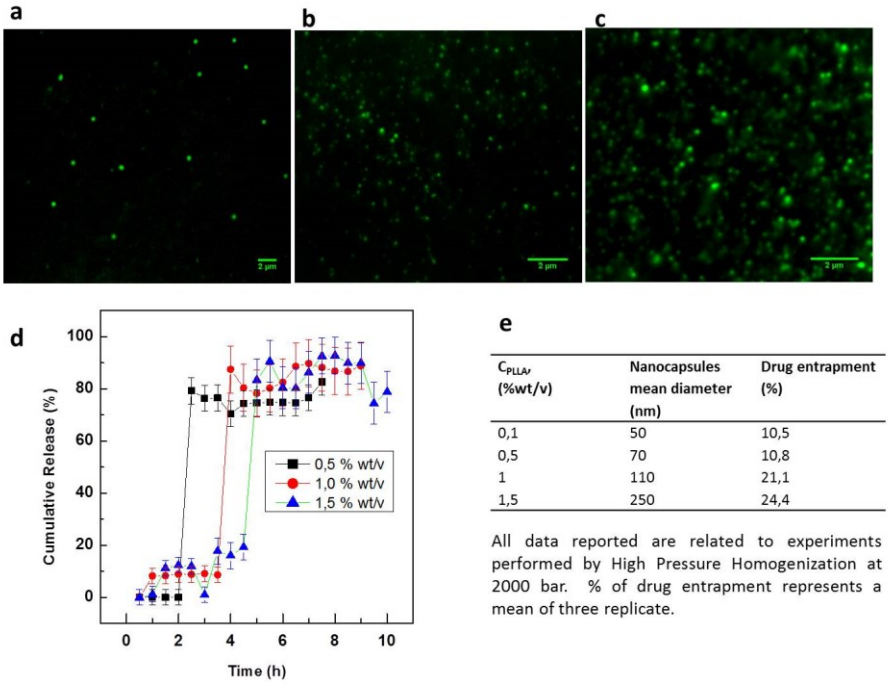


e

| $C_{PLLA}$ (%wt/v) | Nanocapsules mean diameter (nm) | Drug entrapment (%) |
|---|---|---|
| 0,1 | 50 | 10,5 |
| 0,5 | 70 | 10,8 |
| 1 | 110 | 21,1 |
| 1,5 | 250 | 24,4 |

All data reported are related to experiments performed by High Pressure Homogenization at 2000 bar. % of drug entrapment represents a mean of three replicate.

**Figure 29: Loading capability and release mechanism. a-c, STED high resolution images of randomly dispersed fluorescence of (a) 250 nm, (b), 115 nm and (c) 95 nm; d, Effect of polymer concentration on drug release profiles of loaded nanocapsules; e, drug entrapment as function of size and shell thickness for different % of dye loadings.**

In particular, cumulative release was conducted on nanocapsules of different size and shell thickness. The cumulative dye release from our nanocapsules is displayed for nanoparticles of size ranging from 70 to 250 nm. Release experiments were repeated three times and all the profiles obtained were almost superimposable. In the cumulative curves, it can be seen that real release is starting at different time

according to the nanocapsules shell thickness and that, for higher polymer concentration, a first slight release is observed, maybe due to the absorption of the dye within the polymer shell. The sample prepared at higher PLLA concentration, besides showing an increase in their mean diameter, are also giving a slight increase of the loading capacity of hydrophilic compounds from about 25%, calculated on a weight percentage basis, to a minimum of 10 % that can be incorporated into smaller nanocapsules. A different situation is observed in the case of lipophilic compounds or metal nanoparticles where higher encapsulation efficiency is reported (more than 80%). Curves in Figure 29d reveal a release mechanism typical of a nanocapsular structure by degradation of thin wall of the capsules leading to all-or-nothing cargo release. This characteristic is extremely important so that delivery vehicles could be later treated to be responsive to their local environment such that they retain their cargo until their target is reached, whereupon complete release should take place. In this framework, it is important to point out that this burst release via wall erosion can be regulated by tuning shell thickness of the nanocapsules through variation of polymer concentration.

In order to investigate payload capability of the nanocapsules, together with Chromeo 488, other compounds have been easily incorporated in the developed nanocapsules such as Rhodamine B, Nile Red and Gadolinium Chloride, Superparamagnetic iron Oxide nanoparticle (SPIO).

Thus, drug content of the process at different condition is showed in Figure 29e.

## THERMODYNAMIC INTERPRETATION OF THE PROCESS

Generally, TIPS technique is based on changes in thermal energy to induce the de-mixing of a homogeneous polymer solution into a two or multi-phase system domain. In a classical scenario, when the phase separation occurs, the homogenous solution separates in a polymer-rich phase and a polymer-poor phase, usually either by exposure of the solution to another immiscible solvent or by cooling the solution below a binodal solubility curve, where a liquid–liquid phase separation or solid–liquid de-mixing mechanism can occur[20; 21; 22; 23], as described in Figure 30d.

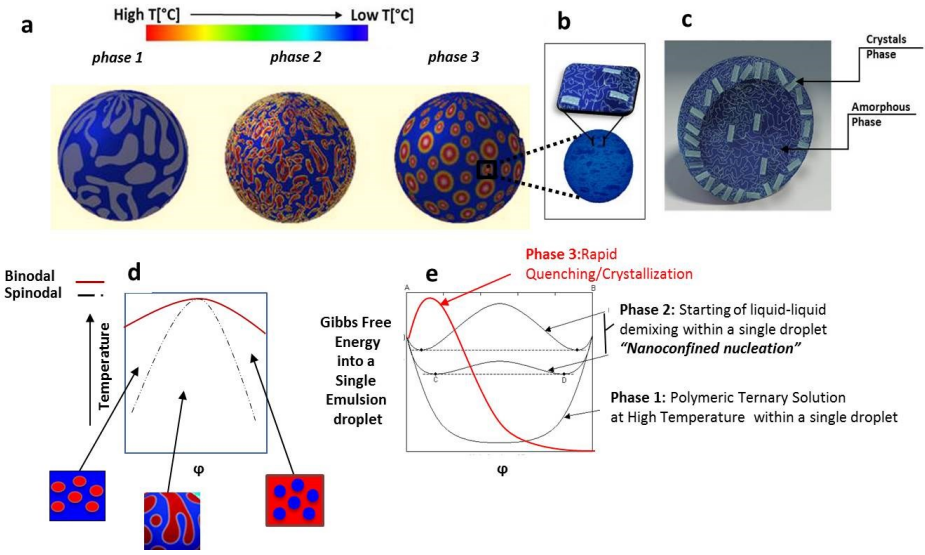


**Figure 30: Schematic representation of demixing of polymer solution in a nanoconfinement. a, Phase morphologies influenced by topological forces. Phase separation patterns are showed by cooling the system at a quench Temperature. In detail, an emulsion droplet containing a polymer solution is cooled below Cloud Point condition (phase 1). At a certain Temperature, phase separation occurs within the droplet (topological nanoconfinement) which inhibits chains from free configurations and pushes them in higher energy state similar to a spinodal phase. This increase of the polymer energy leads to a transition to a more ordered structure, where the polymer sets in a nanocapsular morphology at low free energy (phase 2). While cooling the system, a further segregation will be originated such that chain bending will be preferred. b and c, Schematic representation of nanocapsules and cross section highlighting crystal lamellae within the shell. d, Standard polymer segregation and phase diagram displaying spinodal curves, within the coexistence curves and uppercritical point. e, Energy content of the different phase steps to obtain nanocapsules.**

After that, the solvent is extracted by lyophilization and, depending upon the system and phase separation conditions, different morphologies and characteristics of the materials can be obtained. In this framework, Poly Lactic Acid (PLA) has been largely studied to produce two main types of morphologies by TIPS: *globular-like* and *membrane-like.* However, PLA is a slow-crystallizing material[1], and

crystallization phenomena of PLLA by TIPS are not very effective in terms of control of process-time and material properties.

However, when TIPS is performed in a nanoconfinement, the macromolecules experience an entropy variation of crucial importance for the free energy change accompanying formation of morphologies and crystal domains[24; 25; 26]. The geometrical constraints applied to a free unperturbed polymer chain reduce the number of available conformations of the chain and introduce additional interactions between polymer segments and the surface. For spherical confinement[27; 28], contribution of the entropic penalty is more complex because of excluded volume effects. Indeed, there are two factors influencing the effective coordination number and, hence, the conformational entropy of the polymer in the vicinity of the interface: the excluded volume of the polymer segments and the excluded volume of the obstacle. On the basis of the above principle, here we study the effect of quenching of the ternary system, PLLA-Dioxane-Water, not in a macroscopic environment but in a single droplet of a water-in-oil nanoemulsion. We performed our experiments in the low polymer concentration region (Figure 30d), where a solvent rich phase formation, as well as globular-like morphology, is favorite by decreasing. Briefly, as reported in Figure 30a-c, a polymer ternary solution at fixed temperature and composition is used as disperse phase while a PVA aqueous solution forms the continuous phase (*phase 1)*. Typically, keeping constant the temperature and emulsifying the system under

high shear rate, a mean droplet size lower than 500 nm is obtained. At this point, any emulsion droplet becomes as a single system containing a ternary polymer solution *(phase 2)*. The last step consists in the instantaneous cooling of the emulsion into a metastable region. Under these conditions, the thermodynamic barrier for the formation of a crystalline phase is lower than that for the formation of an amorphous phase, and so, PLLA molecular chains overcome the potential barrier and chain folding will occur also at high cooling rate, in order to maintain the thermal dynamic equilibrium. In details, if trapped in an initially spherical nanoconfinement, the polymer will be unable to fully adopt all its possible conformations through thermal fluctuations, with the consequence that chain segment alignment will probably correspond to the lowest available energy status of the polymer system. Subsequently, some folded chains will immediately aggregate, leading to the formation of crystal nuclei within the droplet. However, at this point, further aggregation phenomena are prevented by a large energy barrier due to intersegment attractive or repulsive interactions, volume effects and presence of antisolvent and only the development of interconnected domains characteristics of spinodal decomposition can proceed. Finally, having a reduced number of available conformations because of the nanoconfinement and trying to be away from the antisolvent, instead of forming an extended or isolated structure, the preformed crystal nuclei will adopt an interconnected nanocapsular

structure to reduce excess of free energy *(phase 3)*, as reported in Figure 30e.

In the framework of the traditional thermodynamics, we can make some considerations: when *phase3* is carried out in a macroscopic system, polymer chains are able to adjust to infinite configurations to reduce their free energy, with the consequence that the formation of a crystalline structure is not energetically favorable at high cooling rate. In a nanoconfined system, instead, chains can adjust a reduced number of configurations to decrease the excess of free energy, with the consequence that chain folding becomes one of those conformations able to bring the system to a reduction of the entropic penalty.

In summary, thermally induced phase separation in a flexible nanoconfinement can promote a spinodal-like regime where even the smallest fluctuations can grow as crystal nuclei because of the shallow energy barriers, driving the formation of nanocapsular structures when surface energetic contributes to create an interface are predominant, in comparison with the volume energetic contributes. Our observations demonstrate for the first time how morphologies resulting from TIPS within a nanoconfinement can be extremely different from those obtained from traditional TIPS in a macroscopic environment. These theoretical considerations are illustrated here for the case of PLLA formation but could be generalized for many other polymer systems. Moreover, the model we propose contributes to advancing the understanding of how polymorphism of some polymers could be

influenced by an energetic nanoconfinement and how this knowledge could influence both fundamental thermodynamic understanding and technological advances in design and scale-up of processes

## References


[1] GARLOTTA, D. A literature review of poly(lactic acid). **Journal of Polymers and the Environment,** v. 9, n. 2, p. 63-84, Apr 2001. ISSN 1566-2543. Disponível em: < <Go to ISI>://WOS:000177985700003 >.

[2] AURAS, R.; HARTE, B.; SELKE, S. An overview of polylactides as packaging materials. **Macromolecular Bioscience,** v. 4, n. 9, p. 835-864, Sep 16 2004. ISSN 1616-5187. Disponível em: < <Go to ISI>://WOS:000223856400001 >.

[3] PANG, X. et al. Polylactic acid (PLA): Research, development and industrialization. **Biotechnology Journal,** v. 5, n. 11, p. 1125-1136, Nov 2010. ISSN 1860-6768. Disponível em: < <Go to ISI>://WOS:000284012300012 >.

[4] SAEIDLOU, S. et al. Poly(lactic acid) crystallization. **Progress in Polymer Science,** v. 37, n. 12, p. 1657-1677, Dec 2012. ISSN 0079-6700. Disponível em: < <Go to ISI>://WOS:000313091300002 >.

[5] ZHANG, J. M. et al. Structural changes and crystallization dynamics of poly(L-lactide) during the cold-crystallization process investigated by infrared and two-dimensional infrared correlation spectroscopy. **Macromolecules,** v. 37, n. 17, p. 6433-6439, Aug 24 2004. ISSN 0024-9297. Disponível em: < <Go to ISI>://WOS:000223448300026 >.

[6] SAWAI, D. et al. Preparation of oriented beta-form poly(L-lactic acid) by solid-state coextrusion: Effect of extrusion variables. **Macromolecules,** v. 36, n. 10, p. 3601-3605, May 20 2003. ISSN 0024-9297. Disponível em: < <Go to ISI>://WOS:000182967300021 >.

[7] BAGARIA, H. G.; KADALI, S. B.; WONG, M. S. Shell Thickness Control of Nanoparticle/Polymer Assembled Microcapsules. **Chemistry of Materials,** v. 23, n. 2, p. 301-308, Jan 25 2011. ISSN 0897-4756. Disponível em: < <Go to ISI>://WOS:000286160800023 >.

[8] BROADERS, K. E. et al. Acid-degradable solid-walled microcapsules for pH-responsive burst-release drug delivery. **Chemical Communications,** v. 47, n. 2, p. 665-667, 2011 2011. ISSN 1359-7345. Disponível em: < <Go to ISI>://WOS:000285300400010 >.

[9] ESSER-KAHN, A. P. et al. Triggered Release from Polymer Capsules. **Macromolecules,** v. 44, n. 14, p. 5539-5553, Jul 26 2011. ISSN 0024-9297. Disponível em: < <Go to ISI>://WOS:000292850100001 >.

[10] HOOGSTEEN, W. et al. CRYSTAL-STRUCTURE, CONFORMATION, AND MORPHOLOGY OF SOLUTION-SPUN POLY(L-LACTIDE) FIBERS. **Macromolecules,** v. 23, n. 2, p. 634-642, Jan 22 1990. ISSN 0024-9297. Disponível em: < <Go to ISI>://WOS:A1990CK43600041 >.

[11] KAWAI, T. et al. Crystallization and melting behavior of poly (L-lactic acid). **Macromolecules,** v. 40, n. 26, p. 9463-9469, Dec 25 2007. ISSN 0024-9297. Disponível em: < <Go to ISI>://WOS:000251724700037 >.

[12] ZHANG, J. et al. Disorder-to-order phase transition and multiple melting behavior of poly(L-lactide) investigated by simultaneous measurements of WAXD and DSC. **Macromolecules,** v. 41, n. 4, p. 1352-1357, Feb 26 2008. ISSN 0024-9297; 1520-5835. Disponível em: < <Go to ISI>://WOS:000253331200043 >.

[13] CARTIER, L. et al. Epitaxial crystallization and crystalline polymorphism of polylactides. **Polymer,** v. 41, n. 25, p. 8909-8919, Dec 2000. ISSN 0032-3861. Disponível em: < <Go to ISI>://WOS:000089272600019 >.

[14] MIYATA, T.; MASUKO, T. Crystallization behaviour of poly(L-lactide). **Polymer,** v. 39, n. 22, p. 5515-5521, Oct 1998. ISSN 0032-3861. Disponível em: < <Go to ISI>://WOS:000075284700029 >.

[15] TABI, T. et al. Crystalline structure of annealed polylactic acid and its relation to processing. **Express Polymer Letters,** v. 4, n. 10, p. 659-668, Oct 2010. ISSN 1788-618X. Disponível em: < <Go to ISI>://WOS:000281954500008 >.

[16] SARASUA, J. R. et al. Crystallization and melting behavior of polylactides. **Macromolecules,** v. 31, n. 12, p. 3895-3905, Jun 16 1998. ISSN 0024-9297. Disponível em: < <Go to ISI>://WOS:000074343700019 >.

[17] YASUNIWA, M. et al. Thermal analysis of the double-melting behavior of poly(L-lactic acid). **Journal of Polymer Science Part B-Polymer Physics,** v. 42, n. 1, p. 25-32, Jan 1 2004. ISSN 0887-6266. Disponível em: < <Go to ISI>://WOS:000187214500004 >.

[18] _____. Melting behavior of poly(L-lactic acid): X-ray and DSC analyses of the melting process. **Polymer,** v. 49, n. 7, p. 1943-1951, Apr 1 2008. ISSN 0032-3861. Disponível em: < <Go to ISI>://WOS:000255130500025 >.

[19] WEEKS, J. J. **emperture and Change of Lamellar Thickness with Time for Bulk Polyethylene**: Journal of Research of the National Bureau of Standards-A. Physics and Chemestry. 67A 1963.

[20] LEE, K. W. D.; CHAN, P. K.; FENG, X. S. Morphology development and characterization of the phase-separated structure resulting from the thermal-induced phase separation phenomenon in polymer solutions under a temperature gradient. **Chemical Engineering Science,** v. 59, n. 7, p. 1491-1504, Apr 2004. ISSN 0009-2509. Disponível em: < <Go to ISI>://WOS:000221030800009 >.

[21] LEE, H.; MYERSON, A.; LEVON, K. LIQUID-LIQUID PHASE-SEPARATION IN CRYSTALLIZABLE POLYMER-SOLUTIONS. **Abstracts of Papers of the American Chemical Society,** v. 201, p. 251-POLY, Apr 1991. ISSN 0065-7727. Disponível em: < <Go to ISI>://WOS:A1991FG89401059 >.

[22] LAXMINARAYAN, A.; LLOYD, D. R. KINETICS OF MEMBRANE FORMATION VIA LIQUID LIQUID THERMALLY-INDUCED PHASE-SEPARATION. **Abstracts of Papers of the American Chemical Society,** v. 203, p. 65-IEC, Apr 5 1992. ISSN 0065-7727. Disponível em: < <Go to ISI>://WOS:A1992HK16200092 >.

[23] LLOYD, D. R.; KIM, S. S.; KINZER, K. E. MICROPOROUS MEMBRANE FORMATION VIA THERMALLY-INDUCED PHASE-SEPARATION .2. LIQUID LIQUID-PHASE SEPARATION. **Journal of Membrane Science,** v. 64, n. 1-2, p. 1-11, Nov 15 1991. ISSN 0376-7388. Disponível em: < <Go to ISI>://WOS:A1991GU01700001 >.

[24] SMYDA, M. R.; HARVEY, S. C. The Entropic Cost of Polymer Confinement. **Journal of Physical Chemistry B,** v. 116, n. 35, p. 10928-10934, Sep 6 2012. ISSN 1520-6106. Disponível em: < <Go to ISI>://WOS:000308339400055 >.

[25] FLORY, P. J. **Principles of Polymer Chemestry**. Cornell University Press, Sage House, 512 East Street, Ithaca, New York 14850: Cornell University, 1953. 647 ISBN 0-8014-0134-8.

[26] KLENIN, V. J. **Thermodynamics of systems containing flexible-chain Polymers**. Sara Burgerhartstraat 25 P.O. BOX 211, 1000 AE Amsterdam: Elsevier Science B.V., 1999. 826 ISBN 0 444 82373 5.

[27] MEHTA, R. et al. Role of curvature elasticity in sectorization and ripple formation during melt crystallization of polymer single crystals. **Physical Review E,** v. 69, n. 6, Jun 2004. ISSN 1539-3755. Disponível em: < <Go to ISI>://WOS:000222502700079 >.

[28] POTEMKIN, I. et al. Spontaneous curvature of comblike polymers at a flat interface. **Macromolecules,** v. 37, n. 10, p. 3918-3923, May 18 2004. ISSN 0024-9297. Disponível em: < <Go to ISI>://WOS:000221394600054 >.

# CHAPTER III: AQUEOUS CHANNEL MANIFESTATION AMONGST BIODEGRADABLE NANOMATERIALS FOR FAVORABLE GADOLINIUM ENTRAPPING

## INTRODUCTION

Enduring volatile evolution of medical imaging technologies have taken place over the past few decades and nowadays play a principal role in clinical oncology. Along with allowing clinicians to see where a tumor is located in the body, molecular imaging also visualizes the manifestation and commotion of unambiguous molecules (e.g., proteases and protein kinases) and biological processes (e.g., apoptosis, angiogenesis, and metastasis) that influence tumor behavior and/or response to therapy[1]. Contemporary clinical cancer actions require specific information such as the exact tumor location; how large is it?; Its confinement to a small area, or its blowing out to lymph nodes? etc. Through the application of traditional anatomical imaging methods such as computed x-ray tomography (CT), magnetic resonance imaging (MRI), and ultrasound (US), the aforementioned interrogations are being dealt with ever-growing spatial resolution[2-4]. MRI provides an obligatory tool to increase the compassion and selectivity of cancer diagnosis; especially in the early stages of tumor. The production of high-resolution three-dimensional maps demarcating morphological topographies of the specimen provides

an edge to MRI comparatively. To establish MRI as a key imaging modality for cell tracking studies, it is necessary to develop a new generation of high-sensitive MRI contrast agents that could allow for the efficient detection of labeled cells in vivo. For enhancing the differentiation between tissues, approved metallic contrast agents such as Mn (Teslasca®), Gd (ProHance®, Dotarem® & Magnevist®) and Fe (Endorem®, and Feride®) have been used[5-8]. Fe comprising nanoparticles (NPs) are being used as cellular probes; they provide a very sensitive "negative" contrast effect, which enables single cell detection. However the induction of a negative contrast effect due to strong magnetic susceptibility of iron oxide nanoparticles greatly exceeds the exact area where implanted cells are located. Moreover, these relics encumber the demarcation of fine vasculature and functional geographies around the labeled cells, and thereby make impossible cell quantification based on contrast enrichment[9-11].

It was considered that the NPs could be one of the ideal molecular probes as the MRI contrast agent and the novel NPs had already been developed for molecular imaging[12]. Although NPs have revealed attractive potential as molecular imaging contrast agent, loading NPs with Gd postures challenge in the development of targeted contrast agents. Three of the common methods being reconnoitered are (i) Encapsulating Gd in the core space of the NPs; (ii) Self-assembling & (iii) Chemical conjugation of Gd on the exterior of the NPs. In combination with gadolinium, polymer micellar NPs are very

promising because of their aptitude to deliver positive contrast (i.e., T1-weighted images), robust structural features, and simple fabrication. In such a micelle assembly product, the rate of water exchange is similar to that observed in Gd–DTPA, because of the exposure of Gd complex in the exterior shell layer of the micelle[13]. However, due to non-biocompatibility of the DOTA, there is necessitated endeavor to study some biocompatible contrast agents. MRI is a powerful medical diagnostic technique: it can penetrate deep into tissue, provide excellent soft tissue contrast with sub-millimeter resolution, and does not employ ionizing radiation. Targeted contrast agents provide an additional layer of molecular specificity to the wealth of anatomical and functional information already attainable by MRI. However, the major challenge for molecular MR imaging is sensitivity: micromolar concentrations of Gd (III) are required to cause a detectable signal change, which makes detecting proteins by MRI a challenge[14]. Excretion of Gd-based contrast agents take place in un-metabolized form, but biodegradability in aqueous test systems is still an issue[15]. Due to their high polarity and good water solubility they exhibit a long half-life[16].

Recently, nanoparticles prepared with biocompatible and biodegradable polymers, such as poly (D, L-lactide-co-glycolide) (PLGA) or poly (D, L-lactide) (PLA), have attracted much attention due to their favorable physico-chemical characteristics in terms of safety,

stability, the relative ease of large-scale production, and lack of intrinsic immunogenicity etc[17-19]. Significantly, idyllic MRI contrast agents voluntarily paves the way to degradation and clearance from the body after its functions were over. Thus, biocompatible and biodegradable nanoparticles, possessing significantly low or trifling safety risks and convenient preparation in large quantities, have been suggested as novel candidates for molecular imaging contrast agents[20]. Block copolymers of poly lactic acid (PLA) and polyethylene glycol (PEG) are few of the commonly used polymers with hydrophilic and hydrophobic blocks which allows the formation of a stable nano-particulate suspension in an aqueous solvent, where PLA chains predominantly form the core and PEG chains are located outside[21]. A systematic variation in their chemical structure, composition, size, and architecture; block copolymers offer advantages in tuning their shape and functionality in comparison to conventional amphiphiles such as low molecular weight surfactants and lipids[22-24]. Recent studies have enriched the scope of block copolymer self-assembly by increasing the diversity of supramolecular aggregates such as micelles[25-27], vesicles[24, 28-32], and toroids[33-36] formed in both aqueous and organic environments or even in the mixture. Diblock PLA-PEG copolymers and triblock PLA-PEG-PLA copolymers allow modulation of the biodegradation rate, the hydrophilicity, and the mechanical properties of the copolymers[37]. Herein we present temperature/time-reliant self-assembly driven simple approach for the development of biocompatible nanostructures for MRI. Endeavor

of the present research was to develop Gd loaded PLA-PEG-PLA NPs as the molecular MRI contrast agents to efficiently target tumor. A low molecular PLA-PEG-PLA have been designated to prepare well-demarcated NPs through optimization of kinetics of the self-assembly viz a viz temperature/time/concentration. The hydrophobic/hydrophilic moieties of block copolymer nanoparticles (BCN) were employed to adsorb $GD^{+3}$ at the surface of BCNs to achieve multifunctional biodegradable NPs for MRI. The paramagnetic properties of the BCNs designed here compare sympathetically with Gd-based agents that have previously been reported. For example, Gd-labeled shell-cross-linked nanoparticles (40nm diameter) exhibit an $R_1$ of $39mM^{-1}$ $s^{-1}$per Gd (0.47 T) but possess only 510 Gd per particle, which results in an $R_1$ of $2x104\ mM^{-1}s^{-1}$ per nanoparticle[38]. This relaxivity is significantly lower than the paramagnetic BCNs presented here.

## MATERIALS AND METHOD

### Materials

For engineering the block copolymer nanoparticles (BCN), a low molecular weight Block polymer (PLA-PEG-PLA, Mw=1500-900-1500 Da) was purchased from Sigma Aldrich. Intended for dispersed phase, various organic solvents such as N,N-Dimethylformamide (DMF) and acetone were also procured from Sigma Aldrich. And the Gadolinium Chloride ($CdCl_3$) used for loading the BCN have been purchased from

Sigma Aldrich. Extra pure Millipore water was used for the self-assembly process.

**Procedural Methods**

In a distinctive procedure three different amounts 1, 5 &10mg of $GdCl_3$ in various round bottom flasks respectively were allowed to dissolve for best labeling efficiency under increased aspiration. The dispersed phase was prepared by solubilizing stipulated concentration of the block copolymer in 3ml of the acetone. A homogeneous dispersed phase was prepared through ultra-sonication for 5 minutes at amplitude of 20%. Under constant and moderate stirring the dispersed phase was poured into 45ml of water at a rate of 1ml/min. Along with the room temperature, the aforementioned pathway was also followed to prepare the BCN for different amounts of the polymer at 40°C. Solvent-evaporation self-assembly during the aforementioned method was allowed for enhanced time intervals of 72 hours at least, while the morphological advances were observed at various time intervals.

**Techniques**

*Dynamic Light Scattering (DLS)*

The hydrodynamic diameter of freshly prepared BCN were continuously observed by a Malvern Zetasizer (Nanoseries) at stipulated time intervals up to 24 hours. Surface Zeta Potential of the BCN was also observed through the same instrument at definite time intervals.

**UV-Vis measurements**

UV-visible spectra of solutions will be measured by Cary 100Scan UV-vis spectrophotometer (UV0901M191) in the wavelength range of 200-900nm. The characteristic UV-vis absorbance properties of colloidal BCN solution in the presence of different concentrations/temperatures have been performed by the dissolution/adsorption of dye in block copolymer solution.

**Isothermal titration calorimetry (ITC)**

The calorimetric experiments were performed with a Nano-ITC instrument (TA Instruments—Waters LLC 109 Lukens Drive New Castle, DE 19720). All heat effects arising from the injection of the solution in the syringe solution into the sample cell solution are actively balanced by a calorimeter feedback system keeping the sample cell and reference one at the same temperature. The calorimeter sample cell was filled with acetone and the titration syringe was loaded with the TBP solution in acetone of a stipulated concentration. Each titration consisted of twenty, 2.5µL injections at 300-second intervals with stirring speed of 150 rpm. A 3000-second baseline was collected before the first injection and after the last injection. Prior to starting the titration, the calorimeter was equilibrated to a baseline with a drift of less than 100nW over a ten-minute period. Two to three individual measurements were performed for each system at different temperatures. The experimental data were analyzed using the NanoAnalyze software for ITC as provided by TA instruments. The thermodynamic properties

using the mass-action model were obtained by applying a non-linear regression routine based on the method of simulated annealing to the experimental data.

**Field Emission Scanning Electron Microscopy (FESEM)**

FESEM instrument from Ultra-plus Zeiss at accelerating voltage of 5-20kV have been used for all SEM studies. For liquid samples the drops were dried on a glass mounted on a stub while the ultra-filtered samples have been observed by fastening the polycarbonate membranes on the stub.

**Transmission Electron Microscopy (TEM) measurements**

The shape and size of BCN have been characterized by transmission electron microscopy (TEM). The samples were prepared by mounting a drop of self-assembly solution on a carbon coated Cu grid and allowing it to dry in air. These samples have been observed with the help of a FEI CM10 transmission electron microscope operating at 120 kV. The system has been provided with an intensified video camera to assist in alignment and a slow scan CCD camera. Final images can be recorded on CCD.

**ICP-MS (inductively coupled plasma mass spectrometry)**

ICP-MS makes it possible to distinguish between different oxidation stages of metal ions (speciation) and between free and bound ions, and thus to determine the effects of the addition of BCNs on the stability of the gadolinium. Aqueous solutions of Gadovist and Magnevist with a gadolinium concentration of 1 mg/L acted as MRI

contrast agents. TBP concentrations of 5, 10 and 20 mg/L were used to investigate the stability of the gadolinium contrast agents.

**Fourier Transformation Infrared spectroscopy**

FTIR spectrum was measured by using a RZX (Perksin Elmer) Fourier transform infrared spectrometer at room temperature in the range of 4000-400 cm-1 with sample mild in KBr.

## Results and Discussion

Gd-labeled biodegradable functionalities have been developed as MRI agents by using $GdCl_3$ and time/temperature driven simple block copolymer self-assembly progression. These biodegradable & biocompatible molecular contrast agents for tumor-sensing have been prepared by encapsulating/loading gadolinium onto BCNs (shown schematically in Fig.3) of low molecular weight block copolymer. The hydrodynamic diameter was determined by dynamic light scattering (DLS). For observing the formation of BCN in a detailed fashion and also for comparison, their formation in the absence of $GdCl_3$ was also carried out and characterized rigorously by DLS & variety of techniques revealed in the experimental section. Fig.1 demonstrates the dynamic light scattering profile of the BCNs self-assembly in DMF. The BCNs were characterized rigorously, by employing DLS which demonstrated that for a lower concentration of the block copolymer, nanostructures were negatively charged having a negative zeta potential, ζ around 35mV and possessed number-averaged hydrodynamic diameter about 100 nm. During the course

of measurement it have been observed that after a certain threshold of time duration of the self-assembly process, the same did not affect the size up to a great extent while somewhat similar trend was observed for ζ of the BCNs. Few of the interesting annotations of the present study were observed in case of the concentration of the block polymer.

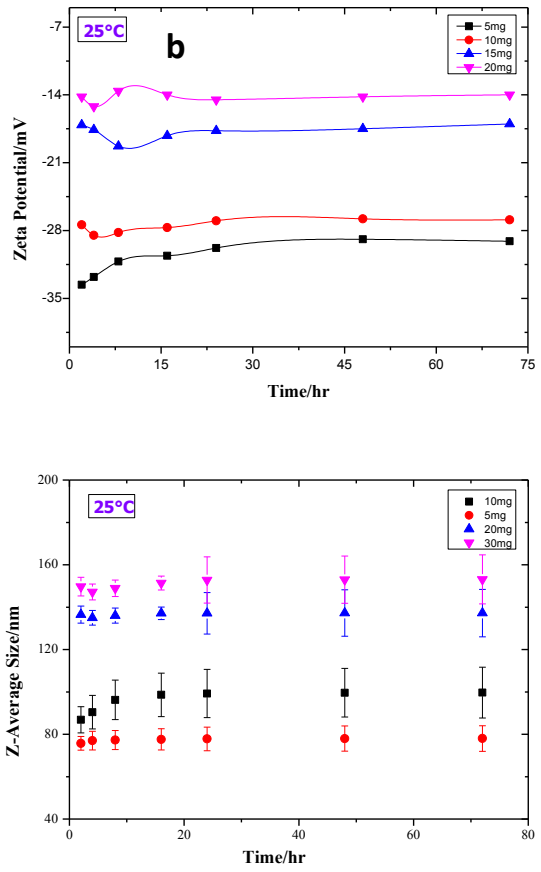


**Fig.1:** a) *Surface Zeta-potential and b) Hydrodynamic Size-Evolution of self-assembled BCNs @Room Temperature in DMF as a dissolving medium.*

As established from Fig.1b, the hydrodynamic diameter of the BCNs have been observed ≤100 for a block copolymer concentrations of 0.43 & 0.86mM, while it was ≤150 for two of the higher concentrations of the block copolymer self-assembly. This upsurge in size at elevated levels of concentration could be driven by an increase in viscosity of the self-assembly solution there by making the emulsion more viscous. The arduous time and concentration oriented study of the BCNs via DLS suggested considerable decrease in surface zeta potential with the increase in concentration of the block copolymer in the self-assembly process, suggesting thereby instability of the BCNs at elevated levels of concentration. This may be attributed to greater amount of polymer present in the same volume of dispersed medium, probably paving the way for enhanced electrostatic interactions among various polymer moieties in far post-micellar regions and same reflection gained strength from electron microscopy profiles of the BCNs demonstrated in the later part of this section.

Since, nonionic surfactants with a PEG hydrophilic segment show a very strong temperature dependent micellization process[39], therefore temperature dependence of BCNs self-assembly was also considered through DLS and other techniques. The DLS profiles of BCN self-assembly have been presented in Fig 2 demonstrating a marked size difference in BCN from that of at 25°C. Evidently from the DLS profiles dilulge that BCN@lowest concentration of the block

copolymer illustrates a negative zeta potential of around 35-40, making these very BCNs more stable in comparison to the BCNs prepared@highest concentration which possess a negative zeta potential of about 15. In terms of size of these morphological architectures we had obeserved an increase in size of BCNs upto about 175nm. One of the point worth mentioning during the course of present discussion is that monodispersity of nanostructures is not very ideal and therefore we observed a diversified morphological structure evolution in terms of shape as well as size (an entirely separate study is underway). Same observation gained prominence after we progressed through the electron microscopic studies (presented in the later part of the discussion). Which may be caused due to highly unstable and complex character of the block copolymer viz-a-viz different types of monomeric identies involved none of which have identical properties in terms of hydrophobicity and solubility in similar kind of solvents. Moreover two PLA monomers on the edges and one PEG monomer present in the middle provides complexity to the block copolymer character.

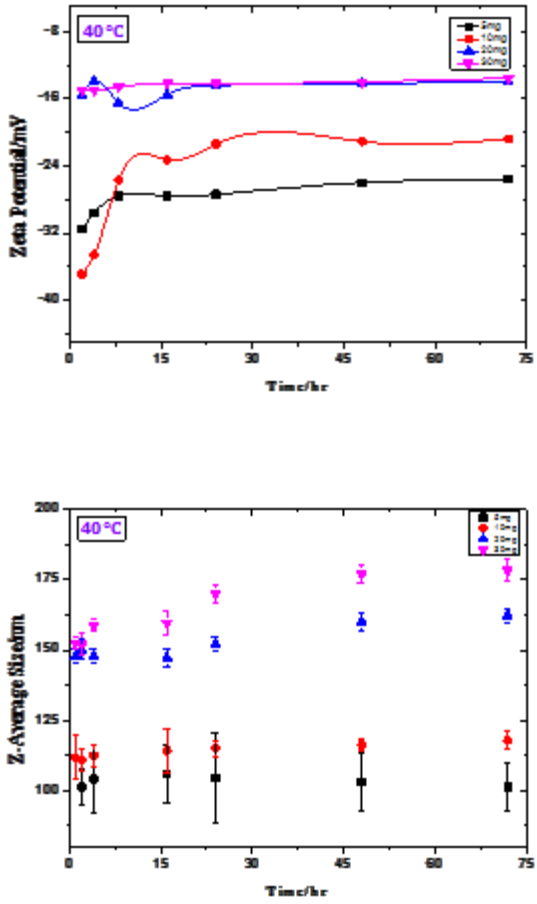


**Fig.2:** a) *Surface Zeta-potential and b) Hydrodynamic Size-Evolution of self-assembled BCNs @40°C*

Because of the the strong temperature dependence of hydrophilic PEG segment the biggest difference in the BCNs for 40°C have been noticed in terms of the shape dependent morphological effects. Moreover, the edifice of triblock copolymer micelles becomes a feeble function of concentration, but changes swiftly with

temperature[40], with association number accumulative and micelle becoming drier, as the temperature is increased and water exorcised from the micelle core[41]. SEM micrographs represented in Fig.4, evidently establish the shapes of BCNs predominently spherical. Moreover a greater temperature provides necessary plateform for the nucleation for the nanostructures evolution towards an ordered geometry. Some of the traces in Fig.4a,b inaugurate that higher temperature leads to the aggregation of nanostructures. At room temperature although the aggregation was totally lacking and the morphology of the BCNs was not orderly spherical (Fig.6a).

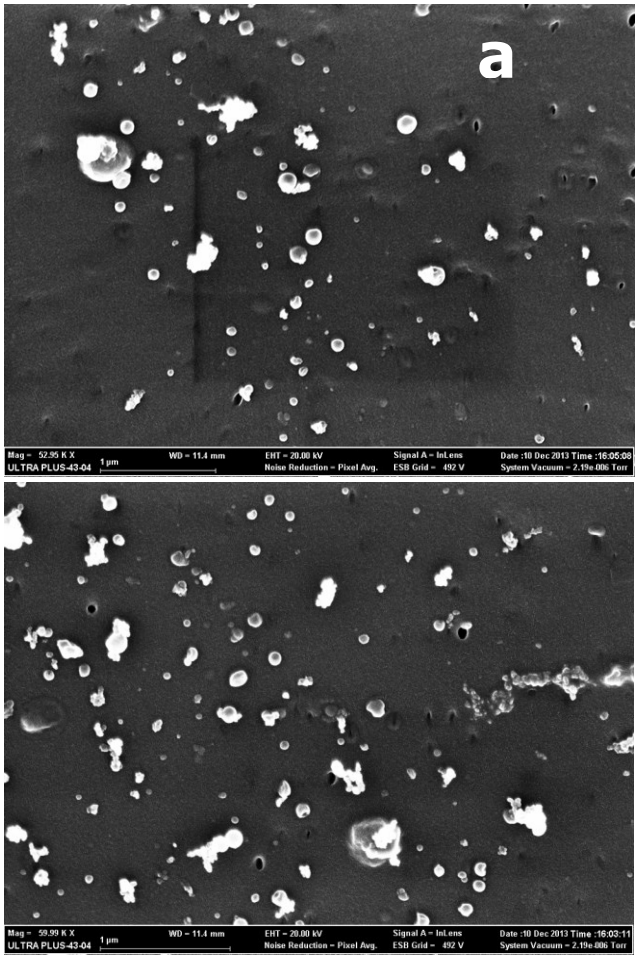


**Fig.3:** a,b *Scanning electron micrographs of BCNs prepared at 40°C.*

The dissolving mediums i.e. solvent contributes in the self-assembly upto a marked extent in terms of diversified properties like size etc of nanostructures. The present study deals with two different solvents DMF and acetone as the dissolving medium for the block copolymer in question. Available literature[42] is enough to suggest that PLA swells when allowed to dissolve in DMF, while it get solubilized completely

in acetone. This inference also gained prominense from the copolymer self-assembly appearance, which was a bit turbid in case of DMF, unlike acetone. This could be the reason for a much larger size of the BCNs in case of DMF as compared to that of acetone (electron micrographs presented in later part Fig.6 onwards). Aforementioned results reveal the electron microscopic and DLS profiles of BCNs in a polar aprotic solvent DMF[43].

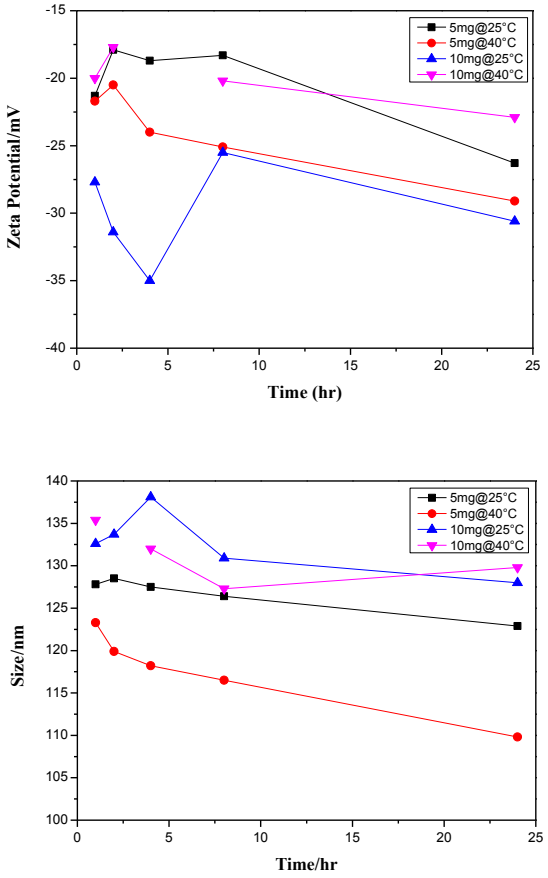


**Fig.4:** a) *Surface Zeta-potential and b) Hydrodynamic Size-Evolution of self-assembled BCNs @Room Temperature & 40°C in acetone as a dissolving medium*

Acetone is a good solvent for PLA, while comparatively it exhibits lesser solubility when dissolved in DMF. In a good solvent the PLA part of the TBP swells more in comparison to a poor solvent, leading there by to smaller nanoparticles in the later. Therefore the size of BCNs obtained in DMF (Fig.1b) is predominantly lesser in comparison

to that obtained in acetone (Fig.5b) as evidenced from the DLS profiles of the same. Various concentrations of the TBP demonstrate a size and zeta potential distribution as embodied in Fig.5.

Fig.6 unveils the scanning electron micrographs of TBP micelles at the lowest TBP concentration we tried during the passage of our self-assembly progression. After enhanced number of experiments for the cmc determination of TBP we had an idea about the cmc of the TBP. ITC was extensively tried to elaborate about cmc determination of the triblock polymer under study. The micrographs clearly demonstrate existence of cylindrical and spherical micelles in the periphery and inside the compound micelle. The size of these micelles have been observed as small as 30-50nm. With the passage of increasing [TBP], size of the micelle nanostructures increases and morphologically these soft nanostructures are converted into comparatively hard ones which can be easily attributed to Fig.7. The black spots on soft micellar nanostructures in Fig. 6b may be attributed to burns caused by elevated levels of magnification during SEM observation. Increasing the magnification during SEM observation does not exhibit burns on the nanostructures thereby making the later hard, unlike the micelles appearing and getting burns at increased levels of magnification for experiments carried around CMC of the TBP. Although polymeric micelles exhibit various biological claims but from MRI and drug delivery point, fondness always subsists for spherical and durable morphologies rather than

soft micellar nanostructures due to unstable character of the polymeric micellar nanostructures.

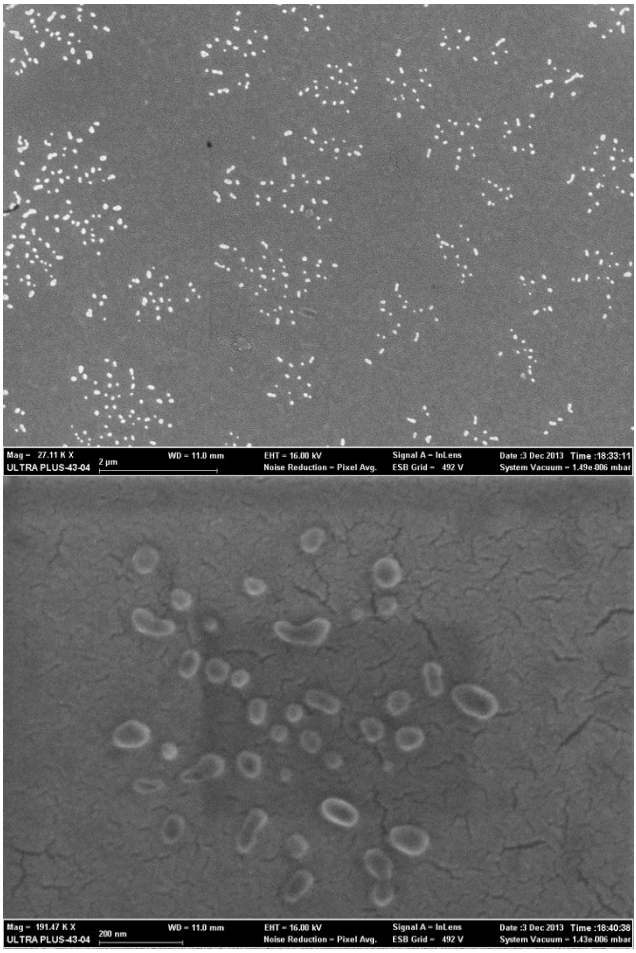


**Fig.5:** *SEM of TBP micelles at lowest [TBP] (around cmc) prepared at room temperature; a) compound-micelles and b) higher magnification SEM construction of a compound micelle.*

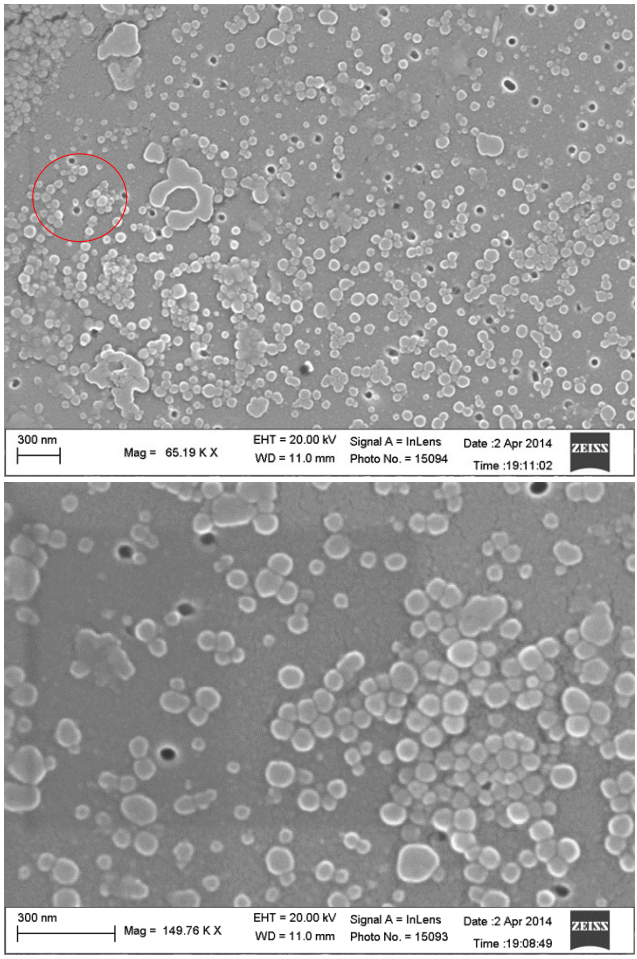


**Fig.6:** a) *Scanning electron micrographs of BCNs at room temperature at moderate [TBP]; b) higher magnification SEM of BCNs.*

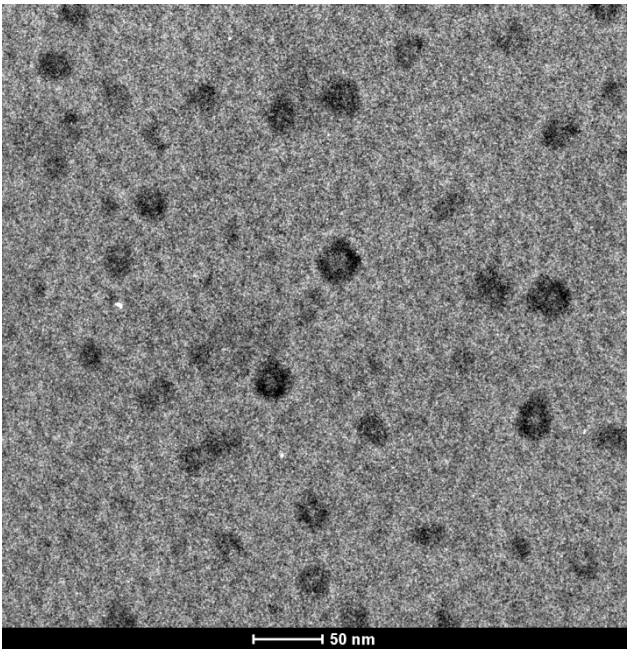


**Fig. 7:** TEM Image of the obtained core shell particles

Numerous experts during the decade have explored micellization of block copolymers up to a great deal but the novelty of present work is the formation of predominantly spherical nanostructures of a very low molecular weight TBP in a phased fashion. To the best of our knowledge, we didn't encounter any literature involving well defined nanostructure accumulation out of very low M.W. TBP. Further, owing to our interests in the field of MRI and targeted drug delivery, the emphasis at the beginning of the present study was laid down for designing spherical nanostructures with a simplest possible path. Cryogenic TEM (cryo-TEM) technique demonstrates the exact morphology of polymeric micelles without being influenced by drying the samples as in case of traditional TEM/SEM or even a bit of

alteration of exact nanostructure size and morphology due to vacuum pressure for cellulose membrane filtration of the samples for SEM. Compared to bright-field TEM where samples were dried on a solid carbon-coated grid, cryo-TEM preserved the size and morphology of micelle nanoparticles in the hydrated state. Cryo-TEM measurements showed that micelle diameters are…

ITC is meanwhile a standard method to determine the critical micelle concentration (CMC) and the heat of demicellization, $H_{demic}$, i.e. the molar enthalpy of transfer of polymer monomers from a micelle into solvent[44-47]. ITC is a widely used method to determine CMC values of surface active agents. In the literature, ITC has been used as a unique technique for studying of micellization [48-52]or used with other complementary techniques such as fluorescence spectroscopy[53], conductivity[54], potentiometric titration[53] and differential scanning calorimetry[53]. Corresponding determination of the micellization enthalpy is another advantageous on part of ITC and CMC later can be further used to determine the Gibbs energy of micellization[48-52]. Following relation can be drawn out of ITC, where

$$\Delta H_{mic} = -\Delta H_{demic}$$

$\Delta H_{mic}$= Enthalpy change when surfactant monomers cooperatively aggregate into micelles & $\Delta H_{demic}$ = Enthalpy change when surfactant monomers de-micellize into surfactant monomers at CMC. Two types

of enthalpograms were obtained; nonsigmoidal and sigmoidal curves respectively (Fig. 7 & Fig. 8) for room temperatures. According to the type of curve obtained, two methods were used for analyzing the enthalpograms. When sigmoidal curves were obtained, the CMC corresponded to the concentration where the first derivative of the curve displayed a maximum; whereas the heat of micellization ($\Delta H_{mic}$) was equal to the enthalpy difference between the two extrapolated lines as shown in Fig 8. The curves that did not present clear sigmoidal features were analyzed by a data treatment analogous to the one suggested by many authors. The enthalpograms may be categorized into two concentration varieties. During the first injections the concentration of the TBP molecules in the sample cell stays below their cmc and large almost constant enthalpic effects appear due to demicellization of the micelles, dilution of the micelles and dilution of the resultant monomers. The second section of the piercing increases (Fig. 7a) or decreases (Fig. 8) of the heat possessions specify that the cmc of the block polymer is reached in the sample cell. In the third concentration range the further addition of a concentrated micellar solution to the existing micellar solution in sample cell leads to heat effects due to the dilution of micelles.

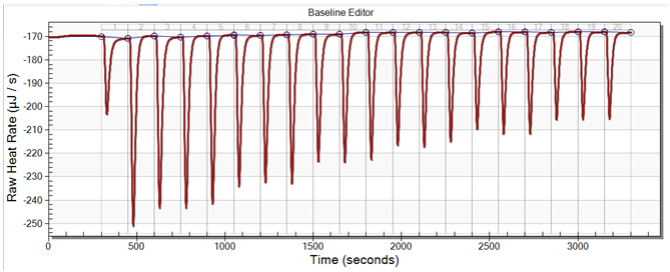


**Fig.8:** *Nano-isothermal calorimetry (Nano-ITC) of the block copolymer*

Reconnaissance was that the incorporation of gadolinium didn't appear to significantly impact BCN size. Probable manifestation of aqueous channels because of the occurrence of PEG in the interior up to a marked extent, along with that on the exteriors of BCNs may lead to entrapment of some of gadolinium amongst the aqueous channels (Fig.3) which may be a contributing factor for insignificant size increase after introduction of Gd. It is likely that the BCN size could not be further reduced due to the energetic constraints imparted by the thick hydrophobic domain. This is significantly larger than the hydrophobic domain of most polymeric micelles, which are typically 3 nm in thickness[55]. Comparative improvement in structural stability of the BCN architectures has made them an attractive alternative to polymeric micelles, which often encounter limitations in clinical applications by their low stability in circulation. In spite of much of endeavor on part of investigators worldwide in the field of monomeric and diblock polymers; the choice of a triblock polymer in the present study could be attributed to the hypothesis that morphologically we expect the presence of PEG on the corona as well

as marginally in the core of BCNs and this may monitor in evading a capture by reticuloendothelial systems (RES) and remain in circulation for a longer duration. Critical micellization allows for vesicle formation while post-micellization concentration paves the way for precise time-tuned control of sequential block collapse and micelle vesicle into BCNs, which might be harmonized with cancer-drug encapsulation with essentially no drug losses. Post-micellization regions have been demonstrated to produce benign, stable nanoparticles made of PLA-b-PEG-b-PLA triblock copolymers that are not only solvent-free and drug-rich, which reduces the body exposure to the excipients, but also nearly burst-release-free owing to the presence of aqueous/PEG channels. Which may reduce if not eliminates its toxic side effects while enhancing its therapeutic efficacy.

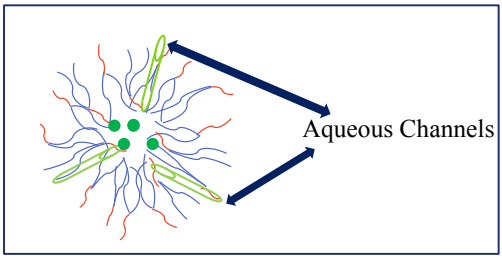


**Fig.9:** Probable model of aqueous channels propagated amongst BCNs

**Conclusions**

Self-assembly driven simple and robust attitude have been developed to prepare well-delineated BCNs of a very low molecular weight block

copolymer. The temperature driven self-assembly generates stable nanostructures in comparison to that at room temperature. Elevated level of temperature provide a higher and rapid nucleation platform for the self-assembly. Although higher levels of concentration of the block copolymer results in the BCNs with higher size (≤150); but evidently zeta potential (35-40) suggests stability of the BCNs at a lower concentration of the polymer. By choosing a suitable system viz a viz dissolution and dispersed medium for the block copolymer constituting monomers, it is reasonable to expect that this simple one-step simple route can be extended to obtain stable nanostructures as a result of the micellization of the polymer. The manifestation of an aqueous environment and the relocation/migration of hydrophilic parts of the block copolymer towards exteriors of the nanostructures have been concluded on the basis of the hydrophilic character of the PEG segment of the block copolymer. Moreover, due to incomplete migration/relocation of the PEG segments towards the exteriors, some part of it remained entrapped in the interiors as well. This PEG present in the interiors of the nanostructures may manifest via aqueous channels which may prove a guiding force for Gd entrapment among the interiors of the nanostructures.

## References


1. Weissleder, R., Molecular imaging in cancer. *Science* 2006, 312, 1168-1171.
2. Juweid, M. E.; Cheson, B. D., Current concepts - Positron-emission tomography and assessment of cancer therapy. *New England Journal of Medicine* 2006, 354, 496-507.
3. Weissleder, R., Scaling down imaging: Molecular mapping of cancer in mice. *Nature Reviews Cancer* 2002, 2, 11-18.
4. Jaffer, F. A.; Weissleder, R., Molecular imaging in the clinical arena. *Jama-Journal of the American Medical Association* 2005, 293, 855-862.
5. Liu, Y.; Chen, Z.; Liu, C.; Yu, D.; Lu, Z.; Zhang, N., Gadolinium-loaded polymeric nanoparticles modified with Anti-VEGF as multifunctional MRI contrast agents for the diagnosis of liver cancer. *Biomaterials* 2011, 32, 5167-5176.
6. Kamaoui, I.; Milot, L.; Durieux, M.; Ficarelli, S.; Mennesson, N.; Pilleul, F., Value of MRCP with Mangafodipir Trisodium (Teslascan (R)) injection in the diagnosis and management of bile leaks. *Journal De Radiologie* 2007, 88, 1881-1886.
7. Sharma, P.; Brown, S. C.; Walter, G.; Santra, S.; Scott, E.; Ichikawa, H.; Fukumori, Y.; Moudgil, B. M., Gd nanoparticulates: from magnetic resonance imaging to neutron capture therapy. *Advanced Powder Technology* 2007, 18, 663-698.
8. Thorek, D. L. J.; Chen, A.; Czupryna, J.; Tsourkas, A., Superparamagnetic iron oxide nanoparticle probes for molecular imaging. *Annals of Biomedical Engineering* 2006, 34, 23-38.
9. Arbab, A. S.; Liu, W.; Frank, J. A., Cellular magnetic resonance imaging: current status and future prospects. *Expert Review of Medical Devices* 2006, 3, 427-439.
10. Weissleder, R.; Cheng, H. C.; Bogdanova, A.; Bogdanov, A., Magnetically labeled cells can be detected by MR imaging. *Jmri-Journal of Magnetic Resonance Imaging* 1997, 7, 258-263.
11. Heyn, C.; Bowen, C. V.; Rutt, B. K.; Foster, P. J., Detection threshold of single SPIO-Labeled cells with FIESTA. *Magnetic Resonance in Medicine* 2005, 53, 312-320.

12. Moffat, B. A.; Reddy, G. R.; McConville, P.; Hall, D. E.; Chenevert, T. L.; Kopelman, R. R.; Philbert, M.; Weissleder, R.; Rehemtulla, A.; Ross, B. D., A novel polyacrylamide magnetic nanoparticle contrast agent for molecular imaging using MRI. *Molecular imaging* 2003, 2, 324-32.
13. Andre, J. P.; Toth, E.; Fischer, H.; Seelig, A.; Macke, H. R.; Merbach, A. E., High relaxivity for monomeric Gd(DOTA)-based MRI contrast agents, thanks to micellar self-organization. *Chemistry-a European Journal* 1999, 5, 2977-2983.
14. Caravan, P., Protein-Targeted Gadolinium-Based Magnetic Resonance Imaging (MRI) Contrast Agents: Design and Mechanism of Action. *Accounts of Chemical Research* 2009, 42, 851-862.
15. Kummerer, K.; Helmers, E., Hospital effluents as a source of gadolinium in the aquatic environment. *Environmental Science & Technology* 2000, 34, 573-577.
16. Kulaksiz, S.; Bau, M., Contrasting behaviour of anthropogenic gadolinium and natural rare earth elements in estuaries and the gadolinium input into the North Sea. *Earth and Planetary Science Letters* 2007, 260, 361-371.
17. Doiron, A. L.; Chu, K.; Ali, A.; Brannon-Peppas, L., Preparation and initial characterization of biodegradable particles containing gadolinium-DTPA contrast agent for enhanced MRI. *Proceedings of the National Academy of Sciences of the United States of America* 2008, 105, 17232-17237.
18. Chen, Z.; Yu, D.; Wang, S.; Zhang, N.; Ma, C.; Lu, Z., Biocompatible Nanocomplexes for Molecular Targeted MRI Contrast Agent. *Nanoscale Research Letters* 2009, 4, 618-626.
19. Doiron, A. L.; Homan, K. A.; Emelianov, S.; Brannon-Peppas, L., Poly(Lactic-co-Glycolic) Acid as a Carrier for Imaging Contrast Agents. *Pharmaceutical Research* 2009, 26, 674-682.
20. Chen, Z.; Yu, D.; Liu, C.; Yang, X.; Zhang, N.; Ma, C.; Song, J.; Lu, Z., Gadolinium-conjugated PLA-PEG nanoparticles as liver targeted molecular MRI contrast agent. *Journal of Drug Targeting* 2011, 19, 657-665.
21. Bazile, D.; Prudhomme, C.; Bassoullet, M. T.; Marlard, M.; Spenlehauer, G.; Veillard, M., Stealth Me.PEG-PLA nanoparticles

avoid uptake by the mononuclear phagocytes system. *Journal of Pharmaceutical Sciences* 1995, 84, 493-498.
22. Hawker, C. J.; Wooley, K. L., The convergence of synthetic organic and polymer chemistries. *Science* 2005, 309, 1200-1205.
23. Segalman, R. A., Patterning with block copolymer thin films. *Materials Science & Engineering R-Reports* 2005, 48, 191-226.
24. Forster, S.; Antonietti, M., Amphiphilic block copolymers in structure-controlled nanomaterial hybrids. *Advanced Materials* 1998, 10, 195-217.
25. Li, Z. B.; Kesselman, E.; Talmon, Y.; Hillmyer, M. A.; Lodge, T. P., Multicompartment micelles from ABC miktoarm stars in water. *Science* 2004, 306, 98-101.
26. Lodge, T. P.; Rasdal, A.; Li, Z. B.; Hillmyer, M. A., Simultaneous, segregated storage of two agents in a multicompartment micelle. *Journal of the American Chemical Society* 2005, 127, 17608-17609.
27. Li, Z. B.; Hillmyer, M. A.; Lodge, T. P., Control of structure in multicompartment micelles by blending mu-ABC star terpolymers with AB diblock copolymers. *Macromolecules* 2006, 39, 765-771.
28. Riess, G., Micellization of block copolymers. *Progress in Polymer Science* 2003, 28, 1107-1170.
29. Potemkin, II; Moller, M., Microphase separation in ultrathin films of diblock copolymers with variable stickiness of one of the blocks to the surface. *Macromolecules* 2005, 38, 2999-3006.
30. Kastle, G.; Boyen, H. G.; Weigl, F.; Lengl, G.; Herzog, T.; Ziemann, P.; Riethmuller, S.; Mayer, O.; Hartmann, C.; Spatz, J. P.; Moller, M.; Ozawa, M.; Banhart, F.; Garnier, M. G.; Oelhafen, P., Micellar nanoreactors - Preparation and characterization of hexagonally ordered arrays of metallic nanodots. *Advanced Functional Materials* 2003, 13, 853-861.
31. Gohy, J. F.; Willet, N.; Varshney, S.; Zhang, J. X.; Jerome, R., Core-shell-corona micelles with a responsive shell. *Angewandte Chemie-International Edition* 2001, 40, 3214-+.
32. Pochan, D. J.; Chen, Z. Y.; Cui, H. G.; Hales, K.; Qi, K.; Wooley, K. L., Toroidal triblock copolymer assemblies. *Science* 2004, 306, 94-97.
33. Chen, Z. Y.; Cui, H. G.; Hales, K.; Li, Z. B.; Qi, K.; Pochan, D. J.; Wooley, K. L., Unique toroidal morphology from composition and

sequence control of triblock copolymers. *Journal of the American Chemical Society* 2005, 127, 8592-8593.
34. Forster, S.; Hermsdorf, N.; Leube, W.; Schnablegger, H.; Regenbrecht, M.; Akari, S.; Lindner, P.; Bottcher, C., Fusion of charged block copolymer micelles into toroid networks. *Journal of Physical Chemistry B* 1999, 103, 6657-6668.
35. Netz, R. R., Micellar morphologies of charged diblock-copolymers. *Europhysics Letters* 1999, 47, 391-397.
36. Jiang, Y.; Zhu, J. T.; Jiang, W.; Liang, H. J., Cornucopian cylindrical aggregate morphologies from self-assembly of amphiphilic triblock copolymer in selective media. *Journal of Physical Chemistry B* 2005, 109, 21549-21555.
37. Wang, S. G.; Cui, W. J.; Bei, J. Z., Bulk and surface modifications of polylactide. *Analytical and Bioanalytical Chemistry* 2005, 381, 547-556.
38. Turner, J. L.; Pan, D. P. J.; Plummer, R.; Chen, Z. Y.; Whittaker, A. K.; Wooley, K. L., Synthesis of gadolinium-labeled shell-crosslinked nanoparticles for magnetic resonance imaging applications. *Advanced Functional Materials* 2005, 15, 1248-1254.
39. Chatterjee, A.; Maiti, S.; Sanyal, S. K.; Moulik, S. P., Micellization and related behaviors of N-cetyl-N-ethanolyl-N,N-dimethyl and N-cetyl-N,N-diethanolyl-N-methyl ammonium bromide. *Langmuir* 2002, 18, 2998-3004.
40. Liu, Y. C.; Chen, S. H.; Huang, J. S., Small-angle neutron scattering analysis of the structure and interaction of triblock copolymer micelles in aqueous solution. *Macromolecules* 1998, 31, 2236-2244.
41. Goldmints, I.; vonGottberg, F. K.; Smith, K. A.; Hatton, T. A., Small-angle neutron scattering study of PEO-PPO-PEO micelle structure in the unimer-to-micelle transition region. *Langmuir* 1997, 13, 3659-3664.
42. Sato, S.; Gondo, D.; Wada, T.; Kanehashi, S.; Nagai, K., Effects of various liquid organic solvents on solvent-induced crystallization of amorphous poly(lactic acid) film. *Journal of Applied Polymer Science* 2013, 129, 1607-1617.
43. Williams, C., Polymer Collapse. *Annual Review of Physical Chemistry* 1981, 32, 433-451.

44. Heerklotz, H.; Seelig, J., Titration calorimetry of surfactant-membrane partitioning and membrane solubilization. *Biochimica Et Biophysica Acta-Biomembranes* 2000, 1508, 69-85.
45. Kresheck, G. C., Comparison of the calorimetric and van't Hoff enthalpy of micelle formation for a nonionic surfactant in H2O and D2O solutions from 15 to 40 degrees C. *Journal of Physical Chemistry B* 1998, 102, 6596-6600.
46. Johnson, I.; Olofsson, G.; Jonsson, B., MICELLE FORMATION OF IONIC AMPHIPHILES - THERMOCHEMICAL TEST OF A THERMODYNAMIC MODEL. *Journal of the Chemical Society-Faraday Transactions I* 1987, 83, 3331-3344.
47. Heerklotz, H.; Lantzsch, G.; Binder, H.; Klose, G.; Blume, A., Thermodynamic characterization of dilute aqueous lipid/detergent mixtures of POPC and C(12)EO(8) by means of isothermal titration calorimetry. *Journal of Physical Chemistry* 1996, 100, 6764-6774.
48. Paula, S.; Sus, W.; Tuchtenhagen, J.; Blume, A., THERMODYNAMICS OF MICELLE FORMATION AS A FUNCTION OF TEMPERATURE - A HIGH-SENSITIVITY TITRATION CALORIMETRY STUDY. *Journal of Physical Chemistry* 1995, 99, 11742-11751.
49. Garidel, P.; Hildebrand, A.; Neubert, R.; Blume, A., Thermodynamic characterization of bile salt aggregation as a function of temperature and ionic strength using isothermal titration calorimetry. *Langmuir* 2000, 16, 5267-5275.
50. Majhi, P. R.; Blume, A., Thermodynamic characterization of temperature-induced micellization and demicellization of detergents studied by differential scanning calorimetry. *Langmuir* 2001, 17, 3844-3851.
51. Beyer, K.; Leine, D.; Blume, A., The demicellization of alkyltrimethylammonium bromides in 0.1 M sodium chloride solution studied by isothermal titration calorimetry. *Colloids and Surfaces B-Biointerfaces* 2006, 49, 31-39.
52. Dai, S.; Tam, K. C., Isothermal titration calorimetric studies of alkyl phenol ethoxylate surfactants in aqueous solutions. *Colloids and Surfaces a-Physicochemical and Engineering Aspects* 2003, 229, 157-168.
53. Klijn, J. E.; Kevelam, J.; Engberts, J., Aggregation behavior of mono-endcapped hydrophobically modified poly(sodium acrylate)s in

aqueous solution. *Journal of Colloid and Interface Science* 2000, 226, 76-82.
54. Wettig, S. D.; Wang, C.; Verrall, R. E.; Foldvari, M., Thermodynamic and aggregation properties of aza- and imino-substituted gemini surfactants designed for gene delivery. *Physical Chemistry Chemical Physics* 2007, 9, 871-877.
55. Discher, B. M.; Won, Y. Y.; Ege, D. S.; Lee, J. C. M.; Bates, F. S.; Discher, D. E.; Hammer, D. A., Polymersomes: Tough vesicles made from diblock copolymers. *Science* 1999, 284, 1143-1146.

# CHAPTER IV: PRELIMINARY DATA ON DEPOSITION OF BLOCK COPOLYMER ON NANOCAPSULAR STRUCTURES TO BE APPLIED IN THE THERANOSTIC FIELD

## INTRODUCTION

There is a vast and growing interest in the medical applications of polymer micelles containing di-block or tri-block-copolymers that consists of hydrophilic and hydrophobic blocks. The micelles cores can be loaded with hydrophobic or hydrophilic drugs that can be released by a change in pH or another external factor. About the enormous advantages of the nanocapsular we have already discussed in the previous Chapter II, so, in this last Chapter we have thought to take advantages from the combinations of these two precious characteristic by covering our semi-crystalline nanocapsules with the TBP. This new architectures could allow us to use the peculiar melting properties and release behavior of the nanocapsules in combination to the ability of the TBP of perform enhanced MRI.[1]

## MATERIALS AND METHOD

### Materials

For engineering the block copolymer nanoparticles (BCN), a low molecular weight Block polymer (PLA-PEG-PLA – Mw=1000-10000-1000Da) was purchased from Sigma Aldrich. Intended for dispersed

phase, various organic solvents such as N,N-Dimethylformamide (DMF) and acetone were also procured from Sigma Aldrich. And the Gadolinium Chloride ($CdCl_3$) used for loading the BCN have been purchased from Sigma Aldrich. Extra pure Millipore water was used for the self-assembly process. PLLA Nanoparticles have been produced by the method reported in Chapter II.

## Methods

### Isothermal titration calorimetry (ITC)

The calorimetric experiments were performed with a Nano-ITC instrument (TA Instruments—Waters LLC 109 Lukens Drive New Castle, DE 19720). All heat effects arising from the injection of syringe solution into the sample cell solution are actively balanced by a calorimeter feedback system keeping the sample cell and reference at the same temperature. The calorimeter sample cell was filled with water and the titration syringe was loaded with the aqueous TBP solution of a stipulated concentration. Each experiment consisted of twenty five injections each of 2µL at 180 second intervals with a stirring speed of 150 rpm. A 3000-second baseline was collected before the first injection and after the last injection. Except the aforementioned room temperature, parallel experiments have also been tried at various temperatures of 30°C, 35°C & 40°C. Prior to starting of the titration, the calorimeter was equilibrated to a baseline with water in water titration so as to standardize the instrument. The experimental data were analyzed using the

NanoAnalyze software for ITC as provided by TA instruments. The thermodynamic properties using the mass-action model were obtained by applying a non-linear regression routine based on the method of simulated annealing to the experimental data. So as to study the thermodynamics involved during a probable combination of PARTICLES with our TBP, separate experiments have been carried out by filling the Nano-ITC sample cell with PARTICLES and inserting the TBP through syringe. The addition pattern and the concentration of the TBP were kept same as was the case previously.

**Field Emission Scanning Electron Microscopy (FESEM)**

FESEM instrument from Ultra-plus Zeiss at accelerating voltage of 5-20kV have been used for all SEM studies. For liquid samples the drops were dried on a glass mounted on a stub while the ultra-filtered samples have been observed by fastening the cellulose membranes on the stub.

**Transmission Electron Microscopy (TEM) measurements**

The shape and size of BCN have been characterized by transmission electron microscopy (TEM). The samples were prepared by mounting a drop of self-assembly solution on a carbon coated Cu grid and allowing it to dry in air. These samples have been observed with the help of a FEI CM10 transmission electron microscope operating at 120 kV. The system has been provided with an intensified video camera to assist in alignment and a slow scan CCD camera. Final images can be recorded on CCD.

## Results

Starting from a particle concentration of 1mg/mL, we worked at different dilution ratio: 1:1, 1:2, 1.10, 1:50, 1:100. Our decision to work at 1:2 ratio was due to the absence of interferences in the heat signal. As showed in the graph a), because of the same height of the peaks only the contribution of the dilution was detected. Two different TBP concentration were studied for this system: 6,67 mM and 13,35 mM.

The reason to try these two concentrations is due to previous data related to the micellization of the TBP in water. Indeed, some experiments related to the CMC and CMT were performed in order to individuate the range of work.[2,3]

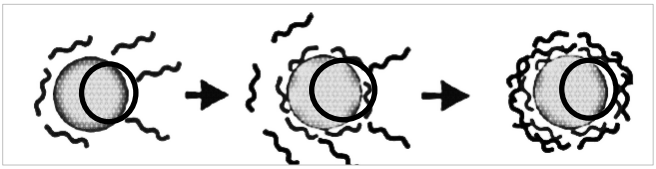

**Figure 3:** Representation of the Block-copolymer depopsition on nanoaprticles after the injection

As reported in **Figure 1-c**, a decrease in the energy rate is observed when the solution of the block copolymer is injected in the sample cell. We have attributed this behavior to the initial deposition of the TBP on the particles. It is important to notice that the exothermic effect in presence of the combination TBP-Particles is much higher if compared to the graph in **Figure 1 A) and B)**.

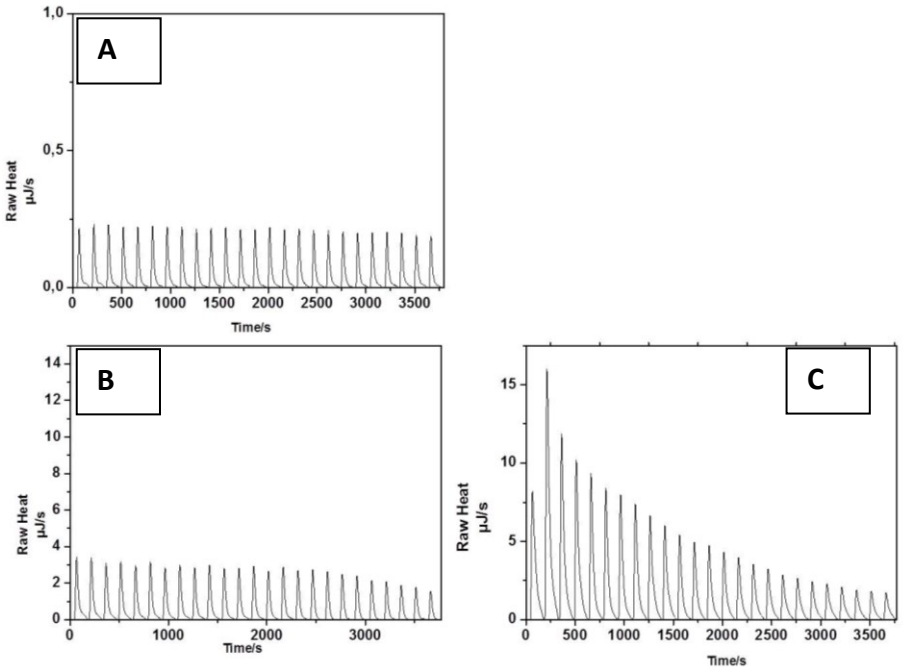


**Figure 4:** Graphs resulting by Titration experiments. A) Heat vs Time resulting by the diluition of the particles within the cell. B) Range of concentration were TBP has already reached its critical micellar concentration able to for regular micelles and to cover the nanoparticles. C) Last results represent the injection the TBP at the concentration of 6,67 mM injected in the sample cell containing nanoparticle suspension 1:2 (0,5mg/mL)

Enthalpy changes/injection were determined and the data was transformed and fit to an equation which shows the “injections” or "Mole Ratio = mole tritant/mole titrate". The line fit to the data in that panel is the best fit line at the selected concentration, Please note that the curve is sigmoidal, as showed in **figure 3**

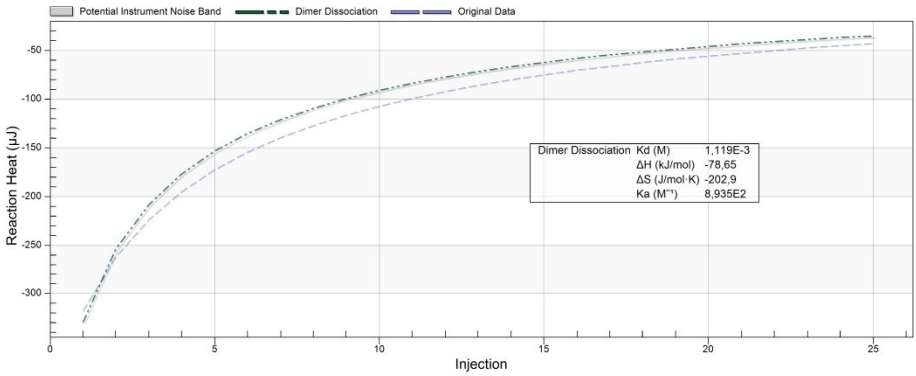


**Figure 5:**Integration of the Heat over the time course of the experiment. The µJ in each peak are plotted against the injection or the male ratio of tritant to tritate.

Predominantly, the two interacting species are probably supposed to interact non-covalently. i.e. via surface hydrophobic patches. Specifically, electrostatic and dipole interactions & a precise pairing of H-bond donors and acceptors may pave the way for binding in the present case. Exposure of the hydrophobic core via aqueous channels of BCNs may deliver an opportunity for the PARTICLES to propagate hydrophobic interactions. ΔG regulates the track in which molecular binding equilibria will instinctively ensue, with more negative values of ΔG favoring higher affinity binding. Decisively, it may be realized that ΔG and its enthalpic and entropic ingredients depend upon differences between free and bound statuses for both of the interacting buddies. Indicative from Fig. 2, the value of ΔG can be calculated from the ΔH and ΔS values and a negative ΔG suggests that the molecular binding in the present case is favorable.

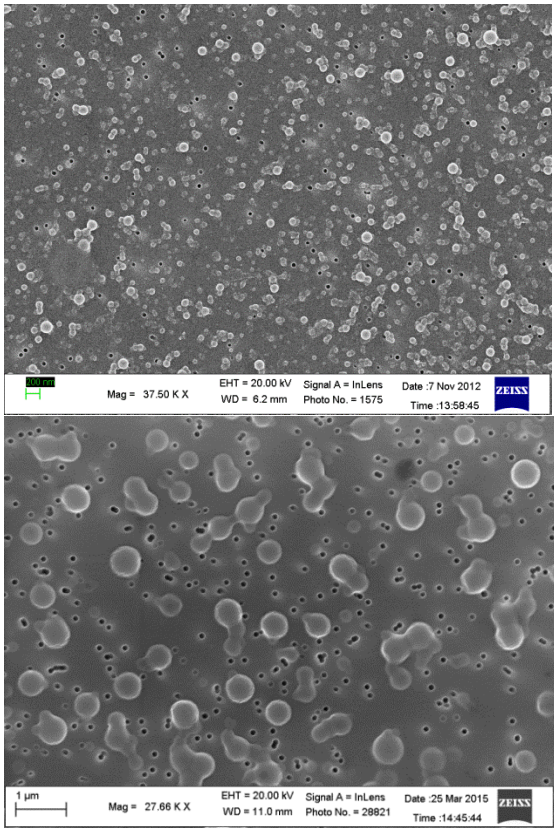


## Conclusions and perspectives

In this last Chapter some preliminary data have been reported related to the deposition of the BCN on the NCs. Further investigations are need to test the nature of this deposition. Indeed, CRYO-TEM in in ordered to evaluate the morphology as so IR to study the interaction between PLLA and Triblock copolymer are needed. Finally, the melting behavior and the theranostic properties of this new-formed system have to be insvestigated.

## References


1 Glover, A. L., Nikles, S. M., Nikles, J. A., Brazel, C. S. & Nikles, D. E. Polymer Micelles with Crystalline Cores for Thermally Triggered Release. *Langmuir* **28**, 10653-10660, doi:10.1021/la300895c (2012).

2 Leavitt, S. & Freire, E. Direct measurement of protein binding energetics by isothermal titration calorimetry. *Current Opinion in Structural Biology* **11**, 560-566, doi:10.1016/s0959-440x(00)00248-7 (2001).

3 Bizley, S. C., Williams, A. C. & Khutoryanskiy, V. V. Thermodynamic and kinetic properties of interpolymer complexes assessed by isothermal titration calorimetry and surface plasmon resonance. *Soft Matter* **10**, 8254-8260, doi:10.1039/c4sm01138d (2014).